EXPERIMENTAL CONTROL OF MORPHOGENESIS IN EMBRYONIC TISSUES

by

Sagar Dattatraya Joshi

B.E. in Instrumentation and Control, Govt. College of Engineering, University of Pune, 2002

M.S. in Bioengineering, Clemson University, 2005

Submitted to the Graduate Faculty of

Swanson School of Engineering in partial fulfillment

of the requirements for the degree of

Ph.D. in Bioengineering

University of Pittsburgh

2011

UNIVERSITY OF PITTSBURGH

SWANSON SCHOOL OF ENGINEERING

This dissertation was presented

by

Sagar Dattatraya Joshi

It was defended on

November 18, 2010

and approved by

Sanjeev G. Shroff, Associate Chair and Professor, Departmental of Bioengineering

Jeffrey D. Hildebrand, Associate Professor, Department of Biological Sciences

Bridget M. Deasy, Assistant Professor, Department of Bioengineering

Dissertation Director: Lance A. Davidson, Assistant Professor, Department of Bioengineering

EXPERIMENTAL CONTROL OF MORPHOGENESIS IN EMBRYONIC TISSUES

Sagar D. Joshi, PhD

University of Pittsburgh, 2011

Embryonic development is a complex phenomenon where embryos construct three-dimensional organ-structures through dynamic cellular rearrangements and cell shape changes. The rapidly dividing epithelial cells spreading over the entire mass of the embryo, the extension of a frog embryonic tissue in the anterior-posterior direction or epithelial-to-mesenchymal conversions are such examples where embryonic cells are undergoing dynamic shape changes. Other events such as bottle-cell formation, blastopore closure, neural tube closure and cement gland formation are examples of dramatic cell shape changes that result is bulk tissue movements. Embryonic development is fundamentally a mechanical process; a developing embryo is shaped by the stresses operating on its mechanical structure. Current studies mainly rely on observations of endogenous cell shape changes and are thus limited by the occurrence of developmentally programmed events. Here we utilize electrical-stimulation, laser-ablation and nano-perfusion approaches to trigger cell shape changes and understand the signaling pathway for externally induced cell contraction. Cell contraction generally and apical cell contraction specifically are the initial steps for numerous morphogenetic events. In these studies we aim to understand the molecular, biochemical and mechanical aspects underlying cell shape change and the role of contractility during morphogenesis. We then refine the perfusion approach to create patterns of differentially responding cells using a precisely controlled spatiotemporal stimulation.

TABLE OF CONTENTS

LIST OF TABLES

LIST OF FIGURES

PREFACE

Performing precise experiments has been tiresome at times. It has been fun on a few junctures. I have had my ‘Eureka’ moments when I had fun. It has been an interesting journey and Isaac Asimov summarized it in very appropriate words: *The most exciting phrase to hear in science, the one that heralds new discoveries, is not 'Eureka!' but rather, 'That's funny...'*

I thank the University of Pittsburgh, the department of Bioengineering and Dr. Borovetz for providing me an opportunity to work and learn in this stimulating environment. I enthusiastically thank the training and financial support from Dr. Lance Davidson who provided me with sufficient scientific opportunities including summer training at the Friday Harbor Labs. I thank the dissertation committee members, Dr. Sanjeev Shroff, Dr. Bridget Deasy and Dr. Jeffrey Hildebrand for their timely advice during my committee meetings. I thank Dr. Ken Webb, my MS thesis advisor for training me in his research lab at Clemson. I also thank Dr. Rohini Mudhalwadkar, my undergraduate advisor for training me in her instrumentation lab at College of Engineering Pune.

I am indebted to the countless embryos and several male and female frogs for their precious contributions to this research project (They demand a paragraph of their own!).

This degree has been an ‘*interesting*’ phase of my life for many reasons. I want to thank the ETD staff at University of Pittsburgh, especially Daryl Bishop for fixing and advising on several issues with the document preparation. I want to thank Tim Cooper for solving numerous

issues with my desktop and laptop computers over the 5 years of Pitt life. I want to thank Lynette Spataro for all her help throughout my stay at Pitt. She has been the “go to” person for me for any and every question I have had.

I made several good friends in Pittsburgh and I would like to thank everyone including Kalpesh, Mangala, Ashish, Shweta, Ashwin, Rich, Yogesh, Komal, Sourabh and Hye Young for their assistance. I also thank all my relatives for their help and assistance. I thank my grandmother for her motivational guidance throughout my life.

My parents are my strength. Without their help and support, I cannot think of being able to start or continue or finish this degree. Throughout this degree I have needed their support to keep my motivation levels up to the mark. This degree is dedicated to all the hard work of my parents over the last several years. Thank you papa and mummy!

I want to thank everyone who has provided any minor or major contributions to help me get through. I may not have written down everyone’s name here but I really mean to thank everyone who has helped me to graduate from a Mr. into a Dr.

I thank God for everything.

1.0 INTRODUCTION

> ‘Let us only imagine that birds had studied their own development and that it was they in turn who investigated the structure of the adult mammal and of man. Wouldn't their physiological textbooks teach the following? 'Those four and two-legged animals bear many resemblances to embryos, for their cranial bones are separated, and they have no beak, just as we do in the first five or six days of incubation; their extremities are all very much alike, as ours are for about the same period; there is not a single true feather on their body, rather only thin feather-shafts, so that we, as fledglings in the nest, are more advanced than they shall ever be ... And these mammals that cannot find their own food for such a long time after their birth, that can never rise freely from the earth, want to consider themselves more highly organized than we?’ (Karl Ernst von Baer)

Embryonic development has fascinated people through the ages. Embryogenesis is a process in which an extremely complex multicellular organism rises out of a single fertilized egg. How is this organism formed? What information does an egg and a sperm possess that dictates the further development of an embryo? These and many other questions have intrigued researchers

since the 18th century. Epigenesis and Preformations were the two proposed models of embryonic development that lasted until the 18th century. 'Epigenesis' theory proposed that the embryo arose progressively (organ by organ) where as 'Preformation' supporters believed that a 'homunculus' was sitting in the sperm head (Wolpert, Beddington et al. 2002). Eventually 'Epigenesis' was accepted with the emergence of cell theory in the 19th century.

Much progress has been made since. Thousands of genes and their functions have been discovered, several morphogenetic disorders have been studied and physics laws have been proposed governing cell behaviors and yet we know so little about the '*embryo*'. Developmental biologists, physicists, bioengineers, molecular biologists and a variety of other researchers have been engaged in understanding and describing embryonic cell behaviors; chemical gradients, physical laws applicable to biology, cell sorting and roles of various genes are some of the areas of scientific interest.

How does a cell know what to do? How does a cell know when to change shape? How does a group of cells know when to contract and cause tissue buckling? How do cells form furrows, pits and cavities? How do chemical gradients originate in cell communities? These and many more fascinating questions have intrigued researchers over time. Subcellular molecules, single cells and multicellular tissues form a close relationship where qualitative or quantitative change in one scale affects the others and vice versa. Microscopic, mesoscopic and macroscopic descriptions can bridge the gaps between scales and illuminate facts that have eluded us so far. A dynamic description, a possible mechanical explanation and a quantitative analysis of the active behavior of the cytoskeleton is a necessary step in this direction (Theriot 1994; Bendix, Koenderink et al. 2008; Bugyi, Le Clainche et al. 2008; Vartiainen 2008).

In this dissertation, complementary stimulation methods were applied to investigate the mechanical, molecular and physical properties of *Xenopus laevis* embryonic cells and tissues. This thesis is structured as follows: In chapter 2, we introduce the fundamental concepts of *Xenopus laevis* embryonic development, describe mechanics in epithelial morphogenesis, and briefly explain the standard methods utilized in this study. The next four chapters (chapters 3 to 6) are dedicated to individual projects. Each of these chapters is subdivided into methods, results and discussion sections. In chapter 3, we demonstrate the stimulation methods and their utility in inducing cell shape change. Using complementary stimulation methods (electrical stimulation, laser activation and nano-perfusion) we aim to understand the embryonic development from morphological, molecular and mechanical perspectives simultaneously. In chapter 4, we uncover the extracellular nucleotides inducing cell contraction. Nucleotides have been studied in different developmental/ physiological roles, but for the first time, we demonstrate their role in inducing a direct cell shape change and thus affecting development through changes in mechanical/ physical properties. In chapter 5, we investigate cell responses to laser-activation. We describe the response of a single cell after a multicellular cell sheet is activated and how the surrounding cells contract with a rapid response throughout the observed field. We propose that embryonic epithelium acts like an “excitable media”. In chapter 6, biology and microfluidic technology have been combined to understand the role of chemical gradients. Using a microfluidic feedback control system, we detect a dynamic spatiotemporal response to periodic chemical stimulation in *Xenopus laevis* tissue. We identify a first order response to stimulation. In chapter 7, a brief summary of our findings is presented and future directions are suggested.

1.1 GOALS AND SPECIFIC AIMS

We investigate mechanisms that drive cell shape change during acutely stimulated *Xenopus laevis* epithelial contraction. We utilize complementary stimulation techniques (electrical stimulus, laser-activation, nano-perfusion and microfluidics-controlled nano-perfusion) and investigate mechanical, molecular and morphological aspects of morphogenesis.

Our long term goal is to investigate the contractile cellular machinery during apical contraction in epithelia and utilize the understanding of this machinery to build tissue-engineered organs. The goal of this study is to investigate stimulated epithelial contraction and understand the signaling pathways that drive cell shape change during induced apical contraction, an apically pronounced form of cell contraction that is purported to be a major tissue-building step during embryonic development and tissue re-building in wound healing. Acute control of apical contraction to stimulate tissue bending is a central goal in tissue engineering and regenerative medicine. The importance of actin microfilaments in driving cell shape change is undisputed yet little is known about the triggers of contraction, cytoskeletal remodeling and physical relocations of F-actin filaments and/ or fragments. Using a combination of three distinct stimulation techniques and a multidimensional approach to understand epithelial morphogenesis, we conduct a thorough investigation of biochemical and morphological changes during apical contraction and address the following questions: (1) What biomolecular physiological factor(s) and signaling pathways may be responsible for inducing cell contraction? (2) What is the role of cell contractility in development? To answer these questions, we proposed and completed studies for the following three aims:

Aim 1: Identify and characterize the kinematics of contraction triggered by electric stimulus, laser activation and nano-perfusion of cell lysate. Using cell lysate perfusion,

electrical stimulation and laser ablation, we have demonstrated our ability to induce apical contraction which peaks within a minute followed by a similar relaxation. These techniques are independent and act as complimentary methods useful to answer different molecular, mechanistic and morphological aspects of the contraction process. Here, we characterize the contraction kinematics and understand the similarities and differences in the stimulation methods.

Aim 2: Identify the molecular pathways involved in exogenously triggered apical contraction and evaluate contractility at sub-cellular, cellular and embryonic levels. Using the nano-perfusion technique, we carry out a screen for molecules capable of triggering contraction and characterize the initial intracellular responses to contraction. Using the laser-activation approach, we collect real time images of F-actin dynamics during contraction. F-actin dynamics in the cell apex that are central to cell behavior provide us with a test-bed to investigate changes in actin-related proteins and signaling responsible to trigger the contraction event.

Aim 3: Evaluate multicellular tissue behavior in response to periodic chemical stimulation. Embryonic development is guided by a complex and integrated set of stimuli that results in collective system-wide organization that is both time and space regulated. These regulatory interactions result in the emergence of highly functional units, which are correlated to frequency-modulated stimulation profiles. Here, we determine the dynamic response of vertebrate embryonic tissues to a highly controlled, time-varying localized chemical stimulation using a microfluidic system with feedback control.

Taken together, these three aims seek an integrated understanding of the underlying molecular mechanisms responsible for apical contraction. Such an understanding is critical to

basic science studies in developmental biology and as well as applications in engineered tissues. By investigating the events of apical contraction at sub-cellular, cellular, tissue and embryonic levels we bring the power of a multi-disciplinary approach to understand this important step in organ generation. Rapid, noninvasive and scaffold-less tissue fabrication technique to produce new organs is purported to be the future of regenerative medicine. By studying the emerging collective behavior of a multicellular tissue, we can understand the embryonic response to chemical stimulation which can help us to uncover a possible unifying theory which governs multiple connected cells in an early embryonic tissue. The success of these aims provides us with new sophisticated tools to rapidly induce cell shape change and will help future bioengineers build complex three-dimensional epithelial organs.

1.2 SIGNIFICANCE

"The aim of art is not to represent the outward appearance of things, but their inward significance" - Aristotle

Our long term goal is to understand the contractile machinery intrinsic to embryonic cells and utilize this knowledge to build three-dimensional tissues. Cell contraction in general and apical contraction in specific is a major driver of tissue morphogenesis (Axelrod 2006; Wozniak and Chen 2009). In these studies, our aim to understand the signaling pathways leading to cell contraction and the knowledge gained through this investigation would extend our understanding of epithelial morphogenesis, help us predict the probabilities of certain birth defects and help tissue engineers to build three dimensional tissues.

1.2.1 Birth defects and diseases

Birth defects are major contributors of mortality rates among infants. 120,000 babies (1 in 33) in the United States are born each year with birth defects (Centers for Disease Control and Prevention (CDC). Birth Defects. March 11, 2009). Furthermore, morphogenetic defects are the leading cause of death in the first year of child life (Mathews and MacDorman 2008).

Morphogenesis is a process by which an embryo is shaped and is a critical period during early vertebrate development when tissues derive their architectural and mechanical properties from complex cell movements. Mechanical irregularities of cell contraction during tissue morphogenesis can lead to severe birth defects (Botto, Moore et al. 1999) such as spina bifida, craniorachischisis and anencephaly and yet the cellular, biochemical and tissue-level mechanics underlying these defects are poorly understood.

Our work is a significant step forward in providing in-depth understanding of the fundamentally "biomechanical" process of embryonic development through cell contractility and investigating the biomolecular and biochemical sources that result in tissue architecture defects.

1.2.2 Tissue engineering

In development, cells rearrange and tissue properties change resulting in architectural and mechanical changes in the developing embryo. This is analogous to the mechanical changes that develop in tissue-engineered constructs either in static cultures or in dynamic cyclic stretching experiments (Joshi and Webb 2008). In tissue engineering, cells and matrices are combined together by tissue engineers to construct organ implants. In tissue engineered implants, cells

modify the properties of the biological matrix resulting in a cell/ biomaterial composites that are to be implanted in patients. A major drawback of current engineered implants is their lack of mechanical strength or their inability to integrate mechanically with host tissues. Since both tissue engineering and embryonic development share similar biological and biomechanical principles, the mechanical principles revealed during studies of morphogenesis will aid future tissue engineers to design efficient and long lasting replacement organs (Ghosh and Ingber 2007). Methods to acutely control apical contraction could be used to engineer three dimensional tissues such as tubes, cavities and furrows. Engineered tissues are currently restricted to two dimensional implants such as artificial skin or engineered scaffolds. The ability to induce cell contraction in specific patterns would extend significantly the capabilities of tissue engineers whose goals are the production of three-dimensional-scaffold-less organ replacements.

1.2.3 Mechanical focus

Although historically embryologists have had an interest in the events of embryonic development, lack of experimental tools have left most questions unanswered. Birth defect studies have focused on the genetic cause of birth abnormalities (De Marco, Merello et al. 2006; Kibar, Bosoi et al. 2009) but molecular genetic analysis has revealed little of the coupling between sub-cellular remodeling and cell shapes change. In this study, we combine biochemistry, molecular biology, image analysis, cell mechanics and microfluidics to seek the links between molecular functions and tissue mechanics to address critical questions about cell contractility and embryonic development.

2.0 BACKGROUND

2.1 EMBRYONIC DEVELOPMENT

Embryos construct tissues using mechanical cues, genetic information and biochemical gradients, but how they do so is unknown (Cowin 2000). Understanding morphogenesis helps us understand the natural ways invented by embryonic cells to build tissues. This knowledge is useful for development biologists and tissue engineers who can utilize it to identify critical steps that a cell undergoes in order to construct tissues and organs. Epithelial morphogenesis is in itself a critical mechanism for embryonic development; understanding the mechanisms by which epithelial cells build three dimensional organs is an important step in understanding the overall morphogenesis. Rapid cell shape changes, signaling pathways and triggering molecules play significant roles in epithelial morphogenesis and we propose to characterize the initial steps of induced cell contraction in embryonic epithelia.

2.2 CHALLENGES FOR BIOLOGISTS AND ENGINEERS

Several fascinating “biological tissue construction” challenges are faced by development biologists and tissue engineers alike. Embryos build three dimensional functional tissues within days of fertilization (Trinkaus 1969). *How does an embryo construct rudimentary tissues?*

Epithelial sheets move, cells elongate and the cell sheet spreads (Vaughan and Trinkaus 1966). *What makes a tightly connected epithelial cell sheet engulf the entire embryo?* Cell cultures, analogous to development tissues, can build three dimensional structures when provided with mechanical or biochemical cues (Matsumoto, Sasaki et al. 2007; Hoque, Conseil et al. 2009). *How do cell cultures form three dimensional structures with distinct apical and basal surfaces?* These and many other questions are central to understanding principles of tissue self-assembly.

Rapidly developing animal model systems are ideal to answer some of these questions. Developing embryos are the best living examples of self-organizing tissues that originate through highly dynamic cell movements such as cell spreading and cell shape change while maintaining homeostasis. Thus, shaping of an embryonic body form is largely dependent on the spreading epithelium that is observed to engulf the entire embryo surface during epiboly in gastrulation (Keller, Davidson et al. 2003). Epiboly is the earliest example of epithelial morphogenesis. The later phases of epithelial morphogenesis shape epithelial organs such as heart, lung and kidney. These organs form as a result of a combination of epithelial folding movements such as ingression, invagination, evagination and involution. During early development and later during organogenesis, another form of epithelial morphogenesis, epithelial-to-mesenchymal transition plays vital role in mesoderm formation, shaping the central nervous system (Shook and Keller 2003), and generating cells with stem cell-like properties (Mani, Guo et al. 2008). Thus understanding how cells change shape and drive morphogenesis is critical to understanding development.

2.3 EPITHELIAL MORPHOGENESIS

Epithelial sheets are cells tightly connected at their apices (Fristrom 1988), constructing a tessellated structure capable of deforming itself by both cell shape change and cell rearrangement. Physical connections attach epithelial cells at their apical ends, lateral cell-cell boundaries and basal surfaces. In principle, each of these connections is capable of transmitting force between adjacent cells to form a mechanically contiguous sheet. In general, epithelial morphogenesis is driven mainly by cell shape change with important exceptions. e.g. epithelial branching morphogenesis where dynamic cell rearrangement is observed (Gjorevski and Nelson 2010; Wells and Patel 2010). Mesenchymal morphogenesis in mainly driven by cell rearrangement.

Cell and tissue shape change form the basis of embryonic body form. Cell contraction, a type of cell shape change, is a major tissue shaping mechanism that alters cell shape and drives epithelial morphogenesis. Cell contraction can be driven by a number of mechanisms 1) apical contraction 2) apico-basal contraction 3) circum-apical or circum-basal contraction 4) apical cortex contraction 5) basal expansion and apical contraction 6) whole cell contraction. Irrespective of the mechanism of contraction, the resulting contracted cell phenotype depends upon F-actin polymerization and remodeling (Vasioukhin, Bauer et al. 2000; Alenghat, Nauli et al. 2004; Lee and Harland 2007; Na, Collin et al. 2008).

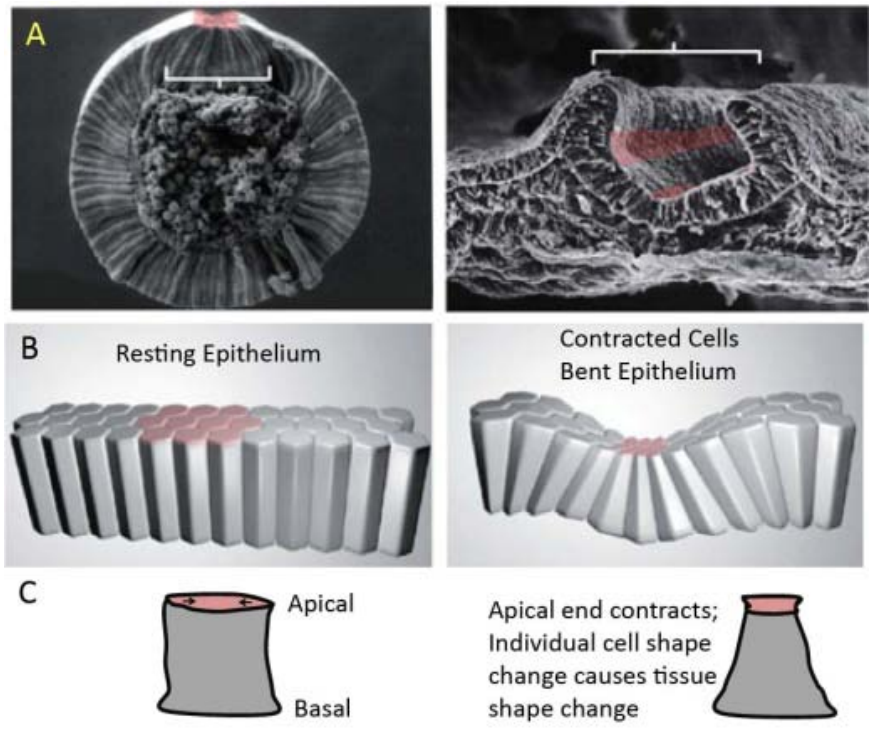

Figure 1. Apical contraction drives epithelial morphogenesis.

A) Epithelial bending shapes the ventral furrow in Drosophila [left panel] and the neural tube in chicken embryos [right panel]. B) Bending is hypothesized to be driven by a group of apically contracting cells (pink apices, shown in C) within an otherwise resting epithelium. Panels A and B are modified from (Lecuit and Lenne 2007).

Cells become wedge-shaped or bottle-shaped during epithelial bending. Apical contraction is but one way this may be achieved (Figure 1). Single cell contractions occur in developing tissues to facilitate neighboring cell movement and / or shape change during morphogenesis. Such a contraction event in a single cell when coordinated among a population of cells, drives epithelial morphogenesis in several model systems (Table 1).

Studies in apical cell contraction in developing embryos have been complemented by cell culture studies that demonstrate control of cell cytoskeleton in kidney epithelial cells (Lagunes, Ruiz et al. 1999; Frixione, Lagunes et al. 2003; Alenghat, Nauli et al. 2004). Thus, cell contractility is purported to drive various morphogenetic movements during tissue formation in development (Haigo, Hildebrand et al. 2003; Rolo, Skoglund et al. 2009) and single cells (Huang and Ingber 2005; Salbreux, Joanny et al. 2007).

Table 1. Cell contraction drives epithelial morphogenesis across species.

Contraction	**Organism**	**Morphogenetic event**	**Phylum**	**Reference**
Single cell	Drosophila	Dorsal closure	Arthropoda	(Toyama, Peralta et al. 2008)
	Xenopus laevis	Wound healing	Chordata	(Davidson, Ezin et al. 2002)
	Amniote	Epithelial to mesenchymal transition	Chordata	(Shook and Keller 2003)
Groups of cells	Drosophila	Ventral furrow formation	Arthropoda	(Leptin and Grunewald 1990)
	Mouse	Neurulation	Chordata	(Smith, Schoenwolf et al. 1994)
	Ascidian	Invagination	Chordata	(Sherrard, Robin et al. 2010)
	Sea-urchin	Gastrulation	Echinodermata	(Nakajima and Burke 1996)
	Xenopus laevis	Neural tube formation	Chordata	(Haigo, Hildebrand et al. 2003)

2.4 MOLECULES AND MECHANICS IN CONTRACTILITY

Role of F-actin microfilaments in cell contractility is undisputed but little is known about spatiotemporal dynamics of the F-actin cytoskeleton that drive cell contraction. There are several studies that attempt to connect biophysical principles, tensegrity, mechanotransduction and biomolecular aspects of contraction (Chen, Mrksich et al. 1997; Wayne Brodland and Wiebe 2004; Klemm, Suchodolski et al. 2006; Chen 2008; Jaalouk and Lammerding 2009; Wozniak and Chen 2009). Though it is critical to understand the relationship between these principles and study them in isolation, it has been difficult to separate them due to the fact that a single protein could have multiple functions or multiple proteins could affect a single outcome.

During development, cells achieve the contracted phenotype using diverse mechanisms depending upon the organism and / or the morphogenetic event. For instance, mouse primary mesenchymal cells contract their apices and extend basal protrusions to form large bottle-shaped cells during ingression (Shook and Keller 2003). In ascidian invagination, apical contraction and apico-basal cell shortening drive the cell contraction in a two-step process (Sherrard, Robin et al. 2010). These examples illustrate the fact that cells utilize diverse steps to alter their shapes that drive tissue buckling and advance morphogenesis.

Many morphogenetic studies have been focused on Drosophila epithelia due to the relative simplicity associated with invertebrate biology and other specific advantages: 1) It has a short life cycle of two weeks which enables study of numerous generous in a short period of time (Sofer and Tompkins 1994). 2) It is easy and inexpensive to maintain colonies. 3) It has a long history in development and genetics research (Rubin 1988). Recent studies involving

sophisticated quantitative approaches and high-resolution imaging have significantly advanced our understanding of the Drosophila morphogenesis (Andrew and Ewald 2009; Martin, Gelbart et al. 2010). Pulsed contractions in actin-rich apical cortex are proposed to drive ventral furrow formation, which is the first morphogenetic movement to occur during *Drosophila* gastrulation causing the internalization of the mesodermal precursors, is thus a mesoderm formation event. (Martin, Kaschube et al. 2008; Puri, Goyal et al. 2008). Actin purse strings and forces from the internalized amnioserosa and expressed proteins in the layer have been shown to drive dorsal closure where epidermal sheets move dorsally to cover the underlying amnioserosa and ultimately fuse in the dorsal midline (Peralta, Toyama et al. 2007; Rodriguez-Diaz, Toyama et al. 2008; Toyama, Peralta et al. 2008), while recently a ratchet-like mechanism has been proposed to drive directed tissue movement in dorsal closure (Solon, Kaya-Copur et al. 2009). These studies seek to connect molecular mechanics with tissue mechanics, however, little is known about the connections between molecular mechanics, cell shape change, tissue folding and morphogenesis.

By using new techniques and complementary experimental tools, we aim to understand how rapid changes in the sub-cellular cytoskeleton translate into cell shape change and how these changes alter tissue-level architecture.

2.5 GRADIENTS IN BIOLOGY

Biochemical gradients play vital roles in providing cues for cell migration, cell shape change, cell differentiation and other cell activities. A gradient a gradual change in the magnitude of a physical or chemical or biological quantity or dimension. Biochemical gradients represent

gradients where biological factors gradually change (increase or decrease) in concentration across the tissue length. In principle, biochemical gradient affects the tissue properties as cells depending on their location in the tissue can sense the change in the biochemical concentration, respond differentially and demonstrate gradient-specific behaviors. e.g. Cell migration in response to biochemical gradients is a widely studied biological process which has wide applications in cell sorting and cellular pattern formation (Brenner, Levitov et al. 1998; Painter 2009).

Embryonic development is a complex, dynamic and highly regulated feedback process where cells actively respond to and control their environment through highly interactive behaviors and in the process form many tissues which result in functioning organ systems (Freeman 2000; Lewis 2008). Vertebrate tissues develop and mature by integrating signaling information provided by several internal and external cues such as mechanical cues and growth factors in the form of gradients (Kessler and Melton 1994; Davidson, Keller et al. 2004; Coudreuse, Roel et al. 2006; Francois, Vonica et al. 2009). In this form of highly regulated development, gradients of diffusible chemical growth factors and morphogens play a fundamental role in processes that shapes animal form (Jaeger, Surkova et al. 2004; Kicheva, Pantazis et al. 2007; Smith, Hagemann et al. 2008). These chemical gradients direct both cell differentiation into specific tissue types and guide cells as they migrate to specific locations (Sater, Steinhardt et al. 1993; Slack 2008). From this perspective controlling these gradients may be the key tools needed to engineer complex tissues for organ regeneration and replacement.

Control of the stimulation profile within microsurgically-isolated tissues serves to reduce the potential complexity of chemical stimuli operating within developing multicellular tissues. For example, chemical gradients can be controlled by manipulating the micro-environment

(Kowalczyk, Byrska et al. 2009; Joshi, von Dassow et al. 2010), delivering growth factors or modulating their activity, overexpressing growth factors to level the gradient or saturate receptors, or genes encoding inhibitory factors or dominant negative receptors (Smith 2009). These approaches have been key tools in identifying factors and mapping pathways that induce differentiation of a range of tissues and testing their physiological function within live embryos (Ariizumi, Kinoshita et al. 2003).

2.6 EXPERIMENTAL PROTOCOLS

Contents of this section have been published in the following journal publication:

Joshi S.D., Davidson LA., Live-cell imaging and quantitative analysis of embryonic epithelial cells in Xenopus laevis., J Vis Exp. 2010 May 23;(39). pii: 1949. doi: 10.3791/1949.

Experimental methods have been described in detail for each project described in subsequent chapters. Here, we present general step-by-step protocols relevant to these projects. These methods include a brief description of the apparatus and tools, simple procedures for tissue isolation and the basic sample preparation methods for confocal microscopy and image analysis. We describe these methods in the following sections: 1) the preparation steps before beginning the experiment, 2) materials and tools required, 3) protocol for explant excision, 4) culture chamber preparation steps, 5) imaging using confocal microscopy, 6) imaging of F-actin microfilaments, and 7) image analysis using Image J.

2.6.1 Preparation steps

1. Synthesize capped mRNA from linearized DNA template encoding the fluorescently tagged protein and purify mRNA by standard methods (AmpliCap Transcription kit; Epicentre Biotechnologies, Madison WI). mRNA should be aliquoted for single time use in 0.2 ml centrifuge tubes and stored at -80°C.

2. Standard methods to obtain eggs, *in vitro* fertilization, and removal of the egg coat have been described previously (Kay and Peng 1991). A procedure to obtain eggs from a *Xenopus laevis* female frog has been demonstrated earlier (Cross and Powers 2008). Fertilize eggs *in vitro* immediately after obtaining them from female frogs using testes previously isolated from a male frog. De-jelly eggs 20 minutes post fertilization and inject mRNA, protein, DNA, or dextran immediately to allow sufficient diffusion of microinjected reagents.

3. Oocyte microinjection has been demonstrated previously (Cohen, Au et al. 2009) using a pressure-valve controlled injector (PLI-100, Harvard Apparatus). Follow a similar method for injecting mRNAs in the animal hemisphere of frog embryos at the 1- to 4-cell stage. Transfer fertilized embryos to 3% Ficoll (Sigma, St. Louis MO) in 1x MBS (MBS-Ficoll) and microinject with the desired volume (2 to 4 nl) of capped mRNA encoding GFP targeted to membrane (mem-GFP) or F-actin (moe-GFP). To obtain even distribution, inject mRNA at 4 equally spaced sites in the animal pole. Embryos can remain in MBS-Ficoll for several hours but need to be transferred to 1/3x MBS before gastrulation starts.

2.6.2 Materials and tools (items marked by * are shown in Figure 2)

1. Dissection stereomicroscope with fiber-optic illumination. A cooled dissection stage is recommended but optional.

2. Hair tools (hair knife and hair loop)*.

3. Forceps (Dumont #5 stainless steel; Fine Science Tools, Foster City, CA)*.

4. Modified Barth's Saline embryo culture media (MBS; 88 mM NaCl, 2.4 mM $NaHCO_3$, 1 mM KCl, 0.33 mM $CaCl_2$, 0.41 mM $(CaNO_3)2$, 0.82 mM $MgSO_4$, 10 mM HEPES (H3375, Sigma-Aldrich, St. Louis MO)).

5. Danilchik's for Amy explant culture media (DFA; 53 mM $NaCl_2$, 5 mM Na_2CO_3, 4.5 mM Potassium gluconate, 32 mM Sodium gluconate, 1mM $CaCl_2$, 1mM $MgSO_4$). Include 0.1% Bovine serum albumin with DFA (BSA; A7906, Sigma-Aldrich). DFA must be sterile filtered but can be aliquoted in 50 ml conical tubes and stored at -20°C. Antibiotics and antimycotics (0.8 % in media; A5955, Sigma-Aldrich) should be added to freshly thawed DFA.

6. 60 or 100 mm Petri dishes*.

7. Large cover glass, 45 by 50 mm (12-544-F, #1.5; Fisher Scientific, Hampton, NH)*.

8. Small cover glass, 24 by 40 mm (12-544C, #1.5; Fisher Scientific).

9. Silicone grease (High Vacuum, Dow Chemical) loaded into a syringe "caulking-gun"*.

10. Custom acrylic chambers or nylon washers (Small Parts Inc.; Miramar, FL)*. Custom chambers can be milled in a Machine Shop from a 25 by 50 by 5 mm acrylic block to provide an inner chamber that is 1.2 cm by 2.8 cm. This chamber has a working volume of 1.68 ml. Optional nylon washers may be selected in a variety of sizes; we prefer sizes compatible with 18 mm diameter circular glass coverslips.

11. Diamond pencil*.

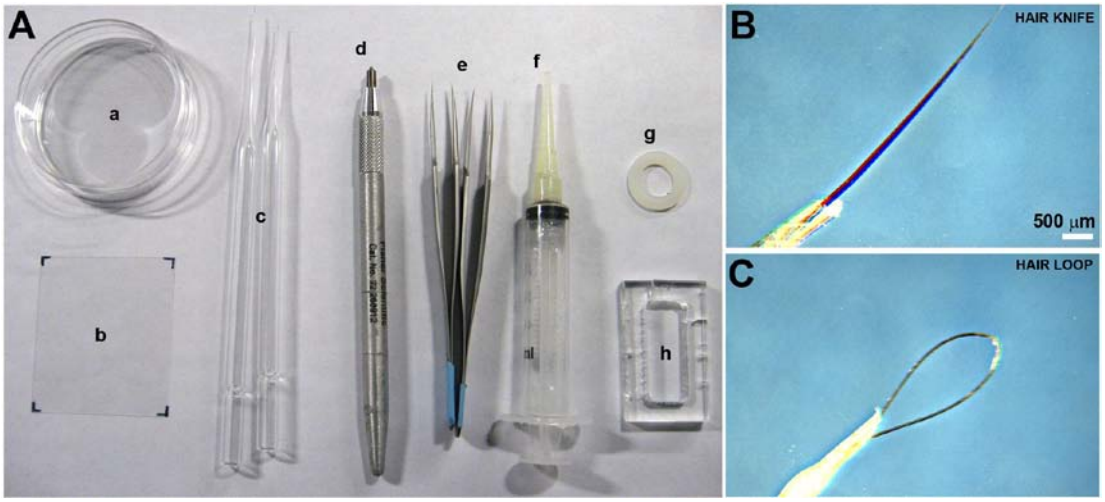

Figure 2. Required tools and materials.

A) Tools needed for microsurgery and assembly of the culture chamber. Petri dish (a), large cover slip (b), hair tools (c), diamond pencil (d), forceps (e), silicone grease "caulking gun" (f), nylon washer (g), and custom acrylic culture chamber (h). B) Close-up of the hair knife, and C) hair loop.

2.6.3 Excision of animal cap explants

Culture embryos to the desired stage in 1/3x MBS. The rate of development can be controlled with culture temperatures between 15 and 21°C so that the experiments can be done at a convenient time of the day. Room temperatures may be used but embryos will develop sooner. Transfer embryos to DFA. Remove vitelline membranes using forceps. Under the dissecting stereomicroscope, excise an animal cap explant using hair-knives and hair-loops. Use the hair-loop to support or hold the embryo at a position and the hair-knife to make a small incision in the animal pole of the embryos. Use repeated "flick-cuts" with the hair-knife to make a 360° incision to remove the animal cap ectoderm from the embryo (Figure 3A). One must be quick while cutting explants, since they have a tendency to ball up quickly. A cooled dissection stage can slow the process or alternatively you can make fewer explants.

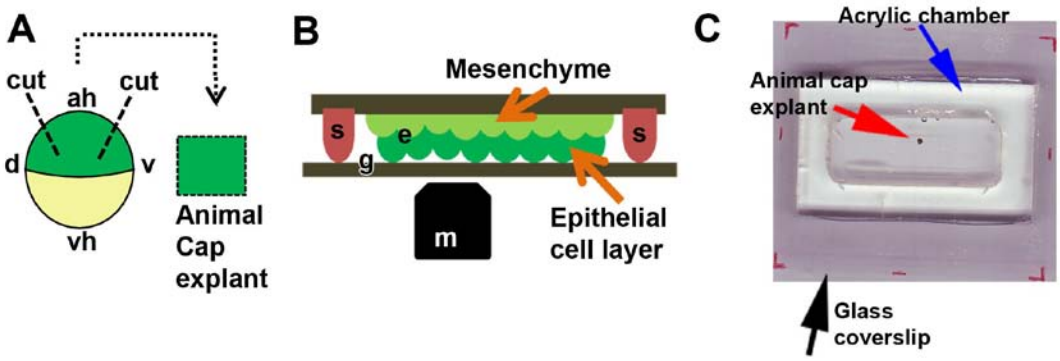

Figure 3. Excision of animal cap explants.

A) Schematic of microsurgical manipulation used to remove an animal cap explant (d, dorsal; v, ventral; ah, animal hemisphere; vh, vegetal hemisphere). B) Schematic of explant (e) positioned under a coverslip fragment held in place by silicone grease (s) with the apical surface apposed to the BSA coated glass (g). The explant is positioned so the epithelial layer is closest to the microscope objective (m). C) Animal cap explant (red arrow) is cultured in DFA and housed in the acrylic chamber (blue arrow) on a large glass coverslip (black arrow) and held in place by glass coverslip fragment and silicone grease.

2.6.4 Culture chamber

Use silicone grease to glue or seal the acrylic chamber to the large cover glass. To reduce adhesion of explants to the glass coat the glass within the chamber with a non-adhesive substrate by incubating the chamber for 2 to 4 hours at room temperature or overnight at 4°C with 1% BSA in 1/3x MBS (BSA-MBS). Prepare small coverslip fragments (approx. 2 by 8 mm) using a diamond pencil. Pre-coat fragments with BSA-MBS. Rinse BSA-MBS from the chamber and replace the media with DFA. Excise animal cap explants and transfer them to the chamber. Position each explant using a hair-loop (with epithelial layer facing the bottom of the chamber) and gently fix the explant in place with a glass coverslip fragment held by small dabs of high vacuum grease (Figure 3B, C). Be very careful while pressing the coverslip since excessive pressure can easily smash the explant.

Multiple explants can be loaded into each chamber based on size of the small coverslip fragments used to hold the explants in place. With practice up to 20 explants can be loaded into the acrylic chamber described here. Fill the chambers with DFA until even with the opening at the top. Use silicone grease to seal the top of the chamber with the 24 by 40 mm cover glass. Add or remove DFA to reduce air-bubbles in the sealed chamber and blot overflow from the chamber. This sealed chamber will allow long term culture and live-imaging of animal cap explants through the large, lower glass surface of the chamber. It is crucial to keep the lower glass surface of the chamber free of dirt, grease, or media for later imaging. We recommend preparing paper-towel bottomed Petri dishes to store chambers as they are prepared for imaging.

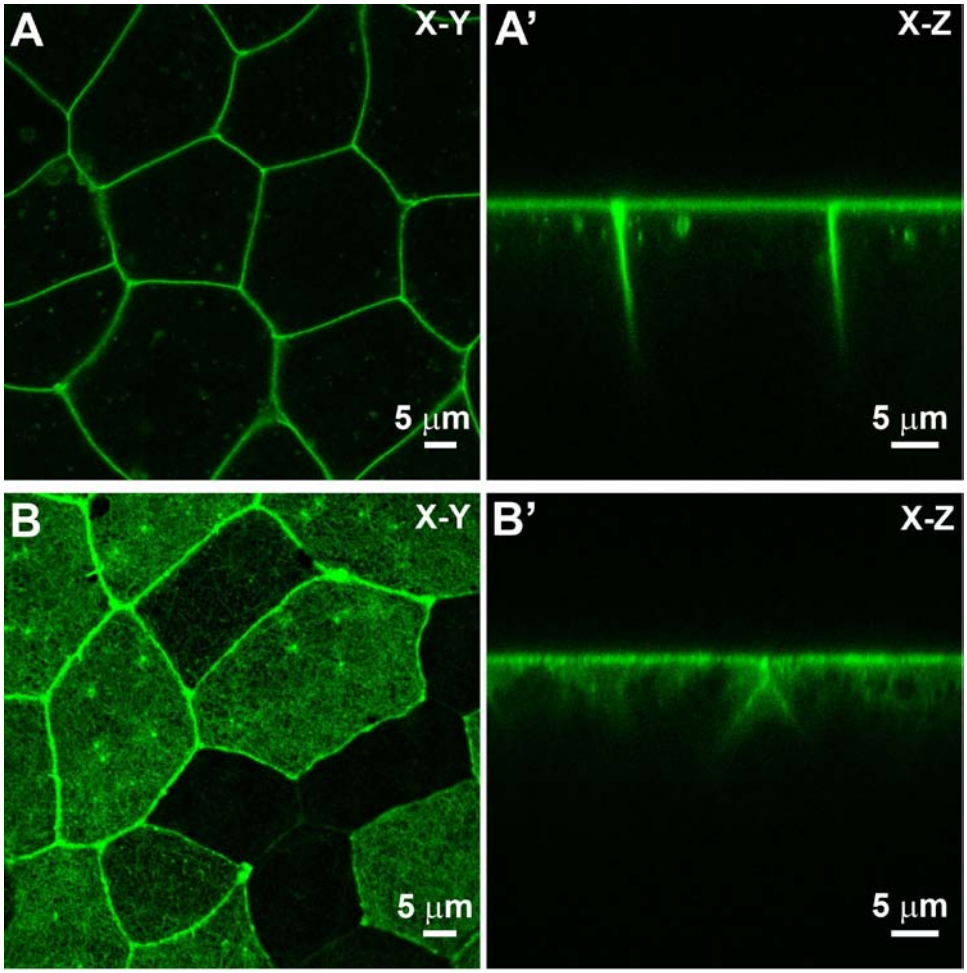

Figure 4. Epithelial cells observed using confocal microscope.

A) An X-Y view and an X-Z (A') view of membrane localizing GFP (mem-GFP) labeled epithelial sheet. B) An X-Y view and X-Z view (B') of a moesin-GFP labeled F-actin apical cell cortex.

2.6.5 High-resolution live-imaging confocal microscopy

This protocol has been developed for a specific confocal microscope (Leica TCS SP5; Leica Microsystems, Bannockburn IL). Different confocal microscopes may require slight modification and we recommend users follow their respective operating instructions.

1. Power-up the system and turn on lasers specific for fluorophores (the Argon laser for fluorescein or EGFP and 543 HeNe laser for rhodamine or RFP).

2. Place the chamber housing the explants onto the microscope stage. Prior to positioning the chamber, move an appropriate objective into place. We recommend using a high numerical aperture 20x air objective (0.7 n.a.) for initial imaging; we recommend using 1.4 n.a. 40x or 63x oil objectives for high resolution imaging and tracking large cell-fields.

3. Use bright-field or fluorescence illumination and adjust the focus until you see the apical ends of the superficial cells. Be careful not to "crash" the objective into the chamber base. Avoid including or producing air bubbles when using the oil immersion objectives. Once the samples are positioned using the "coarse" positioning mode, change to the "fine" positioning mode.

4. Recommendations for tuning the confocal for live imaging:

    a) Laser power should be kept as low as possible: 1) to prevent bleaching, 2) to prevent phototoxic effects, 3) to prevent any accidental triggering of cell shape change.

    b) Use a scan format of 1024 by 1024 pixels for live imaging as it provides good image resolution. If you need very high frame rate (minimum is 1.3s for our system), then use scan format of 512 by 512 pixels.

    c) Adjust the spectral range of the emission, dichroic, and excitation filters.

    d) Adjust the confocal pinhole to between 1 and 1.5 Airy units.

e) Photomultiplier gain must be kept at a minimum level to reduce noise yet provide sufficient signal to identify cell structures and protein localization.

f) Adjust the black level offset to adjust the background to enhance image quality.

g) Steps (a) through (f) are iteratively applied to produce the best quality image possible.

h) Steps (a), (c), (e), and (f) need to be repeated for each additional fluorescence channel to produce the best quality image for possible.

i) When imaging two or fluorescent probes it is important to ensure that there is minimal spectral bleed-through from one protein to a second protein's emission spectra. Bleed-through can be tested by reducing the laser power exciting the first protein and observing the signal produced in the wavelengths used by the second protein. Spectral bleed-through may be reduced with more restrictive choice of filters or by reducing the laser power used for excitation and increasing the gain used for detection of the first protein.

5. With the confocal tuned using these guidelines it should be possible to capture single images at a single focal depth in X-Y mode (Figure 4A).

6. If one is interested in collecting time-lapse movies of a dynamically occurring process such as shape change during cell contraction, one has to choose from the following alternative confocal modes:

1. X-Y-T: This mode allows one to collect a series of images over time, without changing the Z-plane. We use this mode to observe the endogenous fluctuations in the epithelial cells. Normally, we acquire one frame every 5 seconds over 20 minutes to observe endogenous variation or shape changes induced by external stimulation of epithelial cells.

2. X-Y-Z: Using this mode, we can collect a single Z-series stack through epithelial cells. Our default settings to collect Z-series are 0.1 μm steps over a range of 5 μm. We use this

mode to determine whether cytoskeletal changes are occurring only at a certain positions, such as at the level of the adherens junctions, or everywhere in the cell cortex.

3. X-Z-T (Figure 4A'): This mode is mainly used to observe rapid changes in the apical-basal organization of cell in the epithelium. This mode is popular for its utility in confirming that the X-Y-T mode is a reliable reporter of changes in the apical cell domain and that the confocal image acquisition is not drifting along the Z-axis.

4. X-Y-Z-T: This combines X-Y-Z and X-Y-T modes. This mode can provide rich details on the full apical-basal dynamics of the epithelium but is slow to acquire full image stacks and can severely reduce cell viability due to photobleaching and phototoxic effects.

7. The image quality can be improved to a limited extent by using one or a combination of the four following approaches: 1) line averaging, 2) line accumulation, 3) frame averaging, and 4) frame accumulation.

8. With all the settings carefully adjusted, collect and save images, Z-series, and time-series data to an external hard drive, USB-memory stick, or network-attached server.

9. Once you are have completed your experiment, lower the objective for safety, clean the oil from the objective and the microscope stage with lens paper, and power-down the confocal system.

2.6.6 Live-imaging of “subcellular” F-actin microfilaments

As has been shown above, the membrane localizing protein mem-GFP can be used to fluorescently label cell membranes. Live-imaging of sub-cellular components is achieved by using other proteins. A protein such as moesin-GFP that contains an F-actin-binding domain can

be used to label F-actin in live cells. Similar strategies for live-cell imaging and collection of time-lapse sequences follow the procedures outlined earlier. Live-imaging F-actin involves more microscopy skills than imaging mem-GFP since the structures are finer and more tightly localized than the membrane. For instance, any small bubbles in the immersion oil can produce aberration artifacts such as blurring or variable brightness in the captured image. Furthermore, any small drift in the focal or Z-plane can cause moesin-GFP labeled cortical F-actin to move out-of-focus. Thus, one should be re-double efforts to stabilize the stage, the explant, and the chamber while imaging cortical F-actin and other sub-cellular proteins. X-Y and X-Z-T images showing moesin-GFP labeled F-actin are shown as examples (Figure 4B and B').

2.6.7 Image analysis

Images and time-lapse sequences obtained from the live-cell confocal session can be analyzed in order to test hypotheses concerning the shape changes or patterns of protein localization. The naked eye is often the best tool for qualitative analysis but can be augmented or automated by image analysis techniques to extract quantitative data. Image data from Leica confocal systems can be saved in an open format such as .TIF formatted image files or a proprietary .LIF format that retains detailed information on the microscope condition during acquisition. Both .TIF and .LIF files can be directly imported by a freely available image analysis program Image J (Rasband, W.S., U. S. National Institutes of Health, Bethesda, Maryland, USA) using the Bio-Formats plug-in (Kevin Eliceiri, LOCI, University of Wisconsin, Madison, WI). In the following section we offer two examples to illustrate how users might begin quantitative analysis of confocal image data. These examples can allow users to make simple measurements of cell area

and membrane intensity which are initial steps for other complex quantitative analyses. Examples:

1. Open any .TIF or .LIF file (Figure 5A and A') using FILE > OPEN

2. Example 1: Measure the cell area of an epithelial cell (Figure 5B to B'").

    a) Select AREA in ANALYZE > SET MEASUREMENTS.

    b) Select polygon-selection tool from the Image J toolbar, and outline the cell.

    c) Open ROI Manager from ANALYZE > TOOLS > ROI MANAGER and add the outline to it by pressing [control-t], which is the shortcut for adding any new "region of interest" or ROI to the ROI Manager. It is important to add this selection and save ROI-set since you can go back at a later time and make any other parameter measurements. Sets of saved ROIs (click "SAVE") can be reloaded later for further analysis.

    d) One can repeat step (c) with any number of cells in an image and add the ROIs to ROI Manager. Once one has sufficient ROIs recorded, Click "MEASURE" in ROI Manager. In the RESULTS window, one can now see the AREAS against the ROIs. Image dimensions have corresponding values in measurement parameters.

3. Example 2: Measure the intensity of a cell membrane (Figure 5C to C'").

    1. Select "Straight line" tool from the Image J toolbar, and draw a line on the image that is perpendicular to the cell membrane of interest and crosses the membrane. This straight line selection is another type of ROI and can be add to ROI Manager as above.

    2. Plot relative intensities in arbitrary units by ANALYZE > PLOT PROFILE. Save this as image and as list of values by clicking SAVE and LIST > FILE > SAVE AS respectively on the PLOT window.

4. Various quantitative measurements can be made using Image J depending on the researchers' interests and what hypotheses are being tested. Microsoft Excel (Microsoft Corporation, Seattle, WA) or Sigma Plot (Systat Software Inc., San Jose, CA) can be used to plot data graphically.

This protocol can be extended to automate some of the repetitive processes. Macros and plugins can be written to utilize inbuilt Image J commands to achieve complex tasks in image analysis.

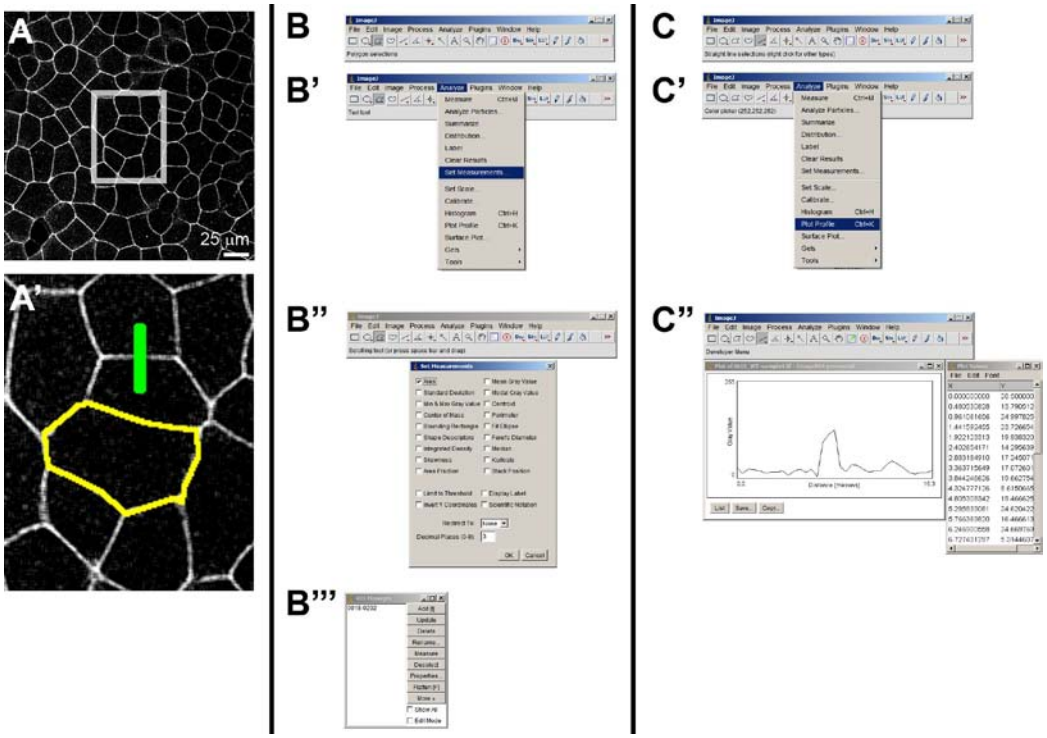

Figure 5. Image analysis using Image J.

A) Original image of a membrane localizing GFP labeled cell sheet. A high resolution view (A') of the box inset in (A) shows two "regions-of-interest" or ROIs. The yellow-outline indicates the boundary of a single cell selected using the polygon tool (see panel B) and the green line indicates the path of an intensity profile across a cell-cell boundary selected using straight line tool (see panel C). B') Method to select the measurement options and choose "Area" (B''). Once the ROI is selected it can be stored in the ROI Manager (B'''). C') The method to select the measurement options for the profile took. C'') Once the straight line or segmented line tool is chosen the intensity profile along the path can be plotted with the "Plot profile" command. A list of intensity values can also be saved in a spreadsheet readable form.

3.0 ACUTE CONTROL OVER STIMULATED EMBRYONIC CONTRACTION

Contents of this chapter have been published in the following journal publication:

Joshi S.D., von Dassow M., Davidson L.A., Experimental control of excitable embryonic tissues: three stimuli induce rapid epithelial contraction. Exp Cell Res. 2010 Jan 1;316(1):103-14.

The experiments for micro-aspiration/ electrical stimulation were conducted in collaboration with Dr. Michelangelo von Dassow.

Cell generated contractility is a major driver of morphogenesis during processes such as epithelial bending and epithelial-to-mesenchymal transitions. Previous studies of contraction in embryos have relied on developmentally programmed cell shape changes such as those that accompany ventral furrow formation in Drosophila, bottle cell formation in Xenopus, ingression in amniote embryos, and neurulation in vertebrate embryos. We have identified three methods to reproducibly and acutely induce contraction in embryonic epithelial sheets: laser activation, electrical stimulation, and nano-perfusion with chemicals released by wounding. Contractions induced by all three methods occur over a similar time-scale (1 to 2 min) and lead to reorganization of the F-actin cytoskeleton. By combining induced contractions with micro-aspiration we can simultaneously measure the stiffness of the tissue and the force and work done by contractions. Laser activation allows real-time visualization of F-actin remodeling during contraction. Perfusion with cell lysate suggests that these three stimuli activate physiologically

relevant pathways that maintain epithelial tension or trigger epithelial morphogenesis. Our methods provide the means to control and study cellular contractility and will allow dissection of molecular mechanisms and biomechanics of cellular contractility.

3.1 EXPERIMENTAL PROTOCOLS

3.1.1 Embryo handling, microsurgery and culture media

Eggs from female Xenopus laevis frogs were collected and fertilized following standard methods (Kay and Peng 1991) and were dejellied in 2% Cysteine solution (pH 8.4) 20 min after fertilization. Embryos were cultured in 1/3x Modified Barth's solution (MBS) to late blastula or early gastrula stages (Nieuwkoop and Faber 1967) and vitelline membranes were removed. Care was taken to minimize wounding of embryos for the whole embryo experiments. For laser activation experiments, animal cap explants were microsurgically removed from stage 10.5 embryos using custom-made hair-loops and hair-knives in Danilchik's For Amy solution (DFA;(Sater, Steinhardt et al. 1993)). With care, microsurgery with hair-tools results in minimal cell lysis. Unless otherwise mentioned, whole embryos at early gastrula stage were cultured in 1/3x MBS and explants harvested from early gastrula stage embryos were cultured in DFA. Bovine serum albumin (0.1 or 0.2 % in media; Sigma-Aldrich, St. Louis MO) and antibiotic/antimycotic (0.8 % in media; A5955, Sigma-Aldrich) were added to both 1/3x MBS and DFA. Unless otherwise stated, experiments were done at early- to mid-gastrulation (stages 10 to 11).

3.1.2 Microscopy and imaging

Three different imaging setups were used for the three stimulation methods. Nano-perfusion experiments were recorded by a digital charge-coupled device (CCD) camera (Scion Corp., Frederick,MD) mounted on a dissecting stereoscope. To visualize embryos and explants during nano-perfusion time-lapse sequences were collected at 1 to 2 sec intervals using computer controlled acquisition software (ImageJ, Wayne Rasband NIH). Electrically stimulated embryos held within the micro-aspirator were visualized using an inverted compound microscope (Leica Microsystems, Bannockburn IL) with either a CCD camera (Scion Corp) or a confocal scan head (Leica TCS SP5). Laser activation experiments were recorded using a confocal scan head mounted on an inverted compound microscope. Timelapse sequences from all three experiments were analyzed either manually or with custom-image processing macros (ImageJ).

3.1.3 Fluorescent probes, lineage labels, and fluorescent proteins

Embryos at the 1- to 4-cell stage were briefly cultured in 3% Ficoll (Sigma, St. Louis MO) in 1x MBS and microinjected with the desired volume of capped mRNA encoding GFP targeted to membrane (mem-GFP) or F-actin (moe-GFP). Capped mRNA was synthesized and purified by standard methods from linearized DNA template (AmpliCap Transcription kit; Epicentre Biotechnologies, Madison WI).

3.1.4 Apparatus for three methods to induce contraction

Three methods of inducing embryonic contractions were designed, implemented and optimized in order to provide consistent results across experiments. We propose to use the three methods – electrical stimulation, laser-activation and nano-perfusion in complementary ways to answer various aspects of the contraction event. All three methods have their pros and cons (Table 2). Laser-activation allows high resolution live cell imaging of the cell cytoskeletal changes. Nano-perfusion allows us to test the physiological factors (small molecules) in the cell lysate that causes embryonic contraction. Electrical stimulation can provide information about the tissue stiffness and the work done by the tissue during contraction. Thus, the three methods provide unique advantages which underline a need to combine the results obtained from them to get a multidimensional understanding about the contraction event.

Table 2. Three stimulation methods for contraction.

Pros/ Cons	Laser-activation	Nano-perfusion	Electrical stimulation
Pros	• Sophisticated method • Precise target site • The only method for high resolution imaging	• The only physiological method • Simple setup • The only method to test biochemical trigger factors	• The only method that can be utilized for mechanics experiments •
Cons	• Complex setup	• Non-specific	• Complex setup

3.1.4.1 Micro-aspiration and electrical stimulation

This protocol was designed and optimized by Dr. Michelangelo von Dassow (von Dassow and Davidson 2009; Joshi, von Dassow et al. 2010). The micro-aspiration device consists of two 90×90 mm chambers, a high-pressure and a low-pressure reservoir, connected by a piece of

poly(dimethylsiloxane) (PDMS) cast around a glass fiber to leave a 120–125 μm diameter channel connecting the two reservoirs (Figure 6A). The pressure difference is adjusted by adjusting water-levels in these reservoirs. This is either done manually with a syringe or using a computer controlled linear actuator (NA08A30A, Zaber Technologies) that drives a piston. Both the camera and the linear actuator are controlled by image acquisition and hardware automation software using a custom macro (LabView VI; National Instruments, Austin TX). Electrical stimulation can be conducted using a Platinum–Iridium electrode (A-M Systems, Sequim, WA). Single electrical pulses (duration = 80 μs; mean voltage = 10 V) were generated using a stimulus isolator (WPI A320; World Precision Instruments, Sarasota FL). To visualize F-actin dynamics within micro-aspirated tissues, a smaller version of the micro-aspirator was built for use with a confocal microscope. Briefly, the protocol for measurement of contraction following electrical stimulation begins with a standard stiffness measurement. At a predetermined time after the start of microaspiration, an electrical pulse, or pulse-train, is delivered across the micro-channel. A visual recording of the time-course of the microaspiration and electrical stimulation is collected and subsequently analyzed to estimate both the mechanical properties and the strength of the electrically stimulated mechanical response (Figure 6B, C).

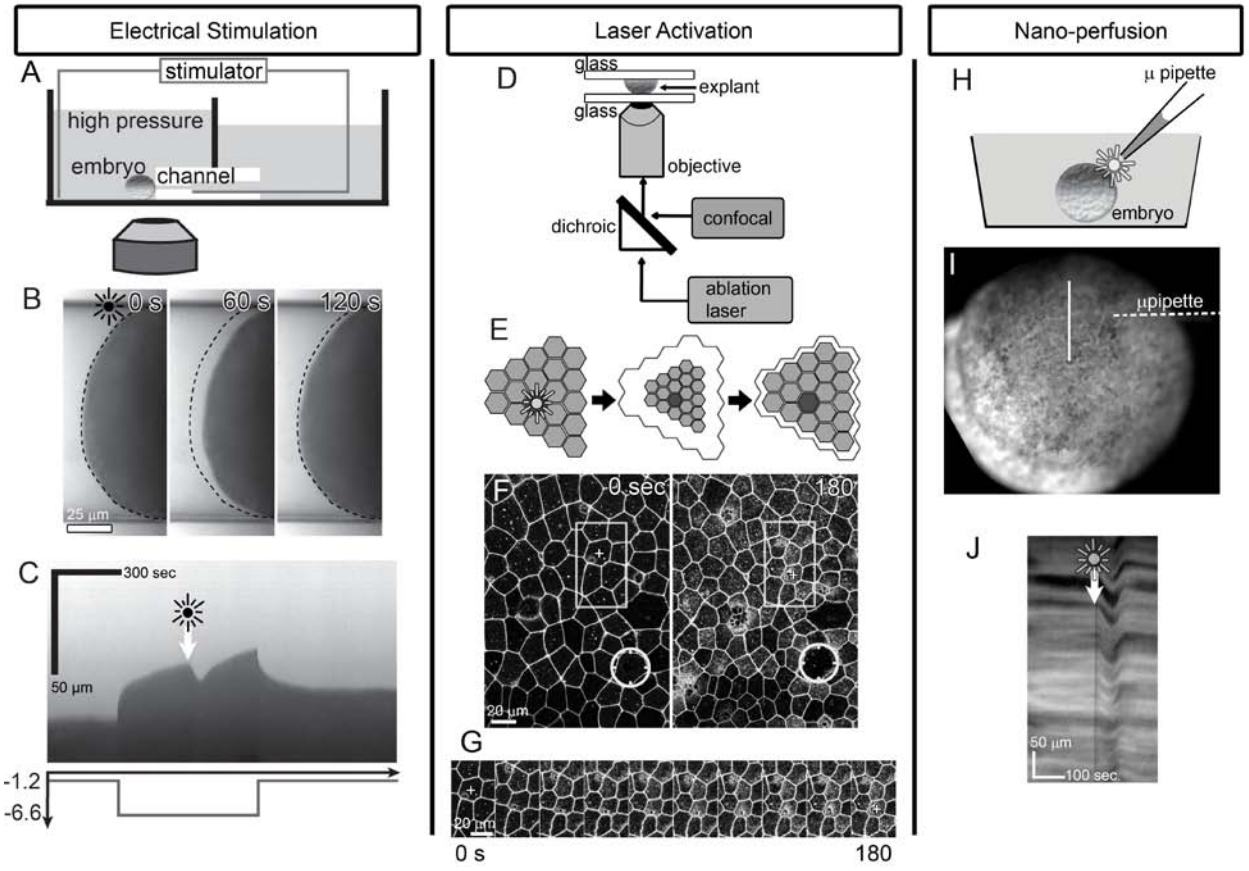

Figure 6. Stimulated cell contraction via electrical pulse, laser activation, and nano-perfusion.

A) Stimulation of an embryo held within a micro-aspirator. B) Aspirated tissues show time-course of stimulated contraction and post-stimulation relaxation (dotted line, limit of aspiration prior to the stimulus). C) Kymograph along middle of the micro-channel illustrates the viscoelastic response to drop in pressure (Pa) over time (graph shown below kymograph) and response to stimulus (arrow and starburst). D) Schematic of laser activation of animal cap explant. E) Activation or ablation of a single cell (starburst) results in contraction of a large field of epithelial cells. F) Time-lapse sequences collected over a large field of cells show contractions spread at least 10 cell diameters away from the ablation site (circle). G) High-resolution view of cells 2 to 6 cell diameters from stimulus (boxes in panel F) contract over 3 min. ("+" cell is the same in F and G). H) Schematic of nano-perfusion shows delivery of 60 nl of cell lysate (starburst) to an embryo (I). J) Time-lapse sequences of the surface of the embryo (in I) resolve the contractile response in a kymograph (along line in I).

3.1.4.2 Laser-activation

We integrated a manual laser ablation system (Micropoint, Photonic Instruments Inc, St. Charles, IL) with the confocal microscope so that we could laser-activate precise locations and collect confocal time-lapse sequences before and immediately following laser activation (Figure 6D). The integrated system consists of a fiber optically delivered beam from a nitrogen-pumped dye laser, beam steering optics and interference filters allowing precise cell membrane ablations or cell targeting. Spatial alignment and focusing of the target illumination is manually controlled. Manually adjustable optical attenuator and collimator allow us to adjust the power of the laser pulse and the size of spot stimulus. In brief, the protocol for laser activation begins with the preparation of an animal cap explant from the animal pole of a gastrulating embryo (between stages 10 and 10.5). Explants and embryos were gently compressed under a glass coverslip bridge held in place with high vacuum silicone grease (Dow Chemical, Russellville, AR) in a custom glass-bottomed confocal chamber. The glass coverslip and confocal chamber were pre-treated with 1% bovine serum albumin (BSA) to avoid sticking or wounding of the embryo. The chamber was then sealed for long-term stable confocal imaging and placed on the stage of the microscope. A suitable field of cells was selected and a pre-activation time-lapse sequence was collected. A predetermined cell or cell–cell junction was targeted and ablated with 1 to 5 laser pulses. A similar number of pulses were used within each experiment. The number of pulses changed in different experiments depending upon the level of pigmentation that could vary between different clutches of embryos. A second time-lapse sequence was immediately started and collected for 3 to 20 min.

3.1.4.3 Nano-perfusion

We adopted a simple yet precise approach for delivering user specified quantities of cell lysate over a defined timecourse on the epithelial surface of the embryo. We first prepared cell lysate by tritrating two early gastrula embryos in 100 µl 1/3x MBS. Lysate was mixed and centrifuged at 13,000 rpm allowing separation of large organelles from supernatant subsequently used for perfusion. 100 µl of lysate was mixed with 3 µl black non-waterproof ink (Higgins Fountain Pen India Ink; Utrecht Art, Cranbury NJ) to allow us to see the applied lysate. To deliver precise amounts of lysate we used a nano-injection apparatus (PLI-90; Harvard Apparatus, Holliston MA), loaded lysate into glass micro-needles, and adjusted the injection time and pressure to deliver 60 nl in a single pulse. Delivery of lysate and the mechanical response of the embryonic tissue were recorded (Figure 6H). Briefly, the protocol for stimulating contraction via nanoperfusion begins with the selection of gastrula stage embryos and removal of the vitelline membrane. Whole embryos are transferred into fresh media and visualized with a CCD equipped stereoscope. The target tissue and micro-needle are aligned so that the epithelial surface is in focus and the opening of the needle is visible within the image field. Since contact between the microneedle and the embryo could wound the embryo, care is taken to ensure that the micro-needle does not touch the embryo. A timelapse collection is started and a bolus of lysate is injected over the tissue surface by manually triggering the nano-injection apparatus. Bulk tissue movements of the contraction response were analyzed with kymographs (Figure 6I, J) prepared from time-lapse sequences (ImageJ).

3.1.5 Analysis of contractile response

An earlier study from our lab (von Dassow and Davidson 2009) demonstrated the existence of clutch-to-clutch variation for stiffness among Xenopus laevis embryos. The existence of natural variation among embryos implies that experiments must be repeated over more than 1 clutch of embryos. To compensate for this variability, experimental and control samples from the same clutch were compared for kinematics of contraction. Also, for timing comparisons, 3 to 4 clutches were considered and a mean of these readings was reported. Statistical tests of significance are carried out with the 2-way ANOVA using SPSS [v. 15] (SPSS Inc. - an IBM Company, Chicago, IL)) which incorporates the clutch-to-clutch variability as well as differences between embryos of the same clutch. A p-value less than 0.05 is considered as statistically significant.

3.2 RESULTS

3.2.1 Mechanical perturbation during contraction

Mechanical stress has been shown to induce expression of Twist in Drosophila embryos (Farge 2003), mechanical stretching has been proposed to induce “hyper-restoration” phenomenon is Xenopus explants (Beloussov, Lakirev et al. 1988) and mechanotransduction has been proposed to play a significant role in defining cell behaviors on a substrate (Ingber 2006). Because mechanically induced effects on cells are being proposed widely, we tested the effect of mechanical microaspiration and physical poking of Xenopus embryos in our experiments. To test

whether mechanical microaspiration of Xenopus embryos would induce cell contraction, previous experiments from our lab (von Dassow and Davidson 2009) indicated to us that microaspirated tissue does not exhibit contractions, meaning that "mechanical" aspiration may not induce contractions by itself. Consistent with these previous observations, we again found no evidence that mechanical stimulation alone induces contractions in microaspiration method. When embryos were "poked" with a micro-needle but care was taken that embryos were not wounded, embryos did not exhibit any contractions (n=7 across 3 clutches). In contrast, embryos when poked with a micro-needle exhibit contractions in cases where a single cell was wounded (see video S4.avi; (Joshi, von Dassow et al. 2010)).

3.2.2 Kinematic parameters of embryonic contraction

Electrical stimulation (Figure 6A through C), laser activation (Figure 6D through G), and nano-perfused lysate (Figure 6H through J) all induce rapid contractions of the epithelial tissue beginning 10 to 20 sec, and continuing for the subsequent 30 to 90 sec after stimulation.

3.2.2.1 Electrical stimulation

After an electrical pulse is delivered to a microaspirated embryonic tissue, the tissue contracts and can partially withdraw from the micro-channel. A visual recording of the time-course of the microaspiration and electrical stimulation is collected and subsequently analyzed for kinematics of contraction. Withdrawal consistently begins within 10 to 15 sec reaching a peak contraction at 45 to 90 sec, and then slowly relaxes towards the original tissue position (Figure 6B, C).

3.2.2.2 Laser-activation

A suitable field of cells was selected, a pre-activation time-lapse sequence was collected, a predetermined cell or cell–cell junction was targeted for ablation and a second time-lapse sequence was immediately started to collect post-activation response. After a laser pulse is delivered to a cell center or cell–cell membrane the surrounding cells, out to the edge of the field of view, begin to contract within 10 to 20 sec. Contraction is rapid over 60 sec and then slows. Because the laser activation damages single or multiple cells (contraction does not require ablation), a long time-scale wound healing response begins about 3 min after activation and culminates in the removal or excision of the damaged tissue (Figure 6F, G).

3.2.2.3 Nano-perfusion

The target embryo and micro-needle are aligned so that the epithelial surface is in focus and the opening of the needle is visible within the image field, a timelapse collection is started and a bolus of lysate is injected over the tissue surface by manually triggering the nano-injection apparatus. Bulk tissue movements of the contraction response were analyzed with kymographs prepared from time-lapse sequences (ImageJ). Nano-perfusion of a bolus of 60 nl of cell lysate stimulates contraction of cells in direct contact with the lysate within 10 to 20 sec. Contractions were not stimulated by nano-perfusion with ink-labeled 1/3x MBS (n=6). Lysate-induced contraction continues and reaches a peak within 45 to 90 sec and then slowly relaxes (Figure 6J).

3.2.2.4 Contraction kinematics are similar across stimulation techniques

Even though the stimuli are different and the methods of visualizing the contractile response are different, all three methods for stimulating contractions produce kinematically similar results. Laser activation contrasts with the other methods in that the contraction response is prolonged;

however, the initial rapid contraction is similar among all three methods **(Figure 7)**. Wounding and wound healing following laser activation could account for the differences in kinematics after the initial phase of contraction. Stimulated tissues respond quickly to activation and the response persists for 1 to several minutes. In all cases the initial response to stimulation is delayed by ~10 to 20 sec, and the response increases over the next 40 to 60 sec.

3.2.3 Biophysical features of induced contractions

3.2.3.1 Reversible and Irreversible contractions

Cells contract and relax in response to all the three stimuli. Depending upon the method of stimulation, different signaling pathways and molecules could play transduction roles. Currently, little is known about the signaling routes for each of the stimulation methods and it is quite possible that the methods could share certain elements of the signaling pathways or have entirely different trigger mechanisms. One way to understand the biophysics of contractility is to understand if any or all induced contractions are reversible or permanent. This study provides us with cues towards a possible shared signaling pathway between the stimulation methods. The stimulation approaches are different in a biophysical sense since laser-activation leaves a wound in the epithelium while nano-perfusion and electrical stimulation do not leave any visible wounds. Contractions after single electrical or nanoperfusion stimulation are often completely reversible producing little permanent change to the tissue. Long-lasting contractions after laser activation “over-shoot” the response needed to remove or replace the tissue damaged by the laser (dotted lines in Figure 7D). In contrast, electrical stimulation does not appear to alter the mechanical properties of the micro-aspirated tissue (Figure 7A).

3.2.3.2 Embryonic tissue response to multiple stimuli

Subjecting embryonic tissues to multiple stimuli can provide us with insight into the downstream signaling pathways. Many signaling systems are down regulated after persistent stimuli. For instance, G protein-coupled receptors exhibit desensitization to repeat exposure to agonist (Ferguson and Caron 1998). Once desensitized, signaling responses will not be triggered unless sufficient rest period is allowed in between pulses.

When stimulated multiple times using all the three methods independently, we found that the tissues could be stimulated a number of times without any desentization. Thus another characteristic shared by these methods is the tissue's response to multiple stimuli. In the course of evaluating the response to differing current polarities, micro-aspirated tissues could be stimulated up to 4 times (Figure 8A) with no detectable differences in the magnitude or timing (Figure 8B) between the first and second stimulus at a given polarity ($P \geq 0.6$ for both comparisons; n=10; outward current; Wilcoxon signed ranks test). Here, four stimuli were given to each embryo, 7 min apart, with two stimuli at each polarity. The order of stimulus polarities was randomized for each embryo. Multiple contractions induced by repeated laser activation (Figure 8C through F) and nano-perfusion (Figure 8G) are qualitatively similar to repeated contractions following electrical stimulation. Even though the physical means of stimulation are different, the contraction responses of tissues subjected to electrical stimulation, laser activation, and nano-perfusion of cell lysate are remarkably similar in their timing and response to repeated stimulation.

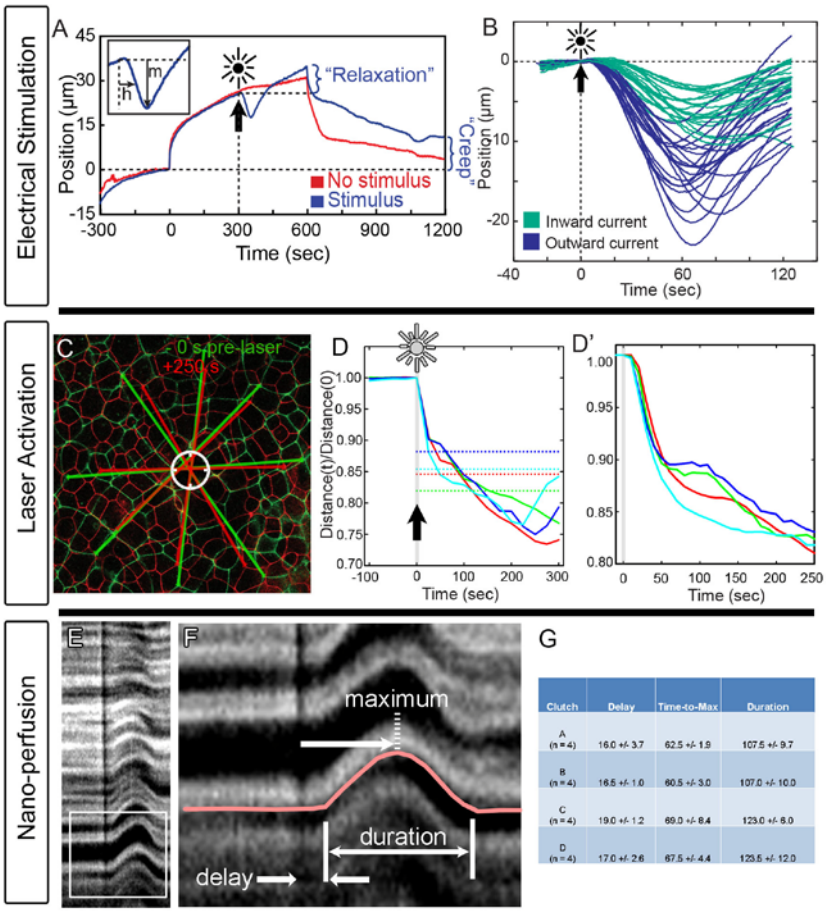

Figure 7. Kinematic responses to stimuli.

A) Response to electrical stimulus is tracked by the distance it retracts down the micro-aspirator channel ("m"), and the time to half maximal retraction ("h"). Pressure drop from−1.2 Pa to −6.6 Pa occurs at 0 s and pressure restored after 600 s. B) Electrical stimulus consistently induces contraction but the magnitude of contraction varies with the polarity of the applied stimulus. Each line records a separate stimulation. C) Tissue contraction response to laser activation (circle) can be seen in an overlay of cell boundaries before and after stimulation. D) The time-course of 4 representative experiments shows a 10 to 20 sec delay followed by rapid contraction over 50 sec (D). Dotted lines indicate the contraction needed to remove or replace tissue damaged by laser in each experiment. E and F). The contraction response to nano-perfusion as seen in kymographs (F: enlargement of box in E) reveals a 15 to 20 sec delay followed by rapid contraction over 40 to 50 sec (G). The black vertical line in E and F indicates perfusion of ink-labeled lysate.

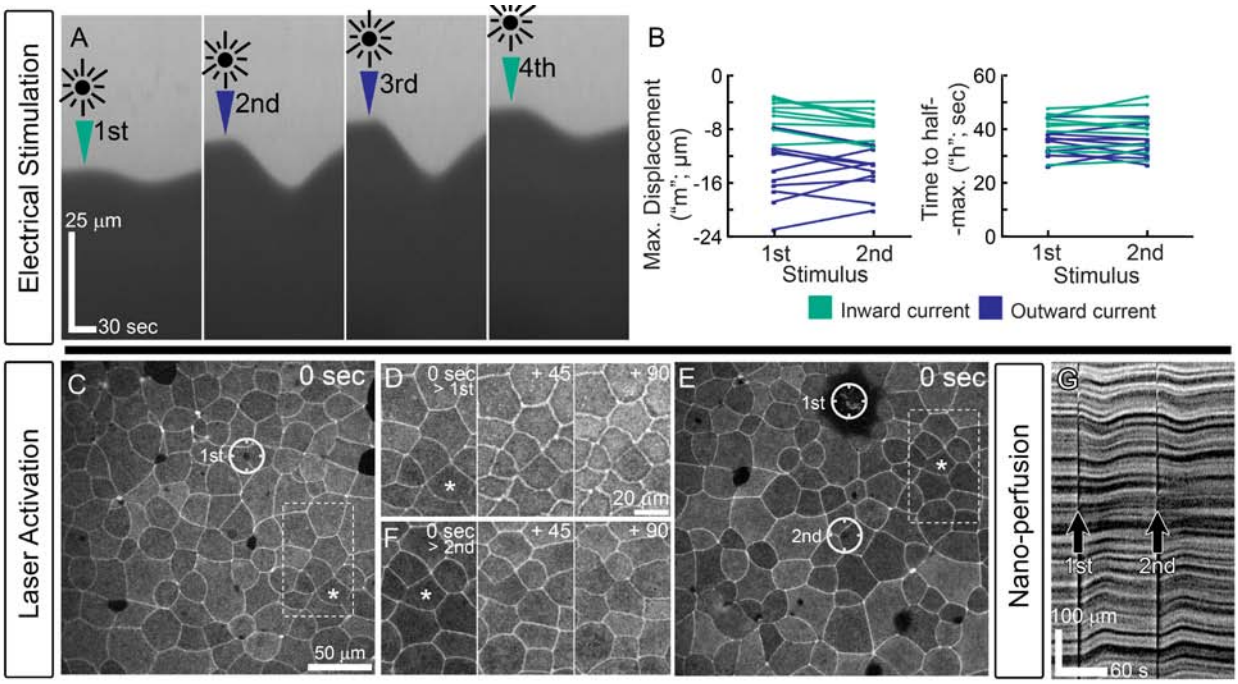

Figure 8. Embryonic epithelium is sensitive to repeated stimuli.

A) Four electrical stimuli applied to micro-aspirated embryos show no difference in the response between the first and second stimulus in a given current direction (B). C) Multiple laser stimulations in the same field (single circle in C and two circles in E) induce similar responses in cells 2 to 6 cell diameters away (D for single stimulus and F following second stimulus; asterisked cell is the same in panels C through F). G) Multiple perfusion stimulations also produce multiple contractions.

3.2.3.3 Site of activation and spread of contraction

All the three methods are very different in the geometry of the stimulation apparatus and the way responding tissue is held. Although technical constraints make it difficult to compare the spreading of contractions from the stimulated site among the methods of inducing contractions, there was some evidence that spreading differed between methods. There was no correlation between the amount of cell contraction and the distance from the site of laser activation within the field of view (Figure 9). In contrast, we did not observe contraction responses in regions far from the site of lysate application. Laser activation required the use of high magnification oil immersion lenses, whereas lysate application required space to expose tissue to the lysate, limiting imaging of most lysate experiments to relatively low magnification stereoscopy. Furthermore, although ink-labeling the lysate allowed visualization of the media containing the lysate, it does not provide information on lysate diffusion.

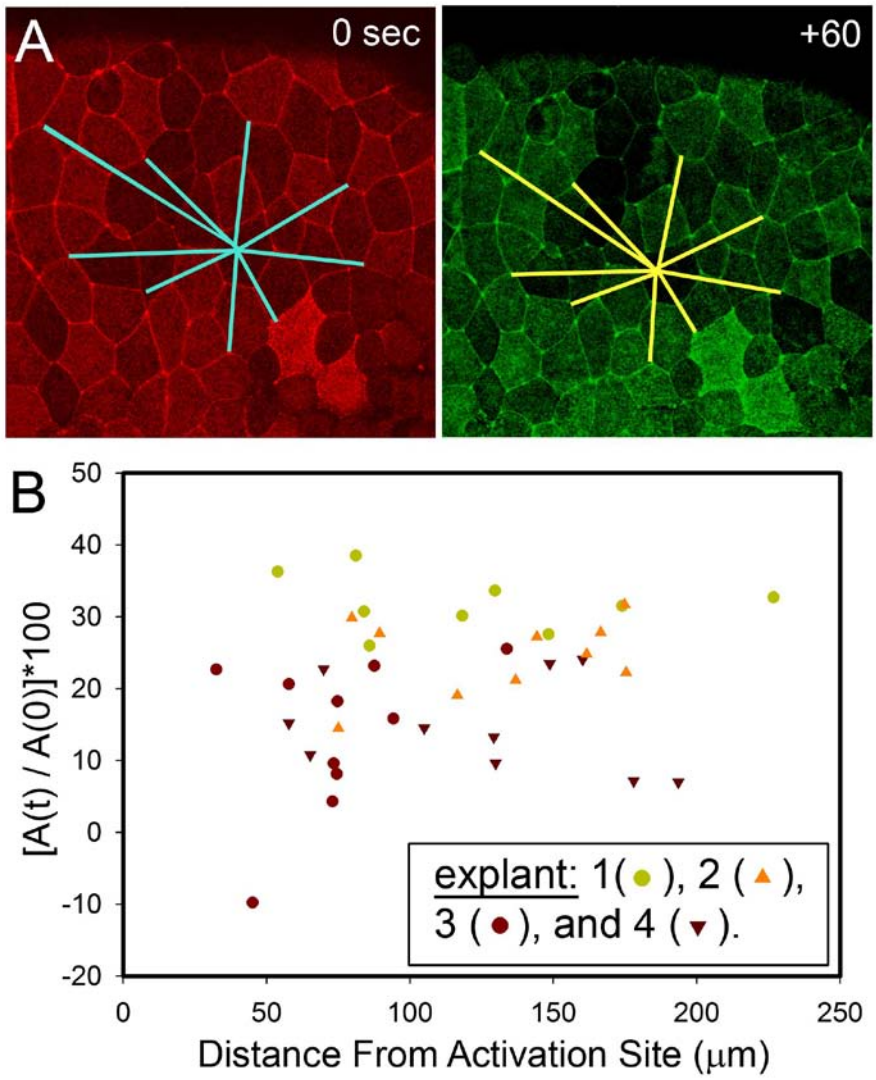

Figure 9. Laser activation induces cell contraction at large distances.

A) Activation of a single cell results in contraction of a large field of epithelial cells. Blue lines denote the distance of the individual cells from the activation site at 0 s post-activation. Yellow lines denote the distance of the same individual cells followed until maximal contraction at 60 s post-activation. B) Thirty-nine cells from 4 explants show cell area contraction, not correlated with the distance of a cell from the laser activation site.

The geometry is more complex during electrical stimulation. There, tissue is firmly held at the channel opening. It is likely that the electric pulse affects only tissue in the channel. Furthermore, since surrounding tissues are obscured by the PDMS block it is difficult to determine whether contractions spread beyond the stimulated area. However our data suggest that laser-induced contractions spread to at least to 10-cell diameter section of the tissue (in the field of view) from the activation site, where as lysate-induced contractions do not appear to spread beyond directly stimulated cells.

3.2.4 Effects on cell cytoskeleton

Because the F-actin cytoskeleton plays an important role in cell contraction, the establishment of tissue mechanical properties, and mechanical events of morphogenesis in general, we wanted to understand how the F-actin cytoskeleton was altered during the course of induced contraction. Cell and tissue contraction is thought to be driven by a number of different cellular mechanisms including: 1) whole cell contraction, 2) apical–basal contraction, 3) circum-apical or circum-basal contraction, and 4) apical cortex contraction. Each of these cellular mechanisms depend critically on F-actin cytoskeletal remodeling (for instance see (Lee and Harland 2007; Martin, Kaschube et al. 2008; Toyama, Peralta et al. 2008).

To visualize F-actin dynamics during stimulation, we expressed a fluorescently tagged fragment of the actin-binding protein moesin (moe-GFP; (Litman, Amieva et al. 2000)) Embryos injected with 0.5 to 1.0 ng of moe-GFP mRNA at the 1 cell-stage allowed observation of F-actin dynamics that were confirmed with a second actin-binding protein, utrophin-GFP (Burkel, von Dassow et al. 2007). Due to the geometric constraints of our three stimulation methods we

focused on the remodeling of F-actin in response to laser activation in the apical face of epithelial cells (Figure 10).

Laser activation of a single cell produced rapid F-actin accumulation throughout the field of view (Figure 10A). The baseline intensity of F-actin within epithelial cells in the animal cap can vary due to different levels of pigmentation in animal cap cells as well as different levels of gene expression based on early diffusion of the moe-GFP mRNA. F-actin intensity (raw values) within the apical cell cortex rapidly increases after a short 10 to 20 sec delay and peaks within 60 sec (Figure 10B). Normalized F-actin intensity profiles highlight variable responses by individual cells after the initial peak (Figure 10C; cell identities correspond to those in A and B). Some cells within the field return to pre-laser activation levels while most show a persistent 50% increase in intensity (20 cells in 4 explants; (Figure 10D). In some instances we observed actin "comets" consisting of moving spots of intense F-actin reminiscent of F-actin structures observed in cultured cells (Schafer, Welch et al. 1998; Orth, Krueger et al. 2002). Visualization of F-actin in XZ-slices confirmed that increases in F-actin intensity following laser activation were the result of F-actin accumulation, rather than displacement of the F-actin cortex from other locations in the cell (Figure 11).

We qualitatively confirmed similar patterns of F-actin dynamics during perfusion and electrical stimulation after adapting these protocols to use confocal imaging. Although visualization through the PDMS and the curved micro-channel was challenging, by reducing the size of our micro-aspirator to fit on the confocal (see methods), we could image the embryonic epithelium and remained able to make out the apical cortex and circum-apical bands of Factin **(Figure 10E)**. After electrical stimulation we were able to confirm increases in F-actin near the

membrane and features such as actin comets and persistent spots reminiscent of F-actin remodeling after laser activation (Figure 10F).

We could see such features in most embryos following electrical stimulation but there was considerable variability. To confirm that we were observing changes in F-actin rather than simply cell shape changes, we electrically stimulated embryos expressing a plasma membrane targeted GFP (Figure 10G, H). The membrane label shows cell shape changes but does not show the same localized spots of increased intensity seen in the case of moe-GFP expressing embryos.

We modified our nano-perfusion protocol to observe F-actin within animal cap explants (Figure 10I through L). Explants were used here because large-scale movements in whole embryos caused considerable lateral movements and prevented continuous visualization of F-actin in the same cells. Lysate-induced contractions appear to be similar to laser-activation in both explants and whole embryos. The challenge to tracking F-actin in perfused tissues lies not with the optics but rather with the delivery of a high concentration of lysate to the tissue. Even so, we were able to confirm F-actin comet formation and F-actin intensity increases at the basal cell cortex (cells adherent to fibronectin; Figure 10I, J) and recruitment of Factin to the lateral cell cortex (Figure 10K, L) after addition of lysate to the confocal chamber. Thus, the kinematics of cell shape change and tissue deformation, and the accumulation of F-actin appear similar after stimulation by laser activation, electrical stimulation, and nano-perfusion.

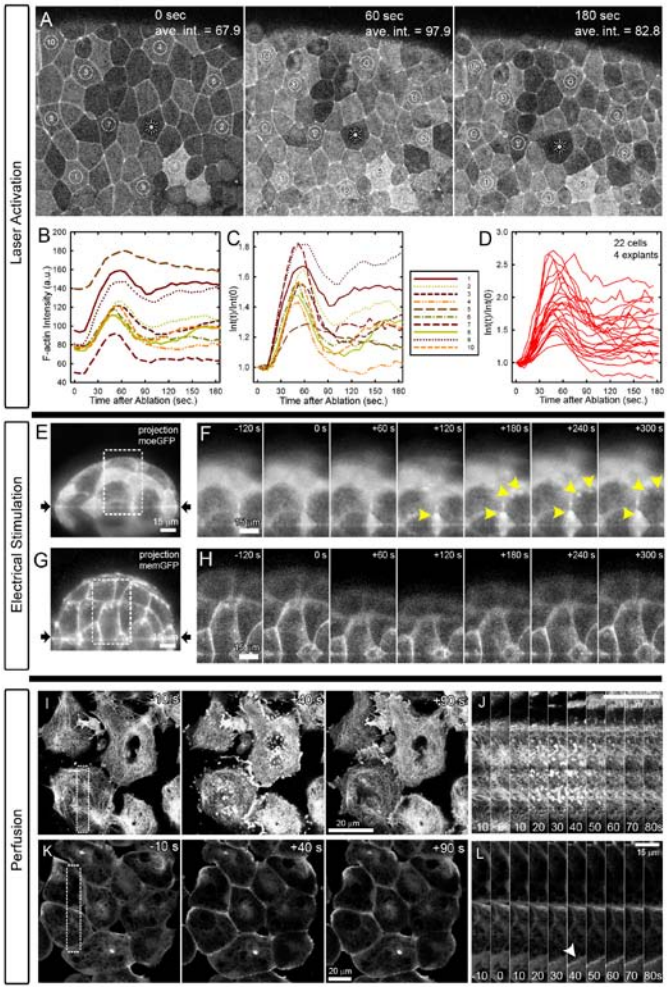

Figure 10. Stimulation induces F-actin remodeling.

A) Laser activation induces F-actin (actin-binding fragment of moesin-GFP) accumulation within surrounding epithelium. B) Intensity of F-actin shows consistent rapid increase followed by variable reduction that does not depend on the initial intensity of the contracting cell (C). D) 22 cells from 4 explants show consistent initial increase followed by variable degrees of reduction. E) Side view of micro-aspirated tissue expressing moesin-GFP shows increasing F-actin (F) within transient actin "comets" (yellow arrowheads). G) Plasma membrane labeled tissues do not show increases (H). I) Response to perfusion of animal cap explants shows rapid disassembly and transient formation of high intensity actin comets and foci within the basal cell cortex over 90 sec (J). K) A deeper confocal section, 5 µmfrom the basal surface shows F-actin within the lateral cell cortex (at cell–cell boundaries: arrowhead) and also intensifies and remodels in response to perfusion of cell lysate (L).

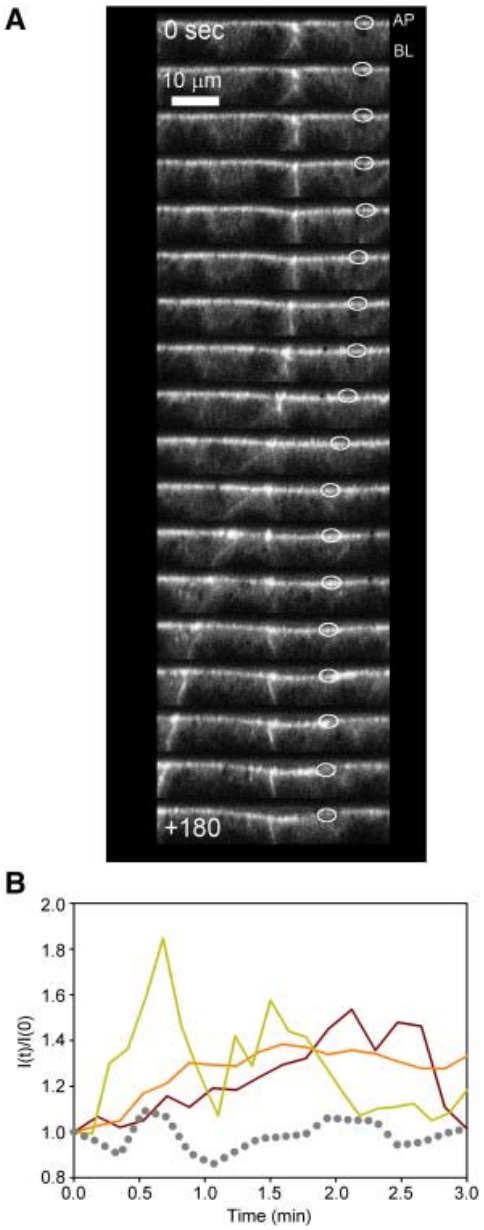

Figure 11. Laser activation induces F-actin increase at the apical cell cortex.

A) Visualization of F-actin in XZ-slices confirmed that F-actin increases in the apical cell cortex. Yellow ellipse shows representative area tracked for changes in intensity in B. (Note: We confirmed the tracked area is within the same cell.) B) Intensity of F-actin (3 solid lines showing 3 different cells in 3 separate explants) show consistent rapid increase that does not depend on the initial intensity of the contracting cell. Dotted line shows no significant changes in F-actin intensity in a non-laser-activated cell in an explant.

3.3 DISCUSSION

We have investigated electrical stimulation, laser activation, and nano-perfusion methods for inducing acute cell contraction within embryonic epithelial cell sheets. Each of these three stimuli produces similar contractions in the targeted epithelium including a 10 to 20 sec delay between stimulation and the start of contraction and rapid movements lasting about 60 sec. However, there are differences in the responses as well. For instance, laser activation appears to stimulate a long time-scale wound healing response causing “over-shoot” in the contraction, whereas electrical- and perfusion stimulated contractions appear to recover fully after a single stimulus. Additionally, laser activation stimulates cells 10 to 20 cells distant from the activation site, whereas nano-perfusion stimulates contraction only within cells that contact the lysate. These differences are relatively minor considering the diverse stimuli and geometries of the epithelial tissues driven to contract. Last, we demonstrate that all three methods drive rapid remodeling of the F-actin cytoskeleton. Recent work suggests that mechanical stimuli may induce contractions in Drosophila embryonic epithelia (Pouille, Ahmadi et al. 2009); however mechanical stimulation was not sufficient to induce contractions.

Each of the three methods to stimulate contraction has advantages in future studies. The micro-aspiration technique is the best suited for biophysical and biomechanical studies, providing mechanical properties such as viscoelasticity of embryonic tissues and high-resolution kinematics of tissue responses to electrical stimulation. Electrically and biochemically induced contractions have been observed previously in chick embryos ((Kucera and Burnand 1987) and (Drews and Mengis 1990), respectively); however the combination of electrically induced

contraction with micro-aspiration provides a novel tool for analyzing the mechanics of contractions.

Previous studies have found that primary invagination during sea urchin gastrulation (von Dassow and Davidson 2007), and Xenopus laevis blastopore closure (von Dassow and Davidson 2009) and dorsal elongation (Zhou, Kim et al. 2009) occur successfully despite considerable variation in tissue stiffness. Little data exist on tissue stiffness in other embryos, and data on forces driving morphogenesis (e.g. in Drosophila (Hutson, Tokutake et al. 2003)) are calculated in relative magnitudes, rather than absolute magnitudes, making direct comparisons between epithelial model systems impossible.

Laser-mediated photo-chemical, photo-thermal, and photomechanical methods have been used to perturb or ablate live tissues (Venugopalan, Guerra et al. 2002; Rau, Quinto-Su et al. 2006). In cell and development biology, lasers have been used to ablate specific targets to investigate questions such as the role of the nucleus in dorso-ventral patterning of the egg (Montell, Keshishian et al. 1991), the role of cell rearrangement in sea urchin gastrulation (Hardin 1988), and the role of actomyosin contractile ring in single-cell wounds in X. laevis oocytes (Mandato and Bement 2001; Benink and Bement 2005). Because of its advantages for visualization, laser activation is best suited for investigating the cell and molecular pathways that mediate cell contraction and biophysical events that couple actomyosin contraction to cell shape change. In some respects, our studies on a complex multicellular epithelial sheet appear analogous to the wounding studies in the single-cell Xenopus oocytes (Mandato and Bement 2003). With laser-stimulated contraction, we observe that neighboring cells contract and F-actin remodeling begins within a few seconds.

We found that laser activation induces epithelial contractility and global up-regulation of F-actin at large distances from the laser-activated site (at least 250 μm). Previous wounding studies have demonstrated increased F-actin and recruitment of myosin to the wound margin in single cells (Benink and Bement 2005), or within immediately adjacent cells after laser wounding in epithelial sheets (Clark, Miller et al. 2009). However, neither of these studies have reported contractile responses within wounded cells or in their neighboring cells. One possibility for these observations could be the freedom of embryonic tissues to deform. Cells cultured on glass or plastic or bound to rigid ECM scaffolds may not visibly deform when stimulated. Based on previous Xenopus laevis studies of wounding responses (Clark, Miller et al. 2009) and Ca^{++} contractions (Wallingford, Ewald et al. 2001), we suggest that laser activation may induce a calcium influx in the surrounding tissue that activates actin polymerization and myosin contractility through Rho and/or Cdc42 dependent pathways. Given the similar kinematics and F-actin dynamics exhibited by contractions induced by the three methods described here, we suggest that at least some of the downstream signaling pathways are shared among all three types of induced contraction.

Neither laser activation nor electrical stimulation is a likely event within the embryo during normal development but perfusion induced stimulation may reflect a morphogenetic or physiological role. Cell contraction in response to chemical stimuli is likely due to a pre-existing receptor that can “trigger” contraction within epithelial cells in the embryo. While both laser activation and lysate may trigger wound response pathways, the factor(s) within lysate may play a signaling role during morphogenesis.

Both spontaneous and periodic contractions have been observed in Xenopus gastrula (Wallingford, Ewald et al. 2001; von Dassow and Davidson 2009) as well as gastrulating chick

embryos (Stern and Goodwin 1977). These rare spontaneous contractions exhibit similar kinematics to the contractions we induce in this report. Such contractions may be more common than reported since they form and dissipate faster than the 2 to 5 min timelapse intervals typically used to study morphogenetic movements. Periodic contractions in epithelial cells accompany epithelial morphogenetic movements in Drosophila and suggest that embryonic tissues are a form of “excitable media” (Martin, Kaschube et al. 2008; Pouille, Ahmadi et al. 2009). We speculate that pathways controlling acute contraction could trigger excitable tissues or coordinate cell contraction during large scale movements such as neurulation. Testing candidate pathways revealed in Drosophila genetic studies and the identification of the factor(s) within cell lysate will be key prerequisites to future progress.

4.0 MOLECULAR AND DEVELOPMENTAL ASPECTS OF CONTRACTION

Contents of this chapter will be published in the following journal publication:

Joshi S.D., Davidson L.A., Extracellular nucleotides lead to severe birth defects in Xenopus laevis embryos by modulating cell contractility driven by actin/ myosin cytoskeleton (in preparation).

Cell contractility is a major tissue-shaping mechanism that drives process such as epithelial bending leading to the formation of pits and furrows in tissues. Previous studies of cell contraction make detailed observations of developmentally programmed cell shape changes such as those that accompany ventral furrow formation in Drosophila and bottle cell formation in Xenopus. We have utilized cell lysate stimulation approach to reproducibly induce acute and chronic contractions in Xenopus embryos. Acutely induced contractions from a single pulse of lysate stimulus demonstrated the importance of actomyosin cytoskeleton that drives contraction. Chronically induced contractions from long term culture of embryos in lysate revealed the importance of coordination between individual tissue parts for successful morphogenesis and Xenopus embryos exogastrulate when there is a lack of coordination. Further, we identify ATP as a primary nucleotide that is capable of inducing contractions identical to lysate. Our findings are the first to demonstrate a link between extracellular nucleotides and epithelial morphogenesis and provide a means to control cellular contractility.

4.1 EXPERIMENTAL PROTOCOLS

4.1.1 Embryo culture, microsurgery, and histology.

Eggs were obtained from female Xenopus laevis frogs, fertilized, dejellied in 2% Cysteine solution (pH 8.4), and cultured in 1/3x Modified Barth's solution (MBS) following standard methods (Kay and Peng 1991). Embryos were staged appropriately (Nieuwkoop and Faber 1967) and vitelline membranes were removed using forceps. Explants were microsurgically isolated and cultured in Danilchik's For Amy solution (DFA; (Sater, Steinhardt et al. 1993)). Marginal zone explants were cut using custom-made hair loops and hair knives at stage 10.5, and cultured on fibronectin-coated glass substrates. Unless otherwise stated, experiments were conducted at early- to mid-gastrulation (stages 10 to 11). Embryos were processed to for gene expression using standard RNA in situ hybridization protocols (Harland 1991). Embryos were processed for protein expression and localization of somitic mesoderm using standard whole mount immunohistochemistry (Kintner and Brockes 1984).

4.1.2 Nano-perfusion

The nano-perfusion method has been described previously (Joshi, von Dassow et al. 2010) and was utilized to deliver 60 nl volumes in a single pulse or repeatedly over several pulses in a series. Perfusion experiments were recorded by a CCD camera (Scion Corp., Frederick, MD) mounted on a dissecting stereoscope. Image acquisition and subsequent analysis of time-lapses sequences were carried out using custom-written macros and plug-ins for image analysis software (ImageJ ver. 1.43, Wayne Rasband, NIH). Lysate and dilute perfusion compounds

were freshly prepared on the day of the experiment. Cell lysate was prepared by tritrating two early gastrula embryos in 100 µl 1/3x MBS. Lysate was mixed and centrifuged at 13,000 rpm for 2 minutes to remove insoluble material. Salts, bioactive compounds, and nucleotides/ nucleosides were diluted in 1/3x MBS (See Table 4 for the list of tested compounds). All the compounds were stored and utilized according to the product guidelines (Sigma-Aldrich, St. Louis MO). To visualize cell lysate and other perfused solutions, 3 µl black non-waterproof ink (Higgins Fountain Pen India Ink; Utrecht Art, Cranbury NJ) was added to 100 µl perfusates.

4.1.3 Statistical analysis

Tests for statistical significance of treatments on blastopore closure and embryonic contractions were determined using 2-WAY ANOVA using commercial statistical software (SPSS v. 15, Chicago, IL).

4.2 RESULTS

4.2.1 Acute and chronic approaches towards inducing contractility

Exogastrula is an abnormal embryo that has the presumptive endoderm increased in quantity and is incapable of invagination leaving the endodermal tissue completely outside the embryo in severe phenotypes. Earlier studies (Chapter 3) revealed that lysate from ruptured embryos (material from cell extracts) could induce acute transient contractions and we suspected if these contractions in the animal cap epithelium were responsible for embryo exogastrulation. To test

this idea, we devised two complementary approaches, “acute” method to induce transient contractions resulting from a single pulse nano-perfusion and “chronic” method of culturing embryos in cell lysate over the long-term. Nano-perfusion of cell lysate (acute method, Figure 12A, B, B’) and long term culture (chronic method) of embryos in cell lysate (Figure 12C, D) are demonstrated. Utilizing the acute method we observe single contraction kinematics while chronic treatment is essential to understand developmental consequences of a constant over-contraction.

As previously demonstrated (Joshi, von Dassow et al. 2010), perfusion of cell lysate over the embryonic surface causes a local contraction beginning 10 to 20 s and continuing for the subsequent 30 to 90 s after stimulation. The stimulated contractions thus have quantifiable kinematic characteristics in the form of the time delay between the stimulus and the beginning of contraction (δT), the time required for the contraction to reach its peak value (T-max) and the total duration of the contraction (T) (Figure 12B, B’). The strength of contraction demonstrates the ability of the embryo to contract in response to the stimulus and can be measured by comparing the distance between two points before the application of stimulus and the distance between the same two points at maximal contraction. Acutely induced contractions are transient and result in no visible long term phenotypic defects. Chronic lysate exposure induced embryos to exogastrulate. The first indication of the lysate effect was that the blastopore closure was completed blocked, evident from significantly large blastopore areas (Figure 12D). Later by stage 12, endoderm protruded from the open blastopore at a time when the blastopore had closed in control embryos. Embryos cultured in lysate until stage 27 developed with a large extending endoderm that remained outside the embryo (corresponding to the protruding endoderm at stage 12) and crumpled epithelial tissue at the anterior end. Thus chronic exposure to lysate results in a severe exogastrula phenotype.

In order to identify a sensitive phase of development and to test whether there were developmental stages more sensitive to lysate exposure, we cultured embryos in lysate for shorter time periods to understand whether lysate-induced contractions could be rescued when replaced with fresh 1/3x MBS (Figure 13). Embryos exposed to lysate for 2 hours after the start of gastrulation develop with minor blastopore closure defects (Figure 13A, B). The embryos cultured in lysate for 8 hours (until stage 15) developed with major defects while embryos in lysate for 27 hours (until stage 27) developed with severe defects (Figure 13C, D). Together, our findings indicate that chronic exposure can cause embryo to exogastrulate and that early stages of development, prior to completion of gastrulation, are especially sensitive to induced contractions.

We hypothesized whether embryos cultured for long periods in lysate continued to contract as acutely exposed embryos and whether prolonged exposure to lysate resulted in a desensitization of the contraction response (Figure 14). To test this we modified our perfusion protocol to induce a series of contractions with different periods of rest between stimuli. When perfused 10 times every 600 sec, the embryonic epithelium recovers after one stimulus is withdrawn and contracts again after every subsequent stimulus is applied (Figure 14A). There is no visible change in the contraction strength for subsequent contractions. Such a long recovery period could provide enough rest time between stimuli, so we reduced the rest period to 60 sec and observed that embryonic epithelium relaxes soon after stimulation and is able to contract again when a new stimulus is applied (Figure 15B). Here, the embryo was perfused 10 times and there was no visible change in the contraction strength. When the rest period was reduced to 30 sec, the epithelium remained contracted during the series of perfusion pulses but recovered soon after the series of stimuli ended (i.e. at the end of the set) or when provided with 60 sec to

recover (arrow, Figure 15C). These results indicate that the epithelial response to lysate does not saturate even when the interval between stimulus is shorter than the response and that lysate is able to produce long term chronic contractions within embryonic epithelia; However, the contraction response in chronically perfused animal caps is not permanent but shows the ability to relax even after 10 repeated stimuli.

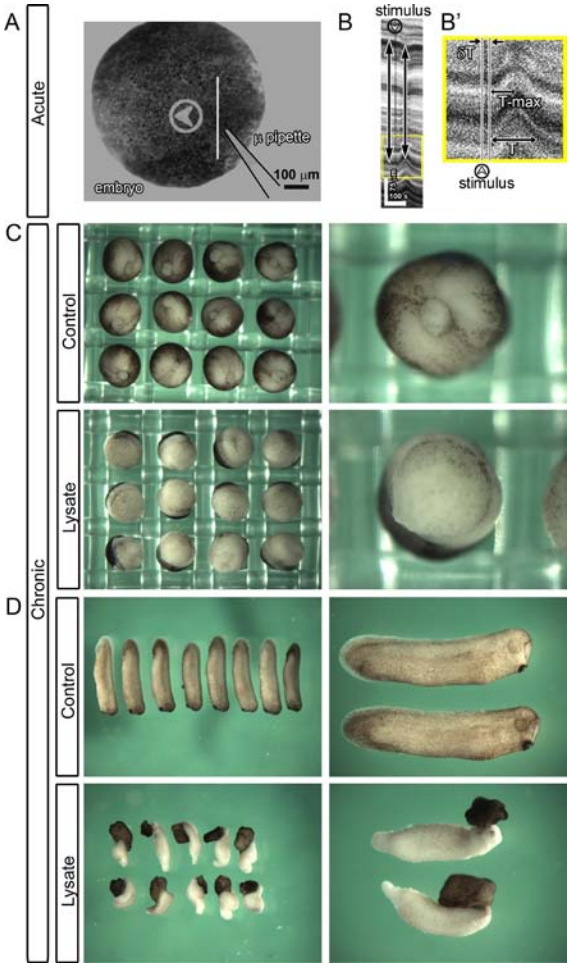

Figure 12. Lysate produces contraction and induces exogastrulation.

A) A representative example of nano-perfusion shows delivery of 60 nl of cell lysate over the surface of an embryo. Arrow head shows the direction of the cell lysate flow from the micropipette. B) Time-lapse frames of the surface of the embryo (in A) reveal the strength of the contraction in a kymograph collected along a line (A). Arrow head indicates stimulus; Vertical arrows indicate embryonic contraction measurement pre-stimulus and at maximal contraction. B') Enlarged view of the contraction (from yellow rectangle in B) showing time of stimulus (arrow head), delay between stimulus and beginning of contraction (δT), time to peak (T-max) and total duration of contraction (T). C) Chronic exposure to lysate induces larger blastopore area and protruding endoderm that lead to severe defects at later stages (D, stage 27). Stage 27 embryos exposed continuously to lysate have crumpled epithelium near the anterior end and extending endoderm.

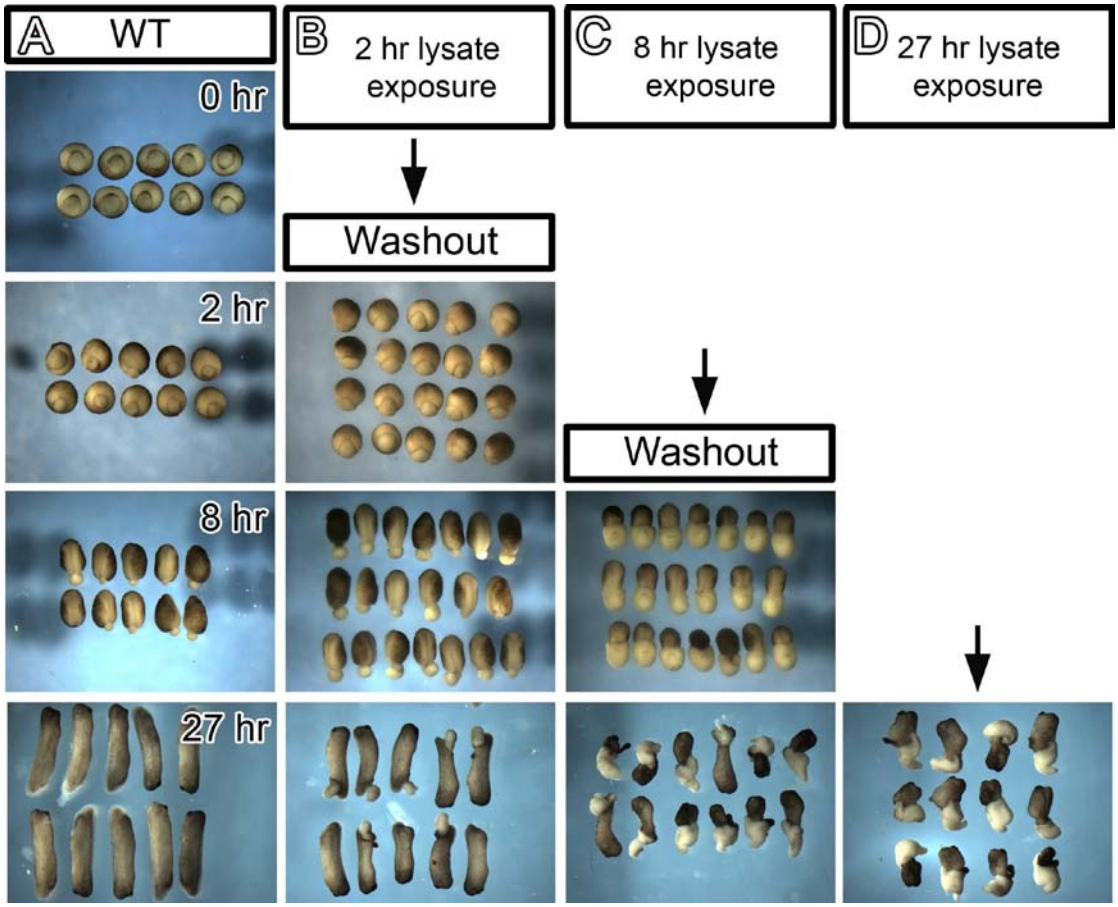

Figure 13. Gastrula Stage embryos are most sensitive to lysate.

A) Controls develop normally from 0 to 27 hours from stage 10.5. B) Embryos treated with lysate for 2 hours from stage 10.5 develop with minor defects. C) Embryos treated for 8 hours develop with major defects. D) Embryos treated for 27 hours develop severe defects. Lysate in media after 2 and 8 hour treatment were washed twice with fresh 1/3x MBS.

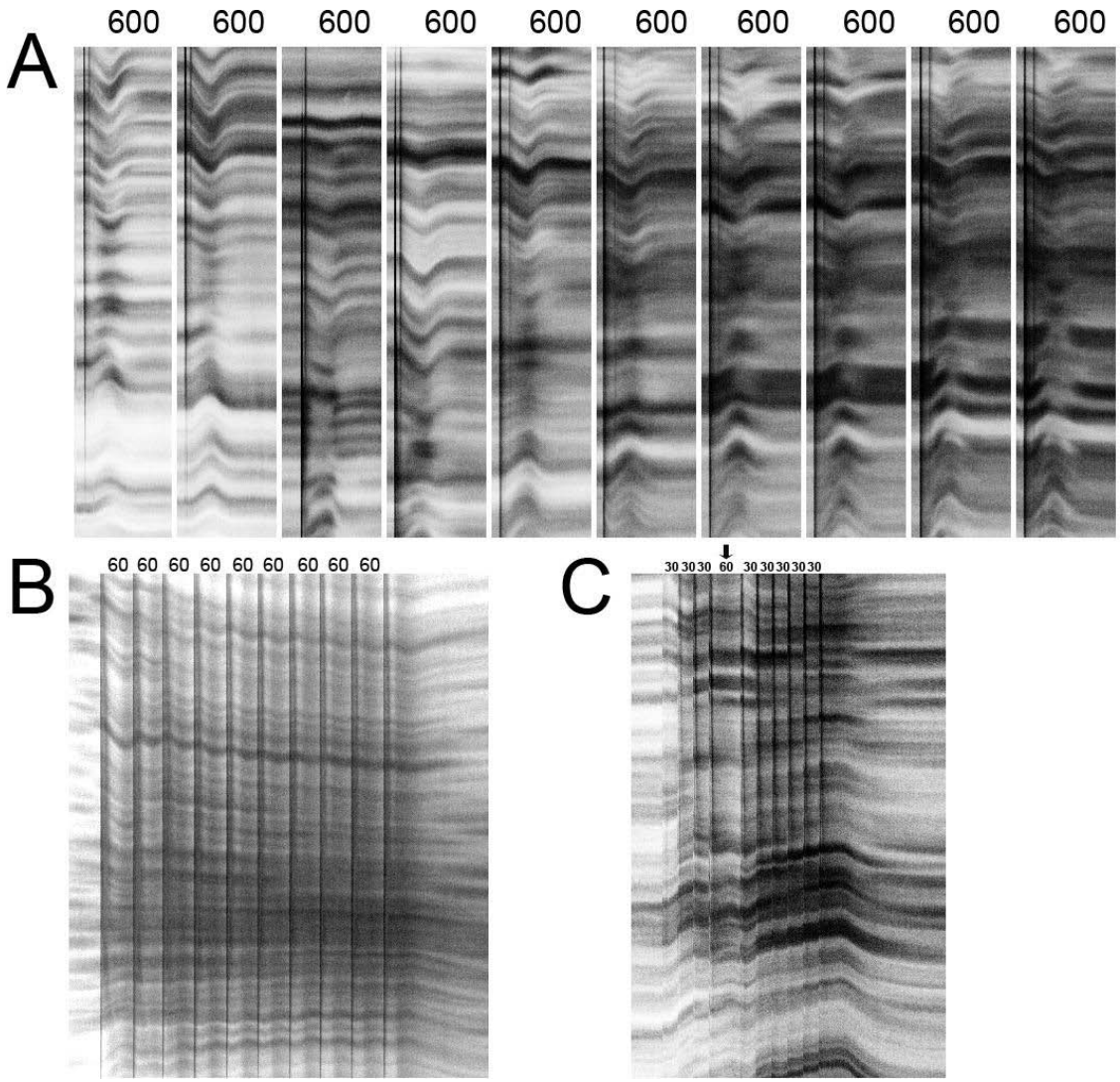

Figure 14. Effects of lysate do not saturate and can produce long term chronic contractions.

A through C) Time-lapse sequences of the surface of the embryo resolve the contractile response in kymographs (similar to Fig. 1B) A) A representative set of kymographs demonstrates the ability of a single embryo to contract when perfused with 60 nl lysate every 600 sec. Embryo recovers soon after the stimulus is withdrawn and contracts again at every instance a stimulus is applied. B) A representative set of kymographs demonstrates the ability of a single embryo to contract when perfused with 60 nl lysate every 60 sec. Embryo recovers soon after the stimulus is withdrawn and contracts again at every instance a stimulus is applied. C) A representative set of kymographs demonstrates the ability of a single embryo to remain contracted when perfused with 60 nl lysate every 30 sec. Embryo recovers soon after the stimulus (at the end of the set) is withdrawn or also when 60 seconds are allowed in between the stimuli.

4.2.2 Embryos have spatiotemporal specificity to lysate-induced contractions

Next we wondered whether the embryonic contractile response was global or whether they were spatially or temporally patterned. To map the spatial specificity, we perfused cell lysate on different locations of a developing embryo (Table 3). Stage 10 and 11 embryos were utilized in all experiments except where response to lysate was tested at the neural plate stages (stage 17). We observed that the animal cap ectoderm, the marginal zone areas and all tissues near or within the neural plate contract in response to lysate. The vegetal endoderm is the only location that did not respond (no visible contractions observed) even when nearby marginal zone cells contract demonstrating that not all tissues are susceptible to induced contractions.

Table 3. Identifying developmental stage and spatial sensitivity to induced contractions.

		Trials[1]	# of embryos[2]	%
Embryonic locations	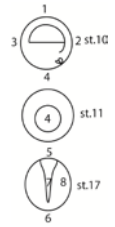	Animal cap ectoderm [1]	58	100
		Vegetal Side (marginal zone above the blastopore lip) [2]	11	100
		Vegetal Side (lateral marginal zone) [3]	11	100
		Vegetal Side (Vegetal Endoderm) [4]	11	0
		Neural Plate (Anterior) [5]	3	100
		Neural Plate (Posterior) [6]	3	100
		Neural Plate (Centre) [7]	3	100
		Neural Plate (Epidermis) [8]	3	100
Developmental Stages[3]		early st. 9 (early blastula stage)	6	0
		late st. 9 (late blastula stage)	6	50
		st. 10.5, 11, 11.5, 12, 12.5 (gastrula stages)	6, 27, 17, 4, 5	100, 100, 100, 100, 100
		17, 18 (neural groove stages)	3, 6	100, 100

[1] Numbers in the square brackets correspond to the numbers displayed on the images showing different embryonic locations. [2] The total number of embryonic for every experimental condition. [3]Embryos were tested for contraction on the animal cap except for the neural groove stage where contraction was tested on the ventral or lateral epidermis.

We next wanted to investigate the developmental onset of this contractile response. We perfused lysate on animal cap from early blastula (early stage 9) to early neurula stages (stage 17, 18). We found animal cap epithelia or epidermis at all late stages responded to lysate (Table 3), but blastula did not. Together, our findings indicate that lysate can induce contractions everywhere except the vegetal endoderm and that embryonic epithelia are susceptible to contractions from late blastula stages onward.

4.2.3 Nucleotides/ nucleosides induce cell contraction

There are several proteins and small molecules in cell lysate that could trigger contraction. Because embryonic lysate contains many factors, we employed several strategies to narrow and then identify candidate molecules. To test whether the factor was a complex polypeptide, such as a growth factor, we first heat-treated (65 deg C, 30 min) the lysate and found contraction activity remained strong, suggesting the active factors were not proteinaceous.

We next began a series of trials with candidate factors known to induce physiological contractions **(Table 4)**. For these tests, we used animal cap tissues since these produced a strong consistent response to lysate in 100% of the cases. Neither 1/3x MBS (solution for all compounds) nor ink (marker for all perfusion experiments) induced any contractions. None of the tested salt compounds (KCl, NaCl, $CaCl_2$ and $MgCl_2$) resulted in any observable contractions. Two other bioactive compounds, sodium glutamate, a well known stimulator of neurons and acetylcholene, known to induce contractions in both smooth and skeletal muscle, did not induce contractions. We next wondered whether phosphorylated factors in the lysate might be responsible and to test this we treated lysate with shrimp alkaline phosphatase (SAP, 30 min 35 deg C [activation], 30 min 65 deg C [deactivation]) and found SAP-treated lysate did not

induce contractions. This suggested that some nucleotides/ nucleosides (NO) could be possible sources of contractions.

Extracellular ATP has been studied extensively for its role as a signaling molecule in epithelial cells (Schwiebert and Zsembery 2003; Zsembery, Boyce et al. 2003; Zsembery, Fortenberry et al. 2004) and we wondered if ATP could have a role in inducing contraction in frog epithelia. We tested ATP and found it to be able to induce contractions as strong as observed with lysate. To test whether ATP rather than ADP or other hydrolyzed products of ATP was the inducing factor, we tested the non-hydrolysable form of ATP (ATPγS) and observed contractions of approximately half the magnitude (contraction strength was compared visually to the induced contraction from lysate or 400 μM ATP). We treated ATP with SAP and observed no contractions. Furthermore, contractions were observed when ATPγS was treated with SAP. Thus ATP is completely able to mimic the acute effects of lysate, however, it is but one of several nucleotides that may contribute to the contraction response.

Lysate contains a rich mix of other triphosphate nucleotides including UTP, CTP, and GTP, as well as other di- and mono- phosphate forms, e.g. ADP, AMP, and cAMP as well as dephosphorylated nucleosides such as adenosine. Of the nucleotides and nucleosides we tested, we found only UTP elicited a strong response while others including UDP, ADP, and adenosine produced contractions that were smaller than lysate, ATP, or UTP **(Table 4)**. For the remainder of this paper, we used either 400 μM ATP or embryo lysate as our experimental due to its ability to induce strong consistent contractions.

Table 4. Identifying ligands that induce apical contraction.

	Candidate Factors	# of embryos[1]	% | Strength[2]	
Controls	Lysate (2 embryos lysed per 100 µl 1/3x MBS)	49	100	
	1/3x MBS	6	0	
	20% Ink (Higgins Fountain Pen India Ink) 1/3x MBS	6	0	
Salts	Potassium Chloride (KCl, 1M)	6	0	
	Sodium Chloride (NaCl, 1M)	6	0	
	Calcium Chloride ($CaCl_2$, 1M)	6	0	
	Magnesium Chloride ($MgCl_2$, 1M)	5	0	
Bioactive Compounds	Sodium glutamate ($C_5H_8NNaO_4$, 1M)	3	0	
	Acetylcholene (3.1 mM)	4	0	
Treatments	Lysate - heat treated (65 deg C, 30 minutes)	9	100	
	Lysate - shrimp alkaline phosphatase treated (SAP, 1U/ 10 µl)	5	0	
Nucleosides / Nucleotides	Adenosine triphosphate (ATP; 400 µM, 40 µM, 0.4 µM)	6, 6, 18	100, 100, 72	+,+, <
	ATPγS (2mM, 1mM, 100 uM)	14, 7, 13	100, 100, 15	<, <, <
	ATP (40 µm) + SAP	6	0	-
	ATPγS (1mM) + SAP	10	100	<
	Adenosine diphosphate (ADP; 40 µM)	4	100	<
	Adenosine (ADO; 400 µM, 40 µM)	8, 5	75, 0	<, -
	Cyclic adenosine monophosphate (cAMP; 40 µM)	5	0	-
	Uridine triophosphate *(UTP; 40 µM)*	6	100	+
	Uridine diphosphate *(UDP;* 40 µM, 0.4 µM)	6, 5	100, 0	<, -

[1]The total number of embryos that the compound was tested for. [2]Strength of contraction is qualitatively measured for nucleoside/nucleotide perfusions of embryos with an observable contraction. Strength is categorized with respect to 400uM ATP or Lysate: (+) contraction is equal or stronger, (<) contraction is weaker, (-) contraction not observed.

4.2.4 Chronic ATP treatment leads to severe developmental defects

Having identified ATP as a prime candidate capable of inducing contractions, we tested whether ATP could produce developmental defects similar to the ones observed after chronic exposure to lysate (Figure 12). 40 μM ATP and 400 μM ATP induced severe gastrulation defects similar to lysate (Figure 15 A, C, E, G, I). ATP-treated embryos also had blastopore closure defects. 40 μM ATP treated embryos produced moderate defects by stage 27 (Figure 15 F). Both, 400 μM ATP and lysate induced severe developmental defects, often producing exogastrula (Figure15 D, H). We conclude from these observations that ATP is capable of inducing contractility during early developmental stages as well as generating defects similar to those induced by chronic exposure to lysate.

4.2.5 Patterning and gastrulation are unaffected by chronic contractions

Because ATP and lysate both produced acute contractility, we hypothesize that developmental defects were due to differential contractility of animal cap epithelial cells. However, prolonged treatment with potent factors such as ATP could alter other processes known to block blastopore closure and induce exogastrulation including: 1) defects in gene expression patterns, 2) defects in convergent extension, and 3) defects in mesendoderm extension. To test these alternate causes of exogastrulation, we carried out RNA in situ hybridization to investigate exposure patterns of dorsal mesoderm markers, Chordin and Brachyury (Xbra), investigated the convergence-extension capacity of sandwich explants (Keller sandwich explants), and observed mesendoderm migration. To test whether patterning was altered, we carried out gene expression and immunohistochemistry studies with Chordin, Brachyury and 12/ 101 (Figure 16). We observed

that embryos cultured in lysate or ATP had visible Chordin expression (Figure 16A). In many cases, medial movement of Chordin expressing notochord cells was blocked in Lysate- or ATP-treated embryos and cells were often spread along the circumference of the blastopore or formed a knot-like structure at the blastopore lip. In contrast, in control embryos, Chordin was observed in a well defined column of notochord tissue. Consistent with these observations, Brachyury expression by pre-involution mesoderm cells is unaffected in Lysate- or ATP-treated embryos (Figure 16B). Because notochord formation was affected in early stages, we wanted to investigate whether somitogenesis was also altered during later development. In stage 27 control embryos, post-segmentation somites stained with the antibody 12/101 form well defined rows on either side of the dorsal axis (Domingo and Keller 1995) while the Lysate- and ATP-treated samples show clustered or curved somites and defective segmentation patterns (Figure 16C). These consistent observations helped us conclude that gene expression was unaffected in the Lysate- or ATP-treated embryos and suggested the phenotypes we observed were due to defects in morphogenesis.

We hypothesized that if cell behaviors are altered in whole embryo experiments, then the gene expression should be identical in explants that have been cultured on fibronectin substrates. We isolated marginal zone (MZ) explants from stage 10 embryos and cultured them on fibronectin (Figure 16D). The Chordin expression in MZ explants cultured in lysate is unchanged in comparison to control MZ explants. These observations help us conclude that contractions induced from lysate or ATP affect the embryonic cell behaviors without altering gene expression in dorsal mesoderm.

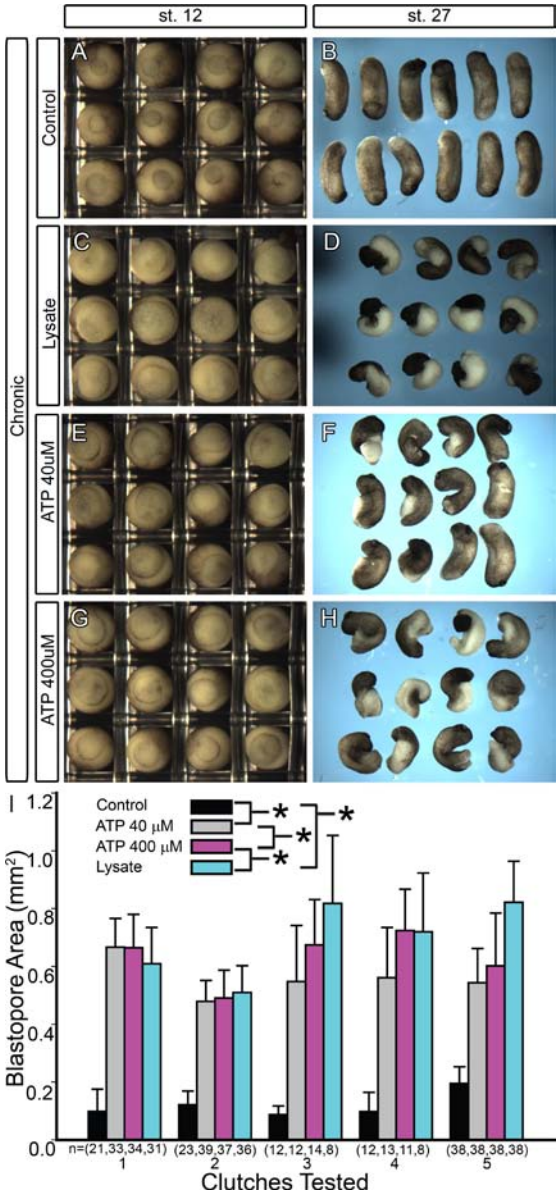

Figure 15. Defects induced by ATP are dose dependent.

A, B) Control embryos develop normally with a small blastopore at stage 12 and form tadpoles by stage 27. C, D) Exposure to lysate from the start of gastrulation blocks blastopore closure and induces severe exogastrula. E, F, G, and H) 40μm ATP (E, F) and 400 μm ATP (G, H) induce dose dependent defects. Defects induced by 400 μm ATP are indistinguishable from lysate. I) Blastopore areas were measured for five independent clutches. Lysate, ATP 40 μm and ATP 400 μm lead to significantly larger blastopore areas than control embryos ($p < 0.01$, 2-WAY ANOVA). The number of embryos in each set is indicated below the bar.

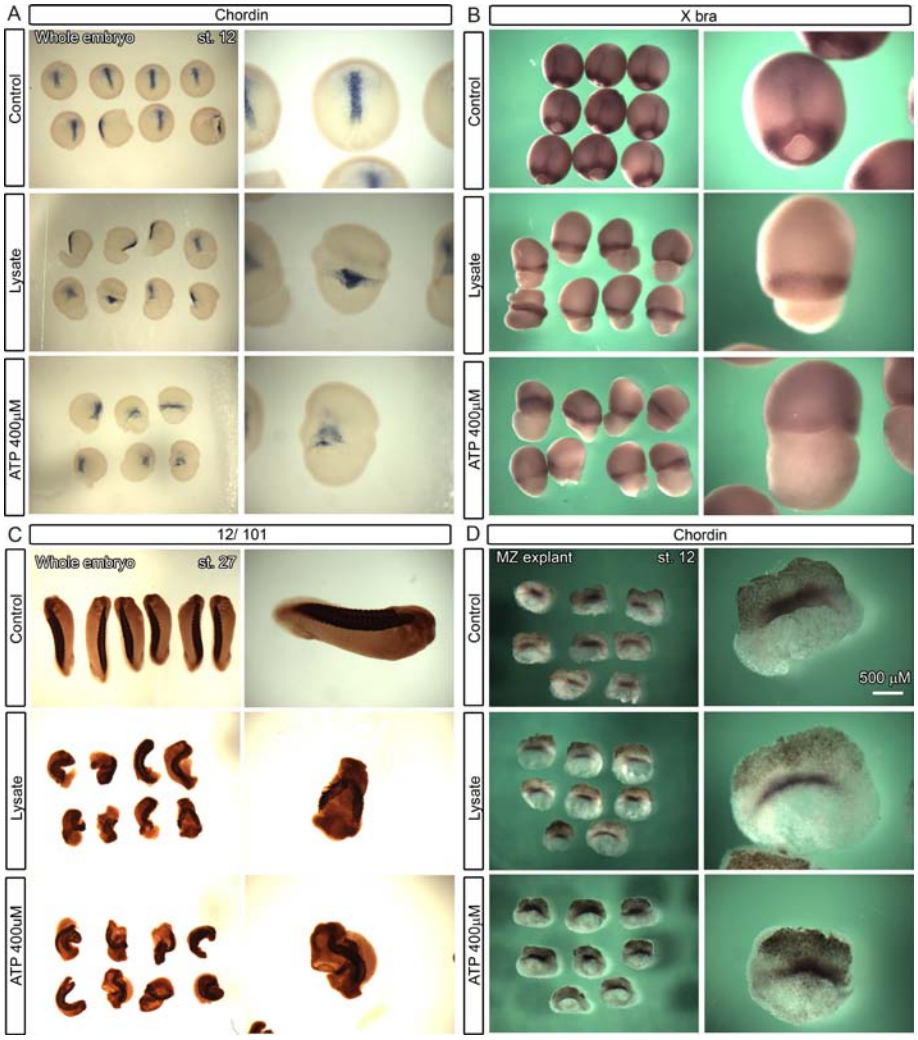

Figure 16. Gene expression patterning is unaffected by lysate or ATP.

A) Medial movement of Chordin expressing notochord cells is blocked in many Lysate- or ATP-treated embryos. In control embryos Chordin is observed in well defined columnar notochord tissue; in embryos treated with either lysate or ATP Chordin expressing cells are often spread along the circumference of the blastopore or form a knot at the mid region. B) Expression of Xbra by pre-involution mesoderm cells is unaffected in Lysate- or ATP-treated embryos. C) Post-segmentation somites stained with the antibody 12/101 form in rows on either side of the dorsal axis while the Lysate- and ATP-treated samples show clustered somites and defective segmentation. D) Marginal zone (MZ) explants cultured from stage 10 on fibronectin-coated glass prevent large-scale convergence of notochord. The pattern of Chordin expression in MZ explants cultured in lysate is unchanged compared to control MZ explants.

Because cell behaviors were altered by lysate, we wanted to investigate whether defects in mesoderm or mesendoderm morphogenesis contributed to the lysate-induced phenotype (Figure 17). Mesoderm convergence-extension and mesendoderm migration are key contributors to overall gastrulation movements and we suspected that either of these two movements could be altered by lysate. We tested the capacity of mesoderm to converge and extend with sandwich explants (Keller, Shih et al. 1992). Sandwich explants develop normally, converge and extend in cell lysate, demonstrating convergence and extension are unaffected (Figure 17B, B', D, D'). Accompanying whole embryos (housed in the same culture dish, cultured in lysate) demonstrated severe defects as previously shown (Figure 12C, D). Mesendoderm morphogenesis was investigated by observing mesendoderm cell migration on fibronectin in MZ explants. MZ explants cultured on fibronectin substrate revealed mesendoderm migration was unchanged in lysate, and strongly suggests exogastrulation is due primarily to differential contractility of the animal cap epithelium and marginal zone (Figure 17E). These results rule out the possibility that lysate alters convergence and extension or mesendodermal cell migration.

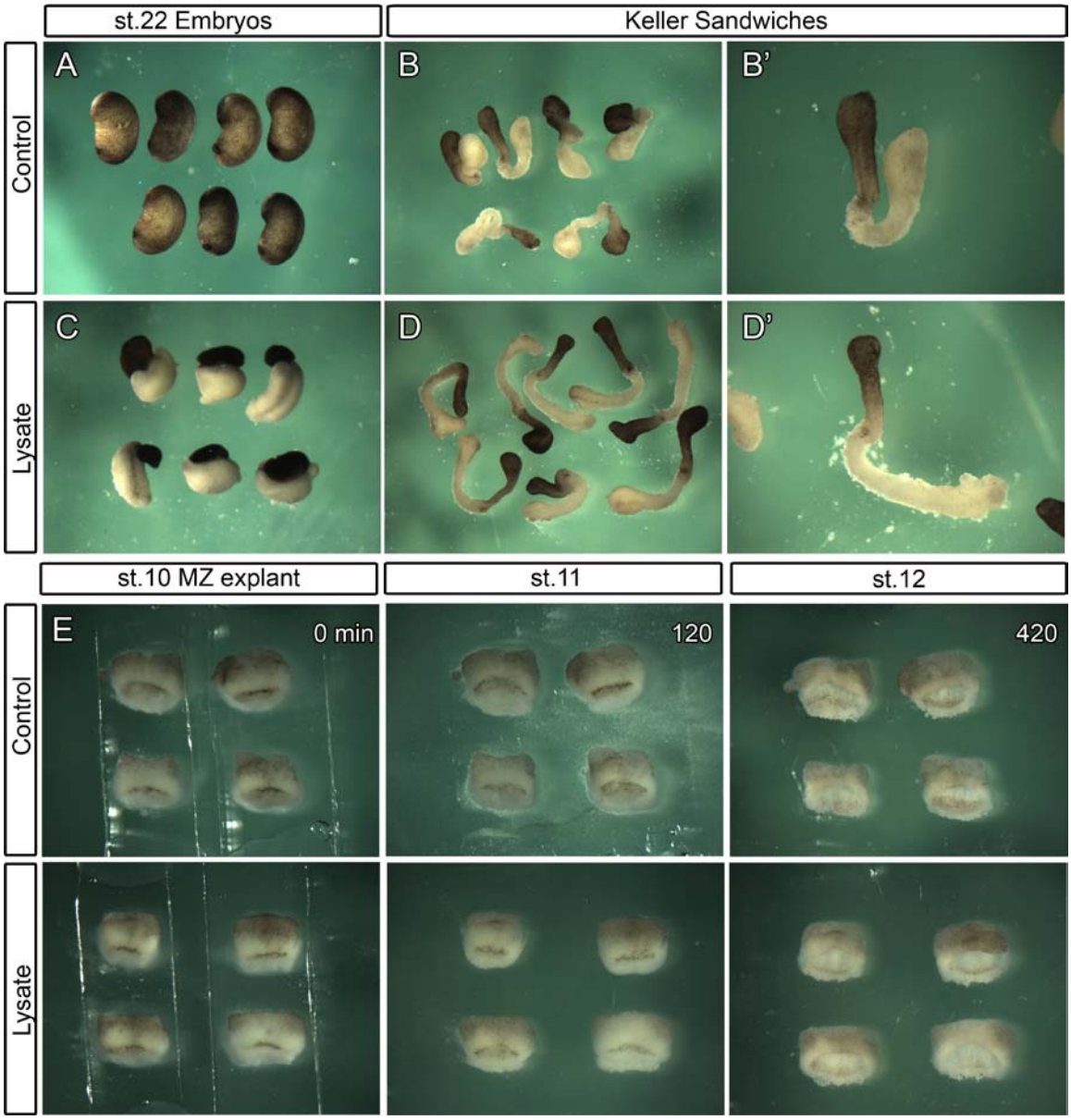

Figure 17. Neither mesoderm nor mesendoderm morphogenesis affected by lysate.

A, B, and C) Whole embryos cultured to stage 22 in lysate exogastrulate (A compared to C) while accompanying Keller sandwiches develop normally in cell lysate (B and B' compared to D and D') demonstrating that unaffected convergence and extension is unaffected. E) Mesenoderm at the vegetal edge of marginal zone explants cultured on lysate spread normally on fibronectin substrate. Lysate was added at 0 min and explants were followed for 420 minutes.

4.2.6 Embryonic contractility is driven by the actomyosin cytoskeleton

Since actomyosin contractility within the apical cortex and circumapical junctions play a key role in epithelial morphogenesis (Sawyer, Harrell et al. 2009; Martin, Gelbart et al. 2010), we strongly suspected these same processes mediated acute contractility in response to lysate or ATP. To test the roles of F-actin and non-muscle myosin II we used an inhibitor of actin polymerization (0.6 μM Latrunculin B; LatB; (Benink and Bement 2005; Lee and Harland 2007; Zhou, Kim et al. 2009), an inhibitor of Rho Kinase (50 μM Y-27632; Y; (Maekawa, Ishizaki et al. 1999; Narumiya, Ishizaki et al. 2000)), and an inhibitor of non-muscle myosin II heavy chain (100 μM Blebbistatin; BBS; (Straight, Cheung et al. 2003; Lee and Harland 2007)). We incubated early gastrula stage embryos for 30 to 60 minutes in each inhibitor, and perfused cell lysate over the animal cap (Figure 18A, A'). Not surprisingly, each of these treatments significantly reduced the absolute magnitude of the contractile response (Figure 18B). Because contractile responses are variable from one batch or "clutch" of embryos to the next, for instance the % contraction varies from 9 to 12 %, we compared results from multiple clutches. BBS produced the largest reduction in the strength of the contraction, in one case abolishing the response altogether, increasing the delay between stimulation and onset of the contractile response, and reducing the time to peak, and the duration of the contraction (Figure 18B through E). Both Y and LatB also decreased the contraction strength, but were considerably less effective. Remarkably, LatB had only moderate effects on contractility, even when the integrity of the epithelium was reduced to the point where cell-cell junctions begin to tear open. Of these three inhibitors, only BBS significantly altered the kinetics of the contractile response (Note: Kinetics were measured only in cases where the contractile response was greater than ~ 2 to 3%).

Together these results indicate an important role for the actin/ myosin cytoskeleton in driving the contraction response that is induced by perfusing lysate on the early embryonic epithelial surface.

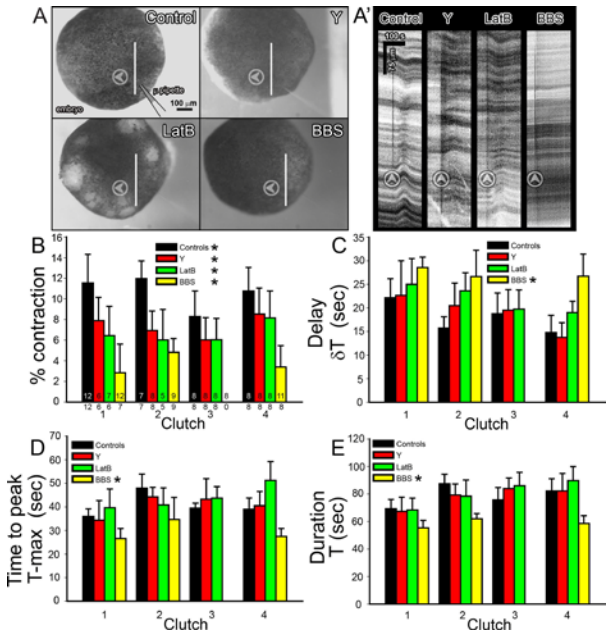

Figure 18. Actomyosin mediates ectoderm contractility.

A) Representative examples of nano-perfusion experiments show delivery of 60 nl of cell lysate over the surface of embryos. Arrow heads show the direction of the cell lysate flow from the micropipettes. Embryos show examples of control, Y-27632 (Y, 100 min treatment, 50 μM), latrunculin B (LatB, 30 min treatment, 0.6 μM), blebbistatin (BBS, 100 min treatment, 100 μM)). A') Time-lapse sequences of the surface of the embryo (in A) resolve the contractile response in kymographs (along lines in A). Arrow heads indicate time stimulus was perfused. Time-lapse sequences demonstrate that cytoskeletal drugs can modulate the kinetics of contractility; moderate effect is seen in Y and LatB examples. Severe effect is seen in BBS treatment. B through E) Kinematic contraction parameters were measured. The strength of contraction is significantly decreased using all the cytoskeletal drugs with BBS inhibiting contraction the most effectively (B). (B) The number of embryos in each set is indicated inside the bar. The numbers below the bars demonstrate the number of embryos that showed a measurable contraction. In clutch number 3, 0 out of 8 embryos contracted when treated with BBS and thus the intensity of the contraction could not be measured. In other cases contractions within BBS-treated embryos was significantly smaller than controls. Other contraction characteristics are significantly different only in Bleb treated samples: i) time-delay increases (C), ii) time-to-peak decreases (D), and the total duration of contraction decreases (E). Statistical significance was calculated using 2-WAY ANOVA across multiple clutches ($p < 0.01$).

4.3 DISCUSSION

Xenopus embryos exogastrulate in response to chronic exposure to lysate and lysate-induced contraction could be a major reason for developmental defects. These defects have been observed by developmental biologists over many years but have been ignored. We propose that ATP is capable of inducing contractions identical to lysate. Lysate and ATP affect biomechanical properties by constant activation of cell contractility when chronically exposed and actomyosin cytoskeleton plays a critical role in driving the induced contractions. Our results extend earlier observations of importance of the epithelial cells in Xenopus morphogenesis (Ninomiya and Winklbauer 2008) and that cell contractility is a key regulator of embryonic development (Armstrong and Armstrong 1992). Our findings are the first to link extracellular nucleotides to epithelial morphogenesis and suggest that differential contractility of animal cap and MZ epithelium drives embryo to exogastrulate.

Embryonic cell-movement in development or morphogenesis is a sum of the movements of different parts of the embryo. Tissues within the embryo move in response to diverse cues using diverse cell behaviors. Different cells in the same tissue may also respond differently to biochemical/ biomechanical cues. e.g. epithelial cells in a animal cap tissue are very different in their behaviors than the underlying mesenchyme (Ninomiya and Winklbauer 2008). Thus exposing embryos with drugs/ compounds could have a differential effect on tissues depending upon the tissue mechanical properties, architecture and tissue location. When different parts of the embryo move individually in a whole embryo, their movements need to be coordinated and any change in one part severely affects the other interdependent parts. When these

interdependent parts are isolated from the embryo, they develop normally and independently (Keller 1975; Keller 1976; Snow 1981). These observations indicate that parts of the embryo could develop normally in isolation since there is no necessity of coordination between these parts for successful morphogenesis. The importance in coordination is highlighted in our studies where processes such as convergence-extension or mesodermal migration individually work in isolation but when these tissues come in contact with epithelium, their functioning is regulated by the excessively-contractile animal cap tissue.

Extracellular ATP has been long investigated for its role in regulating cellular activities, for e.g. triggering 1) calcium waves in PC12 cells (Barry and Cheek 1994), 2) Galectin-1in the extracellular matrix triggering T cell death (He and Baum 2004), 3) deferoxamine inducing inflammatory signals in epithelial cells (Choi, Kim et al. 2004), 4) synringolide1 triggering calcium influx, and 5) potassium eflux in soyabean cells (Atkinson, Midland et al. 1996). These studies point us to the fact that cells have susceptibility to extracellular ligands. Studies of ligands and receptors have been carried out to identify various aspects of specificity and it is evident that the lack of knowledge in this context is due to the existing complexity (Heitzler, Crepieux et al. 2009; Hlavacek and Faeder 2009; Woehler and Ponimaskin 2009). We have identified nucleotide ligands that stimulate contractility and suspect the receptor has the highest affinity for ATP and UTP. Based on these findings and the gene expression studies, we suspect that P2Y class of receptors play a significant role in transducing a lysate stimulus. Further studies will be needed to identify the specific receptors and their role in early gastrulation. It is very important to identify these roles since they may lead to the cause of birth defects and insights into the function of these important class of receptors.

The actomyosin cytoskeleton is a critical cellular that drives the cell to change shape, to direct itself on surfaces, to react to external stimuli and to undergo apoptosis. Futhermore, actomyosin machinery shapes a cell's internal structures controlling the movement of vesicles, exocytosis and endocytosis.

In a previous study, we characterized kinematic parameters of the lysate-induced contraction, identified similarities to other induction methods and also demonstrated that the F-actin cytoskeleton is modulated in each of these cases (Joshi, von Dassow et al. 2010). Cell contractility is primarily driven by myosin motors contracting the F-actin filaments. Many of our treatments, such as disrupting actin polymerization or inhibiting myosin II contractility or even disrupting Rho-activity, reduced contraction strength significantly, but it also demonstrated that perturbations of myosin activity reduced the contraction strength the most highlighting their significance in development (Glotzer 1997; Kelley 1997; Sparkes 2010). Future studies on embryonic contraction will require more specific tools to disrupt protein-specific functions and characterize the individual contributions of the cell architecture to multicellular contractility.

Cell contractility plays important roles in physiology, morphogenesis, tissue engineering and regenerative medicine. A major gap in understanding cell contractility is the identification of molecular factors, segregation of cell receptors and cell-to-cell propagation of contractility in tissues. These factors are highly significant since they could provide insights for 1) engineering three dimensional tissues, 2) producing scaffold-less tissues that could be sculpted by 3D printing and then inducing contractions at specific locations, 3) indentifying the root causes underlying birth defects, which frequently involve defects in epithelial morphogenesis.

5.0 CONTRACTION RESPONSES TO LASER-WOUNDING

Contents of this chapter will be published in the following journal publication:

Joshi S.D., Davidson L.A., Laser-wounding of a single cell in a multicellular epithelial cell sheet triggers large-scale actomyosin contractility in the entire embryonic tissue (in preparation).

Cell contraction is a significant step that shapes tissues and creates three dimensional tissue-forms such as tubes and cavities. Laser-wounding of live tissues has been previously utilized to perturb cell-cell connections in Drosophila (Rauzi, Verant et al. 2008) to understand the cortical forces or to study single cell wound healing in oocytes (Bement, Mandato et al. 1999). We utilize laser-wounding approach to reproducibly induce cell contractions in Xenopus embryos. We propose that embryonic epithelia are an "excitable media" and that the laser-wounding approach utilizes this excitability to generate macroscopic changes in multicellular sheets. We demonstrate a Rho GTPase/ F-actin specific pathway for cell contraction that has connections to epithelial cell protrusions and blebbing. Our findings are the first to indicate a possible link between excitability and cell shape change in Xenopus laevis embryos. This excitability could be used to induce rapid changes in cell shapes needed in the production of three dimensional tissues.

5.1 EXPERIMENTAL PROTOCOLS

5.1.1 Embryo handling, microsurgery and culture media

Eggs from female Xenopus laevis frogs were collected, fertilized following standard methods (Kay and Peng 1991), and dejellied in 2% Cysteine solution (pH 8.4) 20 min after fertilization. Embryos were cultured in 1/3x Modified Barth's solution (MBS) to late blastula or early gastrula stages (Nieuwkoop and Faber 1967) and vitelline membranes were removed. Animal cap explants were microsurgically removed from stage 10.5 embryos using custom-made hair-loops and hair-knives (Joshi and Davidson) in Danilchik's For Amy solution (DFA;(Sater, Steinhardt et al. 1993)). Bovine serum albumin (0.1 or 0.2 % in media; Sigma-Aldrich, St. Louis MO) and antibiotic/antimycotic (0.8 % in media; A5955, Sigma-Aldrich) were added to both 1/3x MBS and DFA.

5.1.2 High-resolution microscopy, laser-activation and image analysis

Laser-wounding experiments were recorded using a confocal scan head (Leica TCS SP5) mounted on an inverted compound microscope. We integrated a manual laser ablation system (Micropoint, Photonic Instruments Inc, St. Charles, IL) with the confocal microscope so that we could laser-wound precise locations and collect confocal time-lapse sequences before and immediately following laser-wounding**.** Detailed description of the laser- wounding / imaging setup is described earlier in Chapter 3. In brief, the protocol for laser- wounding has three steps: 1) collection of before-wounding image, 2) ablation of a predetermined cell or cell–cell junction with 1 to 5 laser pulses, and 3) collection of a time-lapse sequence (3 to 20 minutes) immediately

after step 2. Changes in cell tissue morphology were obtained by analyzing time-lapse sequences either manually or with custom-image processing macros (ImageJ, NIH).

5.1.3 Fluorescent proteins, probes and lineage labels

Embryos at the 1- to 2-cell stage were briefly cultured in 3% Ficoll (Sigma, St. Louis MO) in 1x MBS and microinjected with the desired volume of capped mRNA encoding GFP or RFP targeted to membrane (mem-GFP and GAP43-RFP (Wallingford, Rowning et al. 2000)), F-actin (moe-GFP, (Litman, Amieva et al. 2000) and moe-mCherry, (Clark, Miller et al. 2009)), rho-reporter protein (rgbd-GFP, (Benink and Bement 2005)), cdc42 reporter protein (wgbd-GFP, (Clark, Miller et al. 2009)) and microtubules (tau-GFP, (Kwan and Kirschner 2005)). Capped mRNA was synthesized and purified by standard methods from linearized DNA template (AmpliCap Transcription kit; Epicentre Biotechnologies, Madison WI).

5.2 RESULTS

5.2.1 Experimental control of macroscopic contraction via laser-activation

Previously, we have developed a laser-activation protocol for inducing acute cell contraction within embryonic epithelial cell sheets (Joshi, von Dassow et al. 2010). The preliminary description for laser-wounding has been described earlier in Chapter 3. From these previous studies we can make the following observations about laser-wounding: 1) laser-wounding produces cell contractions in the targeted epithelium with a 10 to 20 sec delay between

stimulation and the start of contraction; the induced contraction is approximately 60 sec in duration. 2) laser-wounding stimulates a long time-scale wound healing response causing over-shoot in the contraction. Laser-wounding activates cell contraction at a distance of 10 to 20 cell-diameters from the activation site and drives rapid remodeling of the F-actins cytoskeleton in these cells. We observed that the magnitude of cell contractions were independent of the distance between an individual cell and the wounding site and all the cells in the field of view contracted without any sign of dampening of the contraction signal, indicating a possibility that the embryonic epithelium might have properties of an excitable media (Bub and Shrier 2002).

5.2.2 Cell fluctuations in an embryonic epithelium indicate excitability

Excitable media are spatially distributed systems which have the ability to propagate signals without damping (Anderson, Janse et al. 1974). Cell fluctuations are one of the indicators that suggest embryonic epithelia are excitable, the other being our previous observations of an undamped spreading of the contraction signal. Such cell fluctuations indicate 1) medium macroviscosity (Tuvia, Almagor et al. 1997) or 2) thermal imbalance of the system or also termed as Brownian ratchet (Gov and Safran 2005; Marcelli, Parker et al. 2005). Macroviscosity is a bulk property and refers to the viscosity measured by conventional approach such as a viscometer (Blacklow, Raines et al. 1988). Brownian ratchets operate isothermally and where chemical energy replaces thermal gradients as the energy source (Peskin, Odell et al. 1993). Following our previous results that contractions spread without dampening, we strongly suspected that embryonic epithelial system might exhibit some properties of an excitable media (Bub and Shrier 2002), as cells contract in response to laser-wounding.

To quantify the cell fluctuations we recorded time-lapse sequences and measured mean squared displacement (MSD) and diffusion coefficient (Dc) of cell boundaries or triple cell junctions (labeled with mem-GFP) and compared them between different embryos and a range of treatments that modulate the cytoskelton. MSD and Dc are two very commonly used parameters in microrheology to identify changes in material properties (Gov and Safran 2005; Daniels, Masi et al. 2006). For quantification, 10 random triple cell junctions in an embryonic epithelium were chosen and their x, y coordinates were noted; centroid coordinates (Figure 19A, red circle) were calculated based on these 10 points (Figure 19A, yellow circles) and the movement of each point with respect to the centroid was calculated over 20 minutes. Centroid calculations were necessary to remove any possible translational movement and derive true fluctuations values. By time-period shifting method, changes in vertex locations were calculated for every time-period (δt), minimum δt being 1 min. Without any fluctuations, we would expect a horizontal line for individual cells. We observe that the MSD is non-linear (Figure 19B) and has variability depending on the cell vertex, which indicates some degree of random behaviors among cells. Similarly, Dc values are non-linear among different cells tracked in the epithelium (Figure 19B, **C)**. The increase of MSD with increasing δt also demonstrates these fluctuations are not mere additions of cell movements over time in one direction (also indicating translation) but are indications of dynamic and active cell behaviors. To confirm these observations, the experiment was repeated for 4 individual tissue samples which also indicated fluctuations among individual cells (Figure 19B', C'). There is a high variability indicated from the large standard deviations. Thus, epithelial cells, labelled with mem-GFP show constant fluctuations in the positions of triple cell junctions (cell vertices) which appear to "shake" or undergo pulsations (also termed as "jiggle", see (Rauzi, Verant et al. 2008)).

Cell fluctuations and excitability are likely indicators of a dynamically changing cell cytoskeleton. We wondered if we could detect dynamic changes in sub-cellular proteins such as the F-actin cytoskeleton. We manually tracked moe-GFP labelled F-actin cytoskeletal contractions in the apical cortex (Figure 19D, red circles). We tracked F-actin intensity in a series of subcellular locations over 250 seconds and observed F-Actin intensity values fluctuate between 10% and 40% in most cases (Figure 19E, E'). These endogenous F-actin fluctuations do not occur in the entire apical surface, but appear to occur randomly and at one or two locations in a cell. The overall F-actin intensity in the epithelium remained relatively constant (Figure 19E, E', pink dotted line). The role of these F-actin fluctuations in epithelial morphogenesis in unknown but it seems likely that the F-actin cytoskeleton contributes to the excited state of cells and may play a permissive role during morphogenesis and may underlie the rapid response to wounds or micro-tears or, as in our case, laser-wounding.

5.2.3 Embryonic fluctuations are driven by the actomyosin cytoskeleton

Since actomyosin within the apical cortex and circumapical junctions plays a key role in epithelial morphogenesis (Adams, Nelson et al. 1996; Vasioukhin, Bauer et al. 2000; Schock and Perrimon 2002; Axelrod 2006) we strongly suspected these F-actin/ myosin dynamics mediated the fluctuations in epithelial cell shapes. Fluctuations, to some extent, are an indicative of the active tendency of a cell to change its shape, and to change its shape, cells utilize their cytoskeleton during development (Lee, Scherr et al. 2007) and in cell culture (Reinhart-King, Dembo et al. 2005).

To test the roles of F-actin and non-muscle myosin II, we used 1) Latrunculin B (LatB): an inhibitor of actin polymerization (0.6 μM; (Benink and Bement 2005; Lee and Harland 2007;

Zhou, Kim et al. 2009) and 2) Blebbistatin (BBS): an inhibitor of non-muscle myosin II heavy chain (100 μM; (Straight, Cheung et al. 2003; Lee and Harland 2007)). We incubated the excised animal caps from early gastrula stage embryos in each of the cytoskeletal inhibitors, and used confocal microscopy to image the epithelial junctions for 20 min. To reduce adhesion of explants to the glass or cell-lysing of explants, bottom glass and overlying cover slip fragments were incubated overnight at 4°C with 1% BSA in 1/3x MBS (BSA-MBS). Not surprisingly, each of these treatments reduced the absolute magnitude of the fluctuations, evident from the reduced values of MSD and Dc (Figure 20). BBS produced a larger reduction in the fluctuations in comparison to LatB. These studies compliment our previous observations of BBS inhibiting lysate-induced contractions (Figure 18). Together these results indicate a critical role for the actomyosin cytoskeleton in driving cell fluctuations.

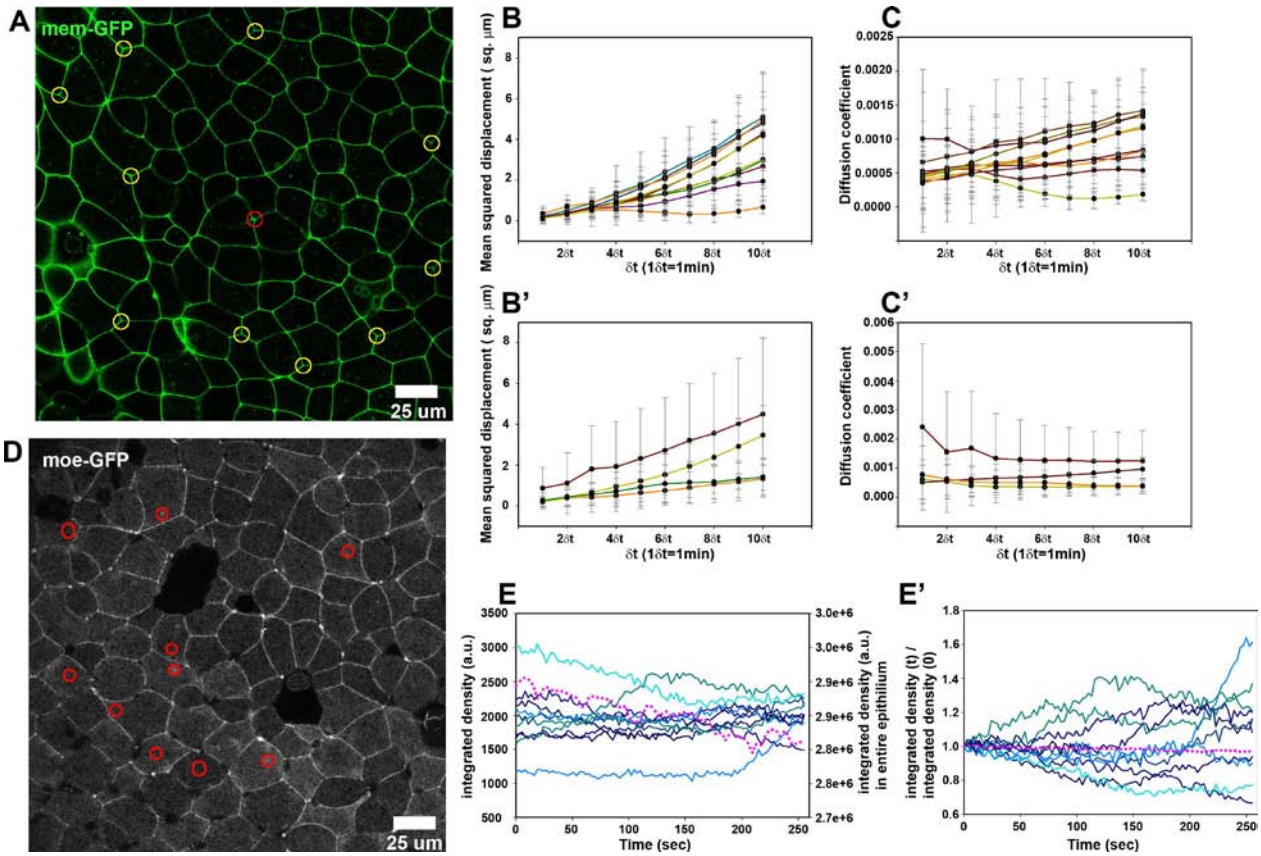

Figure 19. Embryonic epithelium has fluctuations.

Epithelial cell sheet; cells labelled with membrane localizing protein, mem-GFP. Red circle shows the centroid of 10 triple cell junctions (yellow circles) tracked over 20 min. B) Mean squared displacement (MSD) for 10 independent cell junctions (yellow circles) shown in A. Corresponding diffusion coefficient (Dc) values are shown in C. B') MSD values for 4 independent explants from 3 different clutches. Each line represents the mean values for 10 cells each and corresponding Dc values shown are in C'. D) F-actin labeled with moe-GFP; Locations (area inside red circles) in 10 cells were tracked for F-actin intensities over 250s. E) Integrated densities for 10 independent locations (red circles) in D. Pink dotted line represents the overall intensity values of the entire epithelium in the view (follows the y-axis on the right). Corresponding normalized density values are shown in E'. Specific formulas: MSD = (((xt-x0)*(xt-x0)) + ((yt-y0)*(yt-y0))), where t represents positions at individual time spots; Dc = MSD/(6*n*δt), where δt =1 min and n = 1,2,3… varies as the time-period in increased.

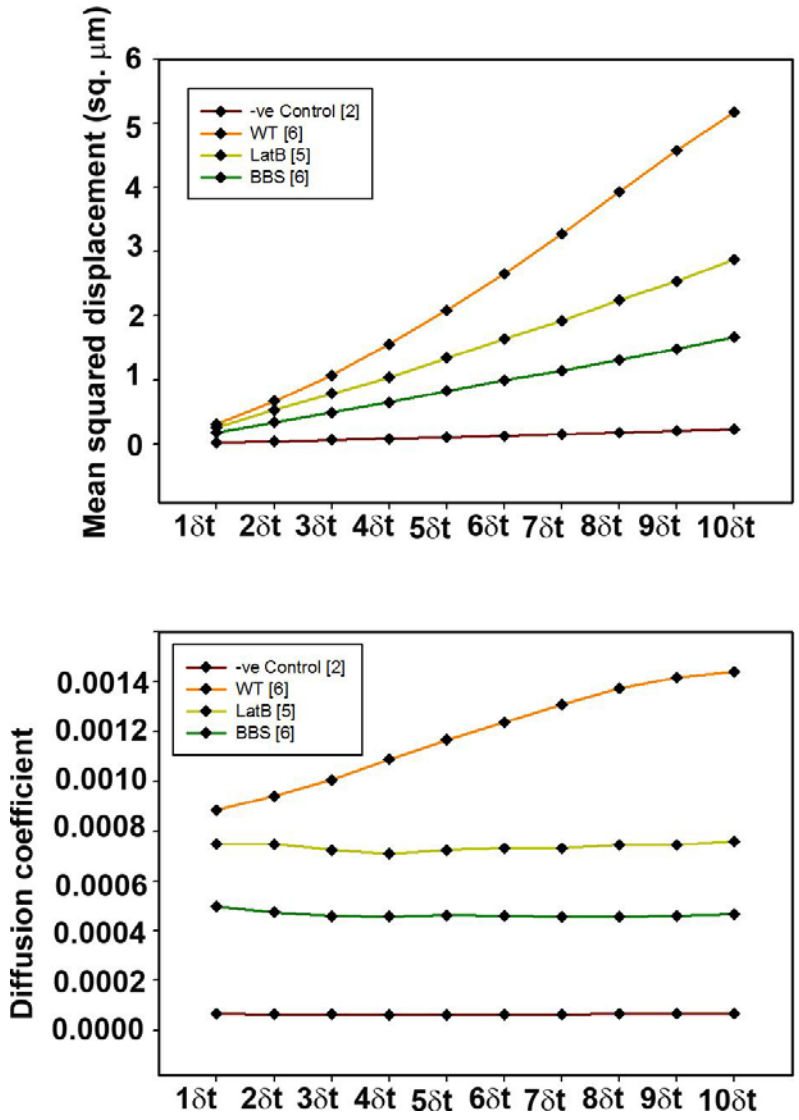

Figure 20. Actomyosin mediates ectodermal fluctuations.

Mean squared displacement (MSD, top graph) and Diffusion coefficient (Dc, bottom graph) is calculated as mentioned in Figure 19. Both, MSD and Dc values, are significantly affected with treatments from latrunculin B (LatB, 30 min treatment, 0.6 μM) and blebbistatin (BBS, 100 min treatment, 100 μM). Negative controls (samples fixed with MEMFA fixation protocol) and digitized to identify any errors in manual tracking demonstrated near zero MSD and Dc values. Graphs demonstrate that cytoskeletal drugs can modulate fluctuations in frog epithelia. In comparison, BBS reduces fluctuations more than LatB (evident from MSD and Dc values). The number of embryos in each set is mentioned in square bracket. The lines represent average values. Standard deviations are very large in all the cases and not shown for clarity in image. The embryos are from 3 different clutches.

5.2.4 F-actin cytoskeleton drives cell contraction triggered by laser-wounding

F-actin intensities in cells fluctuate endogenously while cell vertices undergo fluctuations (Figure 19). Previously, we have reported increases in F-actin intensities in contracting epithelial cells triggered by laser-wounding. We wondered if there was correlation between F-actin intensity changes and the changes in cell area. We first confirmed our previous observations of F-actin intensity fluctuations. F-actin intensities (yellow circles in Figure 21A) and the corresponding cell areas (green boundaries in Figure 21A, A'') were tracked in 10 cells. When compared in a single graph (Figure 21A'''), it shows clearly that as F-actin increases, cell area decreases during contraction and during the following relaxation, as F-actin intensities decrease, cells dilate. In 20 cells from 3 individual explants from 3 independent clutches, we observed variability in the amount of intensity changes (Figure 21B) and area reductions (Figure 21B').

To test whether these intensity increases were independent of increased density as a result of the tighter packing of F-actin in reduced cell areas, we plotted the cell areas against the predicted cell areas, assuming that the F-actin*Area product would be constant in the event of mere packing. Instead we observed that the predicted cell areas would be lower, approximately 10 % lower than the experimental observations (Figure 21C), indicating that there were large F-actin increases than there would have been in case of mere density changes. In most cases, the lines from predicted and experimental data do not match. When 10 cells within each of 3 individual explants were tracked for F-actin intensities and cell areas for initial 90 seconds of the contraction event, we found a very close anti-correlation (Figure 21D). As F-actin intensities increased, cell areas decreased in all the three explants and in all the 30 cells observed. Calculations were conducted over the first 90 sec since post-90 sec, there is variability in the way individual cells recover after contraction. The wound healing response also takes over resulting

in the variable cell relaxation trajectories after the 90 sec. These results indicate that increases in F-actin intensity and decreases in cell area are strongly correlated suggesting that rapid increases in F-actin levels drive cell contraction.

5.2.5 Rho-mediated contraction triggers F-actin remodeling

Laser- wounding of a single cell triggers cell contraction in the entire multicellular sheet and we suspected that other proteins associated with F-actin might also be activated during the triggered contraction. We have previously reported the observations of actin "comets" or "rockets" that have also been described in actin-severing and mechanotransduction studies (Orth, Krueger et al. 2002; Plastino, Olivier et al. 2004; Giganti, Plastino et al. 2005; Revenu, Courtois et al. 2007). These similarities suggest shared mechanisms between cell culture studies and our observations of embryonic contraction.

We next wanted to confirm our F-actin observations with a F-actin cross-linking protein and also examine upstream signaling protein that might trigger F-actin cytoskeleton. Rapid increases in F-actin intensities were confirmed by observations of α-actinin labeled by α-actinin-GFP (Figure 22A, A'). α-actinin is a F-actin cross-linking and bundling protein that demonstrates active F-actin cross-linking sites and highly increased activities. We tracked α-actinin intensities in 9 cells from 3 explants (e.g. white circles in Figure 22A) and observed that intensities increased 3-fold during contraction (Figure 22A'''). When observed in x-z sections, we observed blebbing or cortex delamination (F-actin cytoskeleton separating into 2 layers) in 80% embryos [i.e. 12/ 15 embryos over 4 independent clutches]. Observations in cell blebbing have been reported previously during cell motility (Charras and Paluch 2008; Fackler and Grosse 2008), cell protrusions (Tinevez, Schulze et al. 2009), apoptosis (Coleman, Sahai et al. 2001) and

chemical hypoxia (Harman, Nieminen et al. 1990). There is evidence that blebbing is a major characteristic of injured cells (Babiychuk, Monastyrskaya et al. 2010) and it is quite likely that the epithelial cells in a continuous sheet can sense injury within neighboring cells.

We also suspected that the contraction observations were F-actin specific and that other cytoskeletal elements such as microtubules may not play an active role. In embryos labeled with tau-GFP, when laser-wounded, contracting cells had relatively unchanged intensities in tau-GFP values (Figure 22D, D', D'').

With confirmed results from our observations of α-actinin, we suspected that Rho GTPase protein was actively inducing F-actin remodeling. When laser-wounded embryos labeled with rgbd-GFP were observed in 9 cells from 3 explants, rho-reporter (rgbd-GFP) intensities increase significantly (Figure 22B, B'''), between 40% and 60% in most cases. As before, random locations in a cell were chosen (e.g. white circles in Figure 22B). Active cell protrusions were also observed in contracting cells in the entire cell microenvironment. rgb-GFP labeled punctae were seen at the apical ends of the cells in the x-z slices (Figure 22B') which also represent the protrusions seen in the x-y images. Together these results indicate that rgbd-GFP is activated in the contracting cell protrusions that are rarely seen in epithelial cells. Cell contraction in wgbd-GFP labeled embryos showed that cdc42 was relatively unchanged during contraction (Figure 22C, C', C'') indicating a possibility of rho-specific event.

These results provide evidence that laser-wounding causes a multicellular sheet to contract; these contractions seem to F-actin specific and rho family of proteins and that cdc42 and microtubules may not play active roles in the triggered contraction.

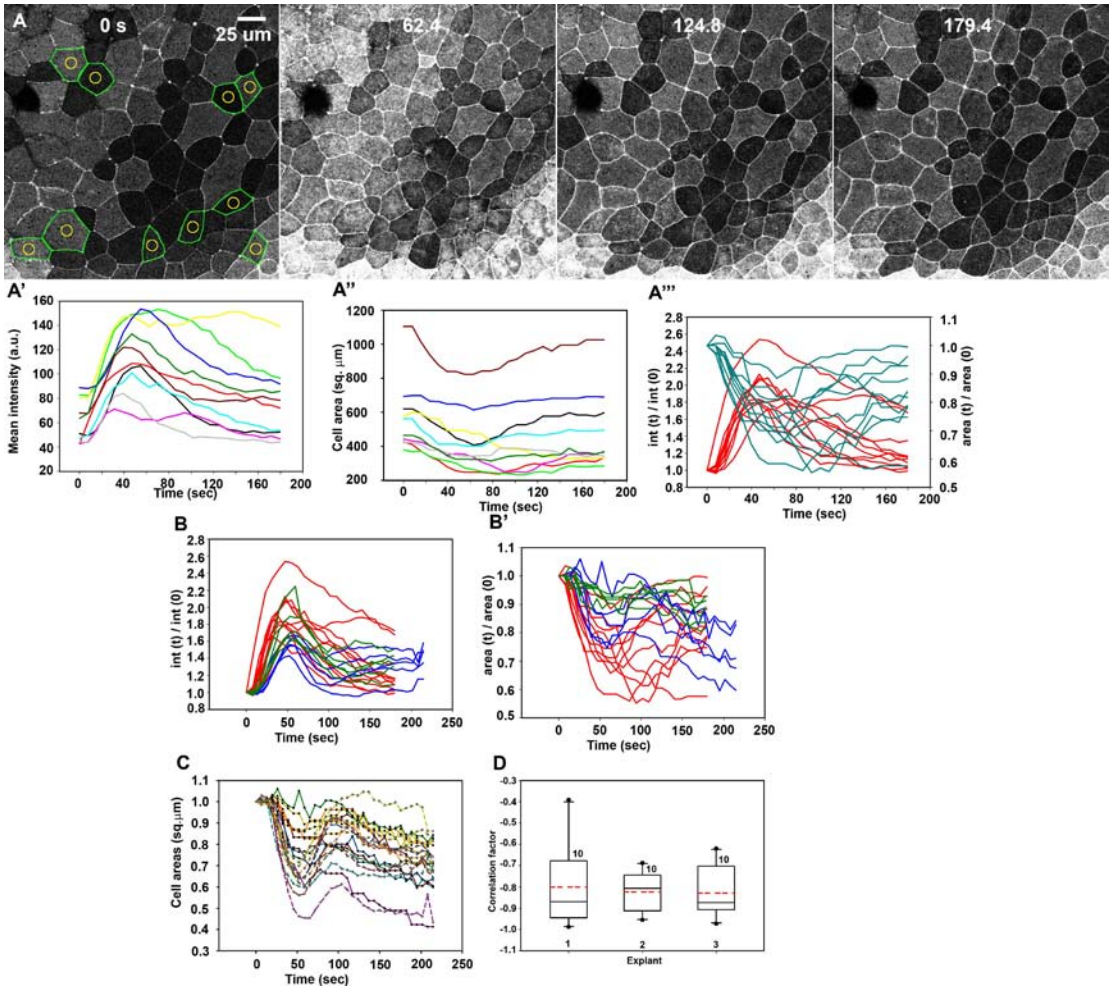

Figure 21. F-actin cytoskeleton drives cell contraction triggered by laser-wounding.

Embryonic epithelial F-actin (labelled by moesin-GFP) changes induced in response to laser-activation of a single cell in the microenvironment. A') F-actin intensities (marked by yellow circles in A) increase and cell areas (marked by green boundaries in A) decrease (A'') for epithelium in A; these changes are independent of initial intensities and/ or cell areas (A'''). B) 20 cells from 3 explants show consistent F-actin increases and cell area decreases (B'). B and B': Blue, red and green lines indicate cells from 3 different explants. C) Comparison between actual cell area changes (solid lines with black markers) and corresponding predicted areas from simple intensity changes (dotted lines with white markers). Lines in same cell represent one cell. D) Correlation factors (between F-actin and cell area) for 3 different explants over initial 90 sec post-activation demonstrating the closely anti-correlated parameters. Numbers above the box plots indicates the number of cells per explant.

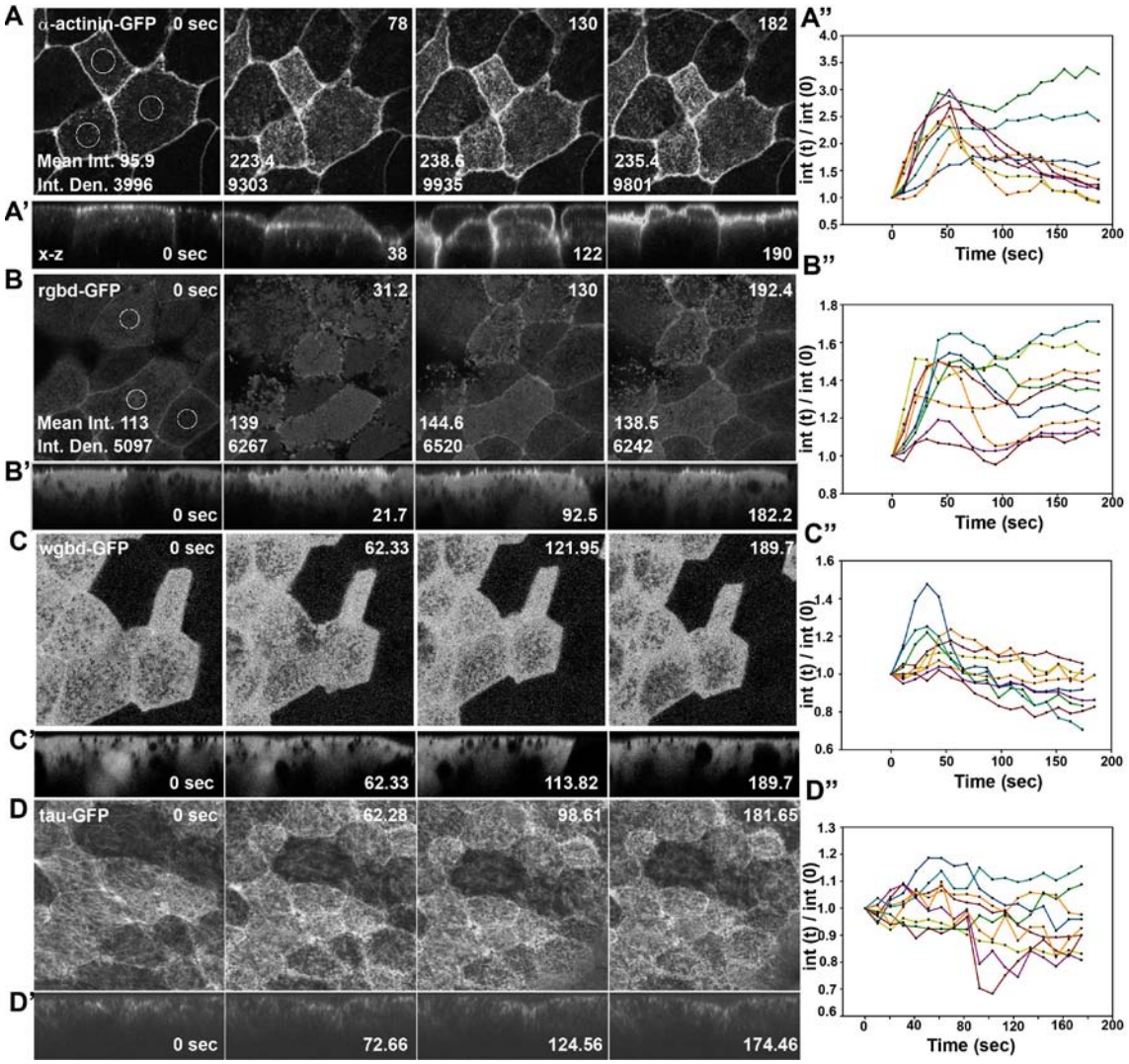

Figure 22. Rho-mediated contraction triggers F-actin remodeling in contracting cells.

A, A' A'') α-actinin (labeled by α-actinin-GFP) changes induced in response to laser-wounding. Intensity ratios (such as intensity in white circles in A) tracked for 9 cells from 3 explants show increases independent of initial intensities (A''). Results confirmed in x-z views (A'). B, B', B'') Rho-reporter protein labeled by rgbd-GFP show corresponding increases in intensity values (such as intensity in white circles in A) for rgbd-GFP during contraction. 9 cells from 3 different explants were utilized for intensity calculations (C''). D, D'D'') cdc42 labeled by wgbd-GFP shows relatively unchanged wgbd-GFP intensities. E, E', E'') Microtubules labeled by tau-GFP demonstrate relatively unchanged tau-GFP intensities during contraction. 9 cells from 3 different explants were utilized for intensity calculations (D'').

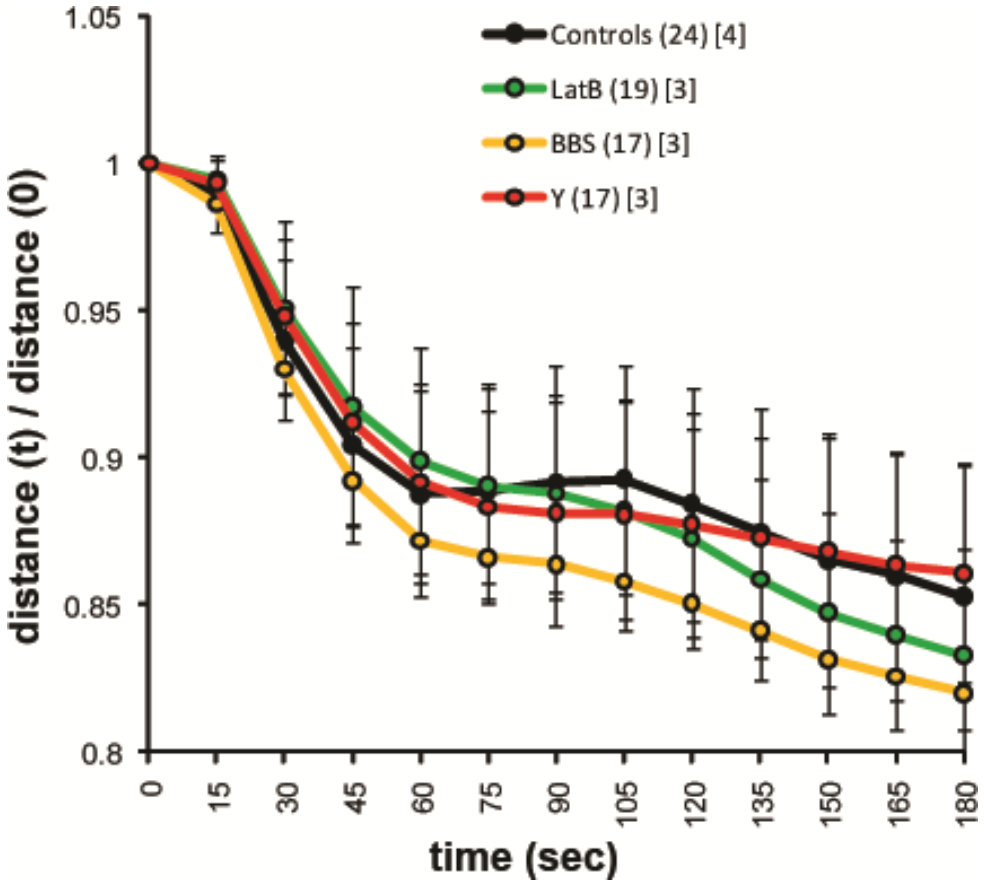

Figure 23. Actomyosin inhibitors are unable to reduce the laser-induced contraction strength.

Distance between two points is tracked in contracting epithelia as previously shown in Figure 9. Treatments from latrunculin B (LatB, 30 min treatment, 0.6 μM, green line), blebbistatin (BBS, 100 min treatment, 100 μM, yellow line) and Y-27632 (Y, 100 min treatment, 50 μM, red line) were unable to reduce the contraction ability of the laser-wounded epithelial sheets. The numbers in round brackets represent the number of embryos while the numbers in square brackets indicate the number of clutches for each set. Graphs demonstrate that cytoskeletal drugs are unable to reduce the contraction ability of the epithelial sheets when laser-wounded.

5.2.6 Actomyosin inhibitors cannot reduce the laser-induced contraction

Actomyosin within the apical cortex of epithelial cells plays a critical role during morphogenesis (Martin 2009). We have demonstrated earlier the importance of the actomyosin cytoskeleton in the observed cell shape fluctuations (Figure 20). Similar to those observations, we strongly suspected that actomyosin plays a critical role in the laser-induced contraction.

To test the roles of F-actin, non-muscle myosin II and Rho Kinase during induced contraction, we used 1) Latrunculin B (LatB, 0.6 μM) and 2) Blebbistatin (BBS, 100 μM) and 3) Y-27632 (Y, 50 μM). We isolated animal cap explants from early gastrula stage embryos, allowed them round up, cultured them in each of the cytoskeletal inhibitors, and used confocal microscopy to collect time-lapse sequences of epithelial cells. We modified our earlier laser-wounding protocol, replacing the laser-gun with high-intensity laser beam in FRAP mode. We collected a pre-wound image, then wounded a target cell-cell boundary or a cell center, and collected a 3 min post-wound time-lapse sequence. To reduce adhesion/ lysing of explants, bottom glass and cover slips were incubated overnight at 4°C with 1% BSA in 1/3x MBS (BSA-MBS). Very surprisingly, none of the three inhibitor treatments reduced the absolute magnitude of the induced contractions (Figure 23). We expected that all the three inhibitors would reduce the contraction abilities of the epithelial caps to a certain extent and that BBS would be a potent inhibitor as in the previous studies (Figure 18).

These results indicate that although F-actin and non-muscle myosin II play a significant role in cell fluctuations, there is a possibility that during contraction, other myosin isoforms may still be active that drive the observed contraction (Smutny, Cox et al. 2010) or BBS is ineffective in blocking all myosins that could play a role in driving contractions (Limouze, Straight et al.

2004). It is also possible that BBS is photo-inactivated by light (Sakamoto, Limouze et al. 2005); if inactivation occurs in our experiment during high laser intensities during wounding, it could explain our observations.

5.3 DISCUSSION

Laser-mediated approaches to wound live tissues have been reported previously (Bement, Mandato et al. 1999; Rau, Quinto-Su et al. 2006). In development biology, lasers have been used to ablate specific targets to investigate questions such as the role of cell rearrangement in sea urchin gastrulation (Hardin 1988), the role of actomyosin contractile ring in wounded X. laevis oocytes (Benink and Bement 2005; Clark, Miller et al. 2009) and the role of cortical forces during in epithelial morphogenesis (Rauzi, Verant et al. 2008). Previously, we have observed that neighboring cells contract and F-actin remodels in the cells in the field of view, when a single cell in a multicellular sheet in laser-wounded (Joshi, von Dassow et al. 2010). Here, we propose Rho Kinase activates F-actin which when rapidly recruited to the apical surface, drives cell contraction. Our results extend earlier observations of wounding responses (Clark, Miller et al. 2009) in Xenopus and are the first to suggest the excitability of embryonic tissues can be used to understand the biophysical features of laser-induced cell shape change.

Sporadic contractions have been previously observed in Xenopus (Wallingford, Ewald et al. 2001) and chick embryos (Stern and Goodwin 1977). These contractions indicate that gastrulating embryos could be in an excitable state when new proteins are getting expressed and tissues are being built. These contractions may also indicate events where embryos “overshoot” their normal behavior in order to compensate for local micro-mechanical perturbations (such as a

round of cell divisions) or local fluctuations in cell-cell signaling (such as expression of new receptors or proteins as the embryos mature). Previously reported contractions (Wallingford, Ewald et al. 2001) may have significant morphogenetic role since their occurrence may be under-reported due to their short duration.

Rudimentary tissues are shaped when cell communities coordinate to modify bulk tissue architecture. It is likely that groups of cells coordinate maximal contraction to shape tissues during macroscopic tissue-shaping movements such as neural plate formation (Schoenwolf and Franks 1984; Benko and Brodland 2007), bottle cell formation (Lee and Harland 2007), and cement gland formation (Wardle and Sive 2003). Periodic contractions and oscillations in cell shape have been shown to precede epithelial morphogenesis (Martin, Kaschube et al. 2008; Solon, Kaya-Copur et al. 2009) which indicates that embryonic tissues are a form of excitable media, and are primed to undergo rapid reorganization during morphogenesis or in response to external perturbations such as wounds and tears. Our studies provide evidence that the embryonic epithelium undergoes cell contraction correlated with changes in changes in F-actin levels.

F-actin plays a critical role during cell motility and is regulated by Rho-family GTPases (rho, rac, cdc42) pathway has been well described in cell culture studies (Nobes and Hall 1995; Popoff and Geny 2009). Our results suggest a model where Rho GTPase drives F-actin remodeling triggered by laser-wounding to force cell shape change in epithelial cells. With laser-wounding, we report 1) intensity increases of rho-reporter protein rgbd-GFP in apical surface of a cell, 2) rarely seen rho-expression in epithelial cell protrusions. With α-actinin intensity increases, we confirm F-actin changes as well as report cell blebbing in response to laser-wounding. These results are a significant step forward since blebbing in a distant cell (3-4 cell

diameters) from the laser-wounding site indicates that the blebbing cells can sense injury to its microenviroment. Of course the same is clear from cell contraction in the entire cell field which also indicates that there is a significant coordination between cells and signal propagation that starts a cascade resulting in macroscopic changes. Our contractions observations are also significant since the event seems to be Rho Kinase/ F-actin specific with microtubules and cdc42 relatively unchanged during contraction.

The induced contractions cannot be reduced by cytoskeletal inhibitors. This is a surprising finding from these studies. Fluctuations significantly dampen with inhibitors but contractions cannot be reduced. There are several possibilities of these outcomes: 1) Inhibitors may not remain effective under harsh light conditions as has been previously demonstrated (Sakamoto, Limouze et al. 2005). 2) BBS may not inhibit all the myosin II isoforms that may participate in cell contraction along with the ones inhibited by BBS. It is quite possible that one isoform of myosin II specifically participates in cell fluctuations, which when inhibited by BBS, dampens fluctuations. This may indicate that fluctuations could be specific to one isoform of myosin II and macroscopic contractions may be driven by many or all types of myosin II isoforms (Limouze, Straight et al. 2004; Smutny, Cox et al. 2010). 3) It is possible that inhibitors are effective and as a result of their effect the tissue reduces in stiffness. Tissues with lower stiffness with cytoskeletal inhibitors effecting reduced cytoskeleton might be able to the contract similar to tissues with normal stiffness and normal cytoskeleton. These results indicate the necessity of further analysis to understand the complex mechanism of cell shape change.

Cell contractility plays important roles in physiology and morphogenesis. It is critical to understand the specific roles of cytoskeletal proteins in order to understand their contribution to the mechanical process of cell shape change and how these changes are coordinated to produce

macroscopic change in tissue architecture. Myosin is shown to localize a variety of receptors to cell surface (Bourguignon 1980; Cyr, Dumont et al. 2002). It appears that actomyosin is a key effecter in the positioning (Dawes-Hoang, Parmar et al. 2005) and establishment of apical/ basal polarity however little is known about the positioning of the cell's growth factor receptors. These too may be localized by actomyosin. Such localization may confound efforts to identify or elucidate principles of mechanotransduction. A major gap in understanding cell contractility is the identification of links between cell receptors and cell cytoskeleton. Another essential aspect of understanding multicellular behaviors is to identify the propagation mechanism between cells. Cells may use gap junctions for signal propagation or mechanical tension to trigger changes throughout a tensed cell sheet. These factors are highly significant since they could provide insights for engineering three dimensional tissues coordinated cell shape change among large cell communities.

6.0 CHEMICAL STIMULATION OF A XENOPUS EMBYRONIC TISSUE

Some of the contents of this chapter have been published in the following publications:

YongTae Kim, **Joshi S.D.,** Davidson L.A., Leduc P., Messner W., Dynamic Control of 3D Chemical Profiles with a Single 2D Microfluidic Platform (submitted)

YongTae Kim*, **Joshi S.D.*,** Messner W., Leduc P., Davidson L.A., Detection of dynamic spatiotemporal response to periodic chemical stimulation in a Xenopus embryonic tissue, PLoS One. 2011 Jan 31;6(1):e14624. **(* equal authors)**

The experiments for this project were conducted in collaboration with a research group consisting of Dr. Phillip Leduc, Dr. William Messner and Mr. YongTae Kim from Carnegie Mellon University. Mr. Kim performed the duties related to microfluidics design, simulations and data analysis in part. I executed the biological portion of this project including injecting embryos with the desired mRNA, tissue isolation, confocal imaging and data analysis in part.

Embryonic development is guided by a complex and integrated set of stimuli that results in collective system-wide organization that is both time and space regulated. These regulatory interactions result in the emergence of highly functional units, which are correlated to frequency-modulated stimulation profiles. We have determined the dynamic response of vertebrate embryonic tissues to highly controlled, time-varying localized chemical stimulation using a microfluidic system with feedback control. Our approach has enabled localized spatiotemporal

manipulation of the steroid hormone dexamethasone (DEX) within Animal Cap (AC) tissues isolated from gastrulating *Xenopus* embryos. Using this approach we investigate cell-scale responses to precisely controlled stimulation by tracking the redistribution of a GFP-tagged DEX-reporter from the human glucocorticoid receptor (GR). We exposed defined regions of a single AC explant to different stimulation conditions—continuous stimulation, periodic stimulation, and no stimulation. We observed collective behavior of the GR transport into the nucleus was first-order. Furthermore, the dynamic response was well-modeled by a first order differential equation with a single time derivative. The predicted responses for periodic stimulations closely matched the results of the frequency-based experiments. We find that periodic stimulation versus continuous stimulation can result in highly distinct responses. This finding is critical as controlled space and time exposure to growth factors is a hallmark of complex process in embryonic development. These complex cellular signaling and transport machinery responses were similar to emergent behaviors in other complex systems, suggesting that even within a complex embryonic tissue the overall system converges toward a predictive first-order response.

6.1 EXPERIMENTAL PROTOCOLS

6.1.1 Embryos, mRNA injections and microsurgery

Embryos were collected and fertilized following standard methods. Embryos at the 1-cell stage were cultured in 3% Ficoll (Sigma, St. Louis MO) in 1x MBS (Modified Barth's solution) and microinjected with mRNA encoding GR-nuc-GFP. Embryos were cultured in 1/3x MBS to early

gastrula stages. Vitelline membranes were removed using forceps. Animal cap explants were microsurgically excised from stage 10 embryos.

6.1.2 Microfluidics

6.1.2.1 Microfluidic device design

Modular microfluidic devices were fabricated using standard soft lithography techniques (Kim, Kuczenski et al. 2009) with polydimethylsiloxane (PDMS) (SYLGARD 184, Dow Corning,c MIDLAND, MI). The microfluidic devices for two modular resistors (R20 and R60) were 20 and 60 mm long and had cross sections 100 μm wide and 50 μm high. The microfluidic channel had three inlet channels that were rectangular cross sections with dimensions of 500 μm wide, 300 μm high, and 5 mm long. The central inlet was used as a temporary outlet for removing air bubbles in the fluidic network. These inlet channels converged to form a single outlet channel (rectangular cross section 1500 μm wide, 300 μm high, and 10 mm long).

6.1.2.2 Air bubbles and microfluidics

Air bubbles are a major problem with experiments involving microfluidic channels (Nakayama, Hiep et al.). The air bubbles have a tendency to move in the microfluidic tubes and cause problems in fluid flow creating vortexes and aberrations in the flow patterns. In our case, air bubbles had a tendency to attach to the walls of the inlet tubes and then flow into the channel and dislodge the explants as they moved out of the channel. Air bubbles were removed before the experiments by flowing DFA for 45 min before the experiment. This ensured that the bubbles would not flow into the channel later during the course of the experiment.

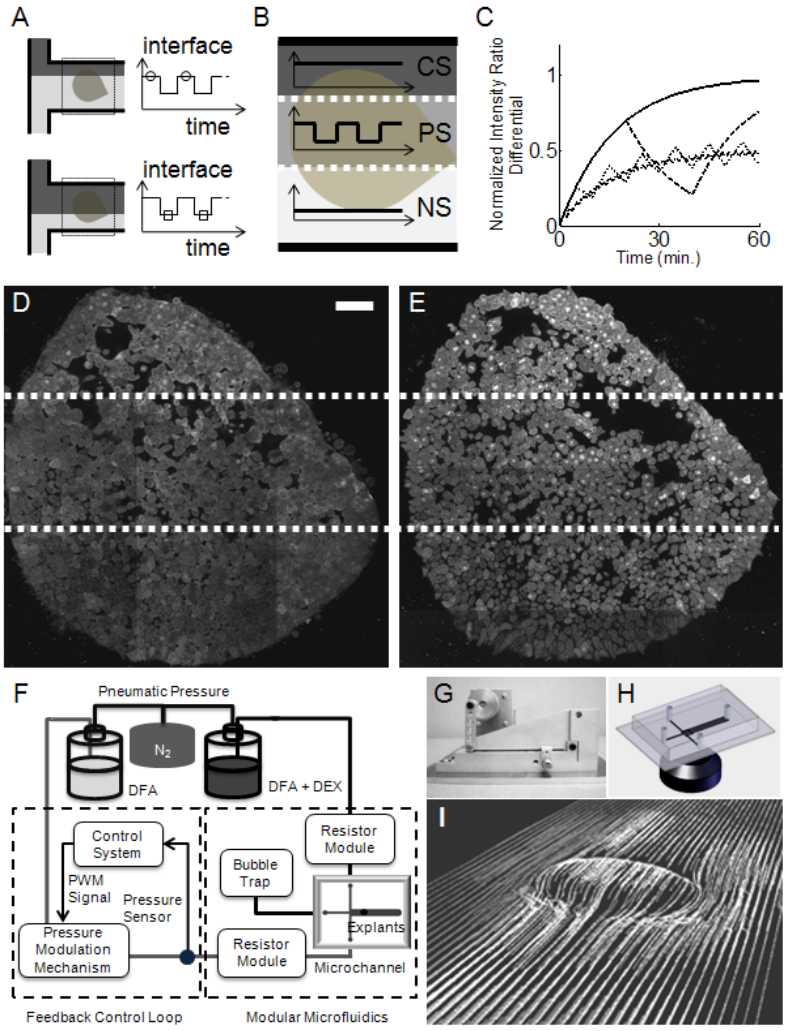

Figure 24. Spatiotemporal control of chemical environment over animal cap tissues.

(A) Laminar flow and fluid interface over the explants. Circles represent initial interface positions while squares indicate repositioned interfaces. (B) Three regions exposed to different stimulation: constant stimulation (CS) with dexamethasone (DEX) in culture media (DFA) (positive control), periodic stimulation (PS) with 50% duty-cycle , and no stimulation (NS) with culture media alone. Dotted lines mark microfluidic interfaces. (C) Simulation results from first-order chemical reaction model depicting normalized intensity ratio differential over time for the cases: CS (solid), 40-minute PS (dashed), 10-minute PS (dotted), and 2-minute PS (dashdot). (D) Image of AC explant before flow. The scale bar indicates 100 µm. (E) AC explant after 60 minutes of three (CS, 2-minute PS, and NS) regions. (F) Microfluidic interface control system. (G) Pressure modulation mechanism. (H) Schematic for confocal imaging setup. (I) Computational Fluid Dynamics (CFD) simulation showing flow patterns with an explant housed in the channel.

6.1.2.3 Control system

Microfluidic interface control system (Figure 24F) is composed of compressed nitrogen gas providing a constant pressure to the two reservoirs (Kim, Kuczenski et al. 2009). One reservoir contains DFA, which flows through the pressure modulation system and the R20 fluidic resistance module before entering the microfluidic channel, and the other reservoir contains 25μM DEX in DFA, passing through the R60 fluidic resistance module before entering the microfluidic channel. The feedback loop modulates fluidic resistance and fluid volumes to regulate the pressure at the channel inlet, which allows both long-term and high-speed control of the microfluidic interface. Different microfluidic resistor modules were used to set an initial interface position at a defined location in the microfluidic channel.

6.1.2.4 Embryonic tissue culture in microfluidic channels

The microfluidic channel is housed on a glass coverslip which forms the base for imaging purposes. Animal cap explants were positioned in the channel by gentle suction using a manual syringe pump. Care was taken to apply suction slowly in order to prevent explants from being destroyed. Explants were allowed to attach to the glass coverslip that had been pre-coated with fibronectin (Figure 25A, B). Explants remain healthy in the microfluidic channels and continue to spread on the glass surface for at least 10 hours (Figure 25C, D, E).

6.1.3 Microscopy and imaging

A digital charge-coupled device (CCD) camera (Scion Corp., Frederick, MD) mounted on a dissecting stereoscope was used for experiments confirming explant attachment. A confocal scanning head (Leica TCS SP5: Leica Microsystems, Bannockburn IL) mounted on an inverted

compound microscope was used to collect time-lapse sequences and z-stacks for translocation experiments. Time-lapse sequences were analyzed either manually or with custom-image processing macros (ImageJ, Wayne Rasband, NIH). Projections of the image stacks obtained in the z-direction (50 sections at 0.2 μm intervals) were used to track cell nuclei and cytoplasm intensities in the explants. Projections were chosen over single images in order to ensure that the entire cell is being accounted for.

6.1.4 Data analysis

To incorporate clutch-to-clutch variability, all experiments were repeated three times. Statistical analysis for verifying the significance of the intensity ratio values were carried out with the non-parametric Mann-Whitney U-test using commercial software, Minitab (Minitab Inc., State College, PA).

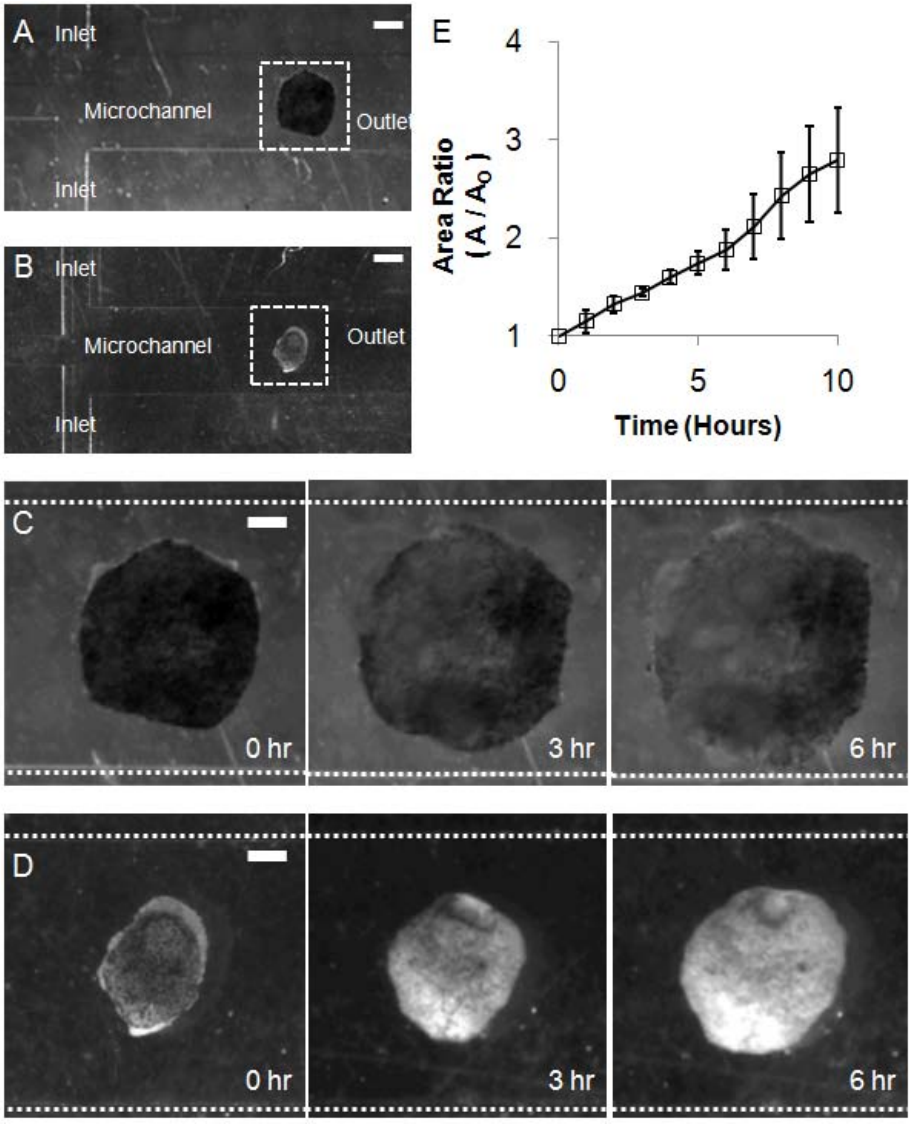

Figure 25. Animal cap tissue spreading in microfluidic channels.

(A and B) Tissue explants from two different female frogs attached to the substrate in the microfluidic channels. The scale bar is 500 µm. (C and D) High resolution images of the tissue explants (in A and B) spreading over time. The scale bar is 200 µm. (E) Ratio of the area of the tissue explants normalized by the initial area versus time (n=3). Error bars represent standard deviations.

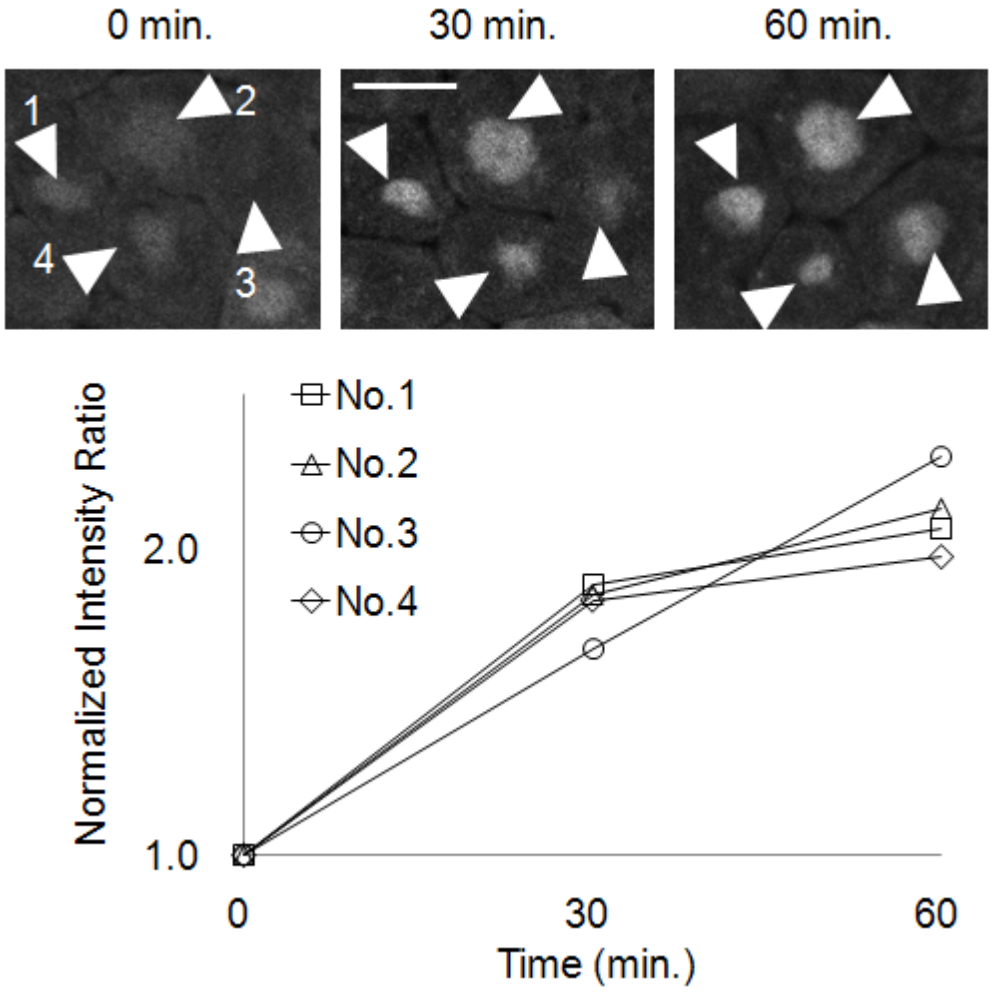

Figure 26. High resolution images of four individual cells to DEX stimulation.

Tracking nuclear intensities of four cells over time allowed us to quantitatively determine the responses using ratios of nuclear to cytoplasmic intensities. The ratios were first normalized by the initial value at time zero. The scale bar is 20 µm.

6.2 RESULTS

6.2.1 GR-nuc-GFP construction and characterization

To probe the kinetics of cellular responses within a multicellular embryonic tissue to chemical stimulation we first created a synthetic stimulation-response network using the human glucocorticoid response system. To detect activation by the glucocorticoid hormone dexamethasone (DEX) we constructed a GFP-based biosensor that reports the level of hormone stimulation in *Xenopus* cells through fusing the hormone binding domain from the Human glucocorticoid receptor (GR) (Kolm and Sive 1995) with a nuclear-localizing green fluorescent protein containing a nuclear import sequence (NIS; nuc-GFP) (Htun, Barsony et al. 1996; Kroll and Amaya 1996). In the absence of DEX, GR-nuc-GFP accumulates in cytoplasm, but translocates to the nucleus after the addition of DEX to the system. We demonstrated the function of this biosensor in a multicellular embryonic tissue by monitoring the dynamics of 4 individual cells in a tissue and calculating the normalized intensity ratio of GFP levels in the nucleus to GFP levels in the cell cytoplasm in the tracked cells over time (Figure 26). These trials have been verified earlier in a manual experiement that was conducted in petri dish (Figure 27).

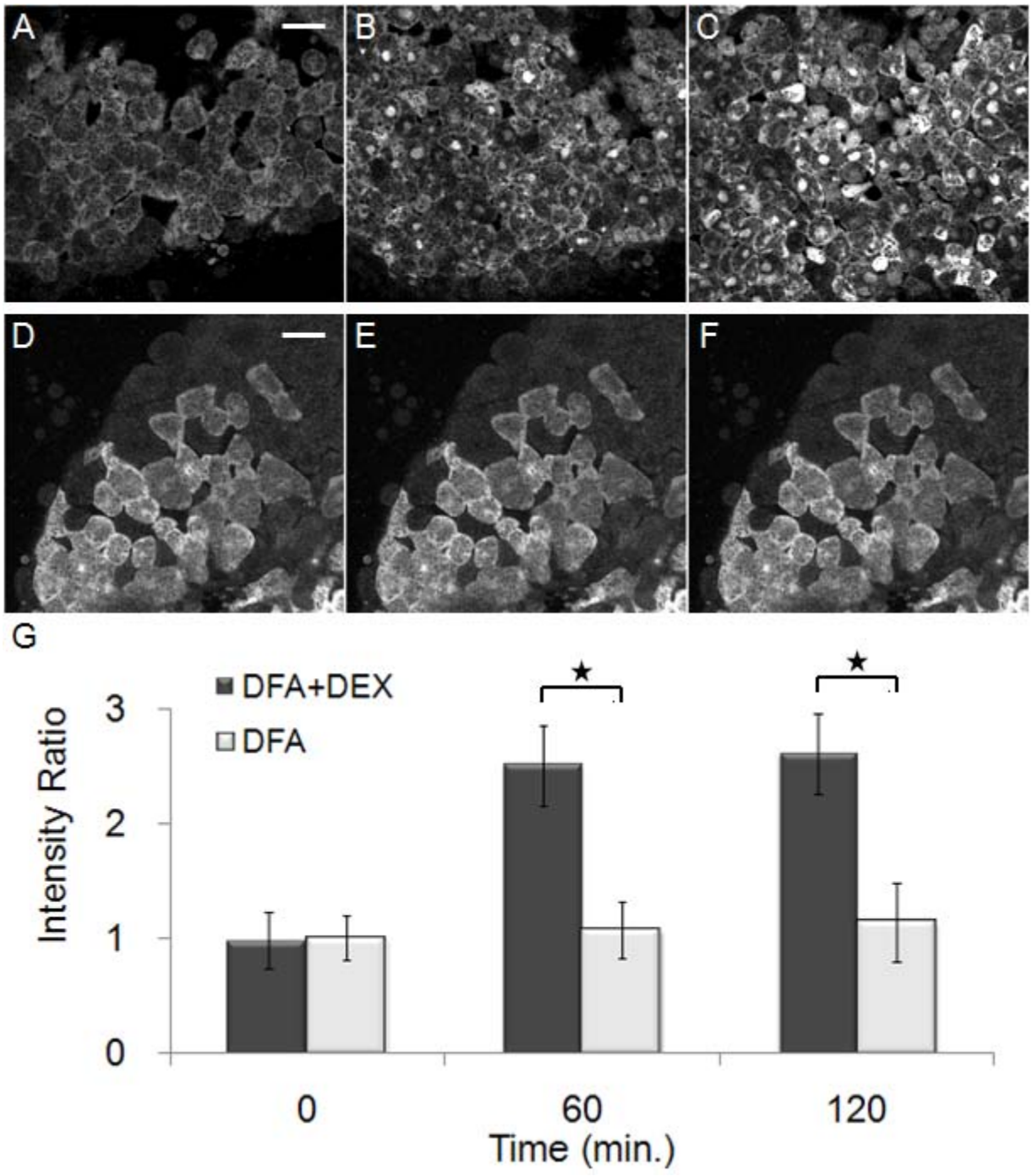

Figure 27. The response of GR-nuc-GFP in animal tissues housed in a petri dish.

(A through C) Stimulated AC explants with DEX after 0, 60 and 120 minutes. (D through F) Control regions without DEX after 0, 60 and 120 minutes. (G) Ratio of the nuclear intensity to the cytoplasmic intensity (from A through F). Error bars represent standard deviations for 20 cells. The scale bar is 30 µm.

6.2.2 GR-nuc-GFP translocation using microfluidic control

With GR-nuc-GFP as a reporter of DEX we followed responses of cells within the embryonic tissue to a precise spatiotemporal pattern of chemical stimulation. We used a large microfluidic channel to accommodate the larger size of AC explants and provide continuous and periodic stimulation over longer duration (Figure 24A, B). We then observed the response pattern of the explant over time (Figure 24C) as well as GR-nuc-GFP nuclear translocation response (Figure 24D, E). As expected GR-nuc-GFP accumulated in cytoplasm before stimulation (Figure 24D) but translocated with spatially distinct responses to a sharp gradient (Figure 24E). Our microfluidic control system (Figure 24F) using a custom designed pressure regulation mechanism (Figure 24G) delivered precise doses of DEX to defined regions, images of which were taken using confocal microscope. The integration of the techniques enabled both long-term and high-speed manipulation of laminar flow interfaces in microfluidics for spatiotemporal regulation of DEX stimulation of AC explants.

One important issue to consider when delivering chemical factors to multicellular tissues using microfluidics is the effect of the shape of a three-dimensional (3D) tissue on flow patterns around the tissue. We examined the contribution of these factors to create a functioning system by modeling the fluid interactions with the geometry of a 3D tissue using computational fluid dynamics (CFD) simulations (Figure 28). We found that the presence of the explants does not significantly disrupt flow in the channel (Figure 24I). CFD simulations also provide limits on the range of exploitable flow rates critical to precise stimulation (Lucchetta, Lee et al. 2005).

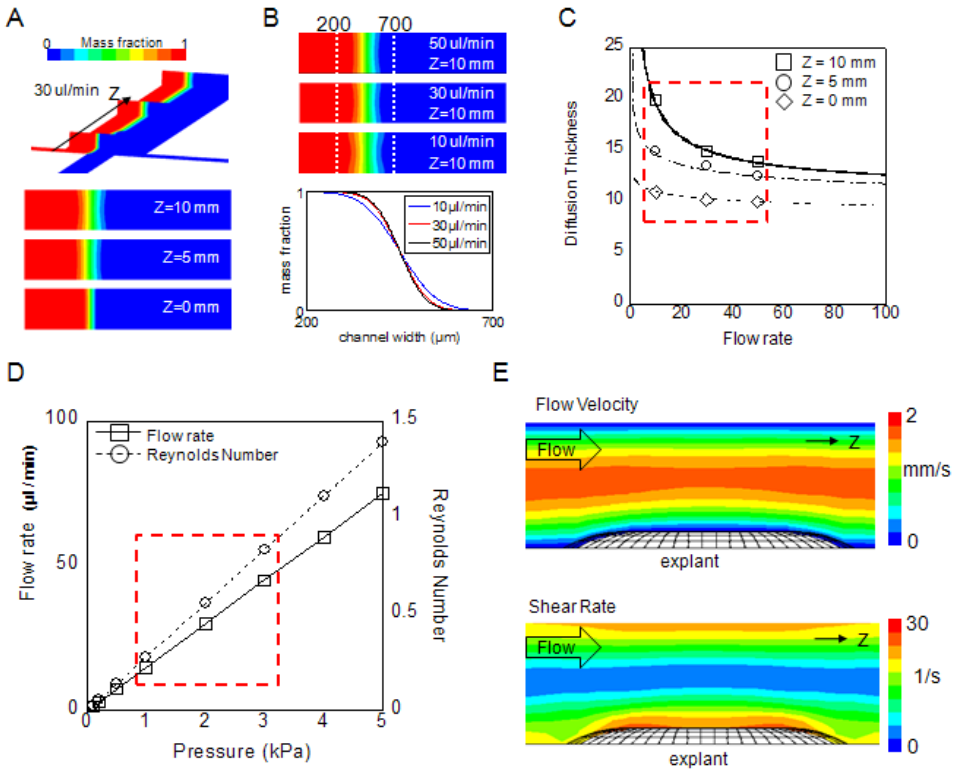

Figure 28. CFD simulations: flow patterns around the explant housed in the channel.

(A) Diffusive dispersion through the channel at the AC explants at a flow rate of 30 µl/min. (B) Diffusion profile in the cross section to the downstream flow at flow rates of 10, 30, and 50 µl/min. The lowest flow rate useable for our approach was determined to maintain a diffusion thickness of less than 20 µm. (C) Diffusion thickness at different sections downstream at the middle layer relative to channel height. (D) Relative effects for flow rates, pressures, and Reynolds number. The red dashed box represents a useable range of the pressure in the experiment to prevent large diffusion and high shear stress based on the simulations. We then experimentally determined the highest flow rate possible for the experiment where the explants did not experience high shear force. An appropriate range of the flow rate was between 10 µl/min and 50 µl/min where the Reynolds number was less than 1. From these experimental and simulation results, we selected a flow rate of 30 µl/min for the experiment, which corresponded to an inlet pressure of 2 kPa. (E) Flow velocity and shear rates around the explant at a flow rate of 30 µl/min. This flow rate corresponded to a fluid velocity around the explant of less than 1.0 mm/s and a shear rate of less than 30 s^{-1}.

6.2.3 Response to stimulation

6.2.3.1 Response to spatially patterned stimulation

To investigate cellular response to a sharp gradient of stimulation we positioned the interface between the streams of DEX and DFA over the center of an explant for 120 minutes (Figure 29A). One region of the explant was exposed to DEX continuously (CS) while the other region was only exposed to DFA (NS) (Figure 29B). We found no significant localization of GR-nuc-GFP in the explant at the beginning of the experiment (Figure 29D), but after 60 minutes, the CS regions exhibited a stronger localization of GR-nuc-GFP in nuclei than the NS regions (Figure 29E); the trend continued over 120 minutes (Figure 29F). We analyzed the subcellular spatial pattern of cell responses by calculating the ratio of the GFP intensity in the subcellular nuclear region divided by the intensity in the subcellular cytoplasmic region (Figure 29G). Quantitatively, CS regions of the explant had a significantly higher intensity ratio of 91% at 60 minutes when compared to the NS regions which reached steady-state by 120 minutes.

6.2.3.2 Response to spatiotemporally patterned stimulation

Simple forms of frequency stimulation such as “pulse-chase” experiments have been used to explore the role of long range factors in developing embryos (Kicheva, Pantazis et al. 2007). To investigate the developmental response of integrated embryonic tissues to complex signals we applied frequency controlled stimulation to a single AC explant. We began testing tissue responses by stimulating with a 2-minute periodic flow with a 50% duty cycle (we define the duty cycle as the fraction of the period that the localized region of the explant is exposed to DEX) for 120 minutes over the center region (PS) while maintaining CS and NS over other

regions (Figure 30A, B). Responses to continuous, periodic, and no stimulation were qualitatively similar to earlier experiments (Figure 30C through F). The cells in the CS region exhibited significant increases in the number of GFP-labeled nuclei (Figure 30D through F).

In contrast to the CS region, some cells in the PS region showed apparent translocation while other cells had little response. Cells in the NS region had very few significant changes in intensities. A higher magnification image provided more spatial details on events at the critical interfacial region (see rectangular region in Figure 30B; response after 0, 60, and 120 minutes in Figure 30G, H, I respectively). Cells within this region were neither “on” nor “off” but rather they had higher or lower nuclear intensities compared to the cytoplasm, indicating a more nuanced response to the temporally complex chemical microenvironment in this region (Figure 30J). By applying continuous and periodic stimulation with the microfluidic control system, we were able to elicit spatially distinct responses within a single tissue explant.

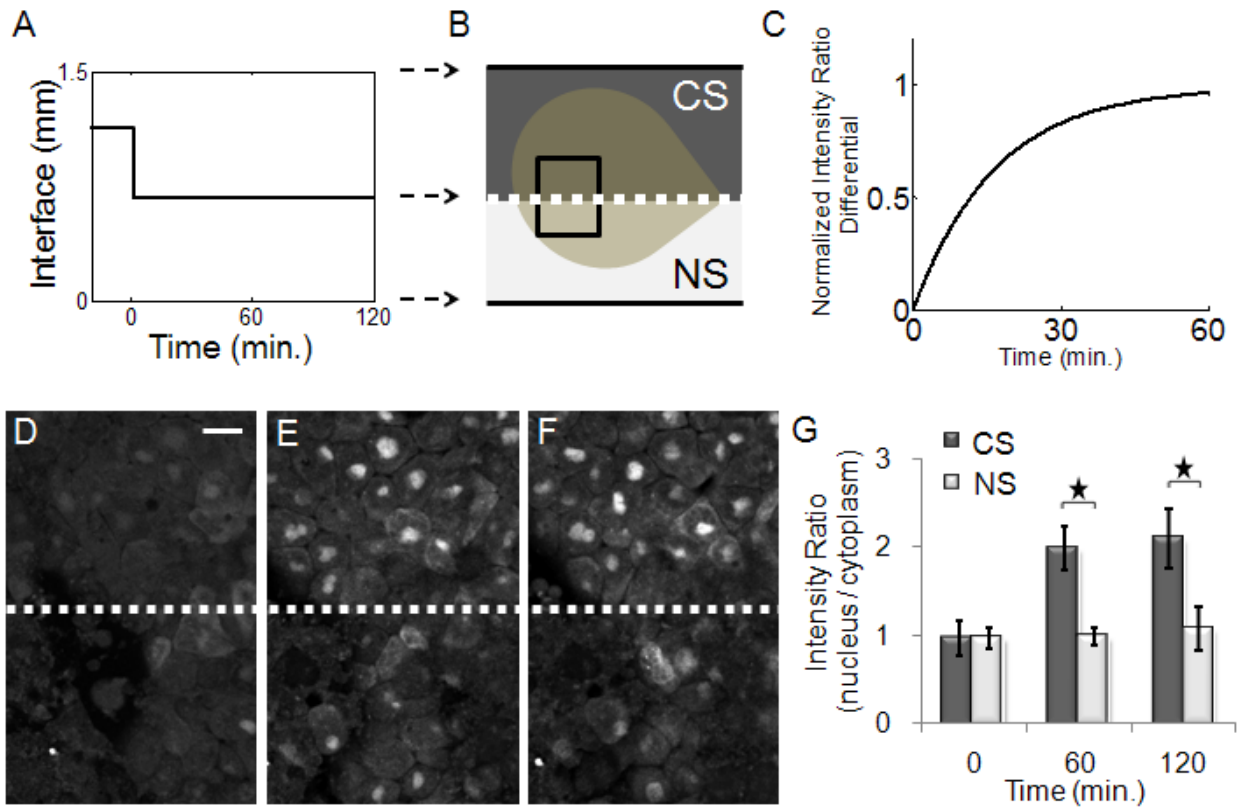

Figure 29. Localized response to spatially defined continuous stimulation.

(A) Laminar flow interface profile over time. (B) Schematic showing two regions within a single AC explant constant stimulation (CS) and no stimulation (NS). (C) Simulated response to CS. (D through F) Images of the explant subjected to CS and NS (from B) at 0, 60 and 120 minutes. The scale bar is 20 µm. The dotted line marks the interface (correlates to the dotted line in B). (G) Intensity ratios of GFP levels in nucleus relative to cytoplasm. Error bars represent standard deviations for 20 cells (* indicates p<0.01).

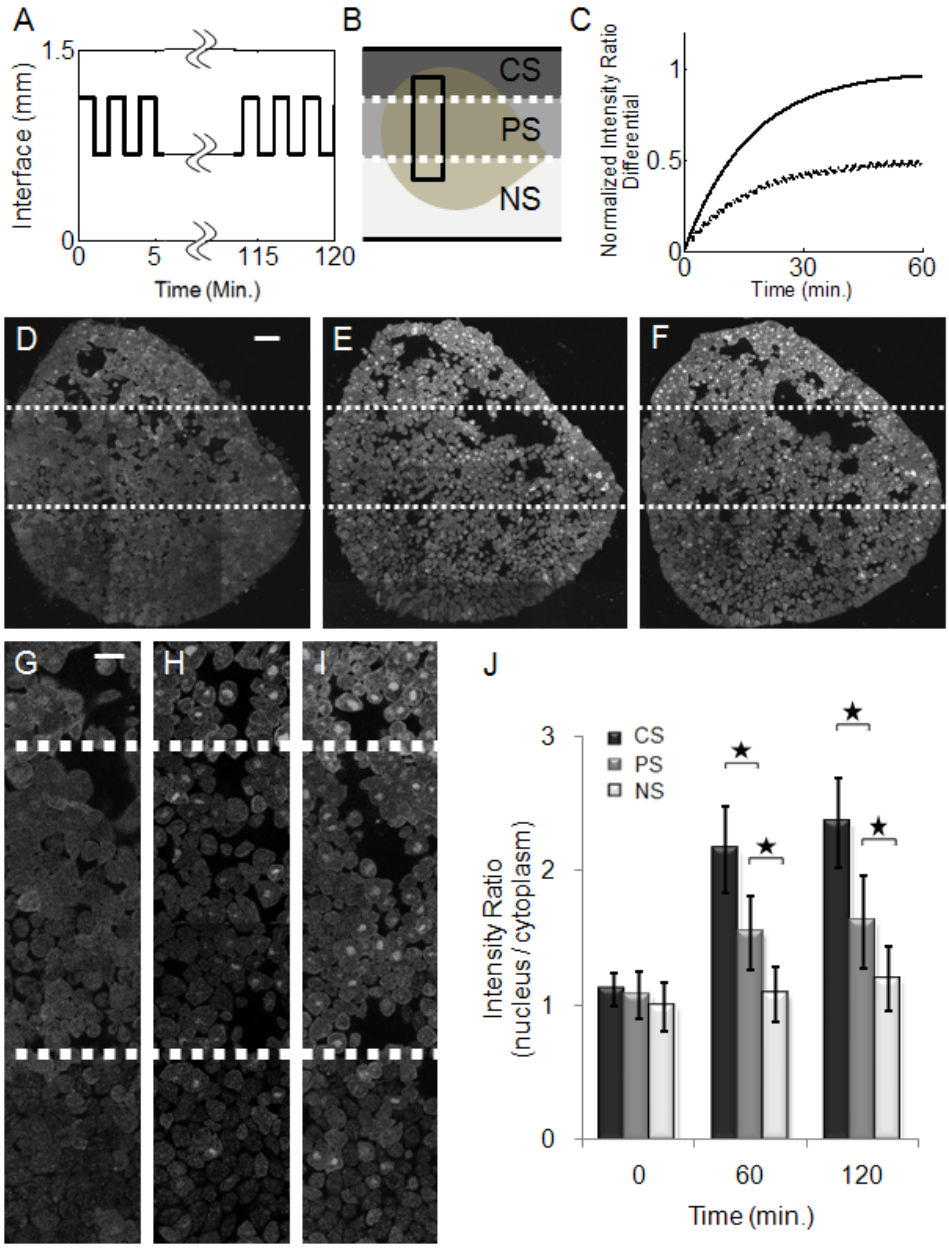

Figure 30. Localized response to spatiotemporal periodic stimulations with 50% duty cycles.

(A) Laminar flow interface profile over time. (B) Schematic showing three regions of a single AC explant exposed to different stimulation conditions: CS, 2-minute 50% duty cycle PS, and NS. The dotted lines mark the interfaces. (C) Simulated response to CS and PS. (D through F) AC explants exposed to CS, PS, and NS regions of (in B) at 0, 60 and 120 minutes. The scale bar is 100 µm. (G through I) High resolution images of explants shown in D, E, and F. The scale bar is 25 µm. (J) Intensity ratios of GFP in the nucleus versus cytoplasmic intensities. Error bars represent standard deviations for 20 cells (* indicates p<0.01).

6.2.3.3 Response to temporally patterned stimulation

To investigate the dynamics of the DEX/ GR-nuc-GGFP signaling and transport system we applied a more complex program of stimulation. We wondered whether cells could "integrate" a stimulating signal or whether only concentration was sensed. For instance, whether an explant responds the same to 50% stimulation over a certain time period as it would respond to alternating stimuli between zero and 100% for equal amounts of time; or whether an explant exposed to 100% stimulation followed by an "off" cycle simply resumes its response at the same level when the 100% stimulation is reapplied. Using time-lapse confocal microscopy we tracked responses of 30 individual cells from 3 explants (10 cells in each explant) exposed to continuous (squares) and periodic stimulation (40 minute - diamonds; 10 minute - circles; 2 minute - triangles in Figure 31A). In general, the stimulation profiles approach a constant level after 60 minutes, however we found translocation can reverse in cases of longer period stimulation (Figure 32, 33, 34, and 35). In addition, the cell responses to 2-minute and 10-minute periodic stimulations with 50% duty cycles were both approximately half the response to continuous stimulation. In contrast, the response to the 40-minute periodic stimulation with 50% duty cycle was approximately the same as the response of the continuous stimulation for the first 20 minutes (the "on" part of the period) and then decreased between 20 minutes to 40 minutes (the "off" part of the period). The response again increased between 40 minutes and 60 minutes (the "on" part of the second period; Figure 31A). Thus, we conclude that responses to periodic stimulation depend on the duration, frequency, and duty cycle of the stimulus and that manipulating the duty cycle can be used to mimic stimulation with lower concentrations of DEX.

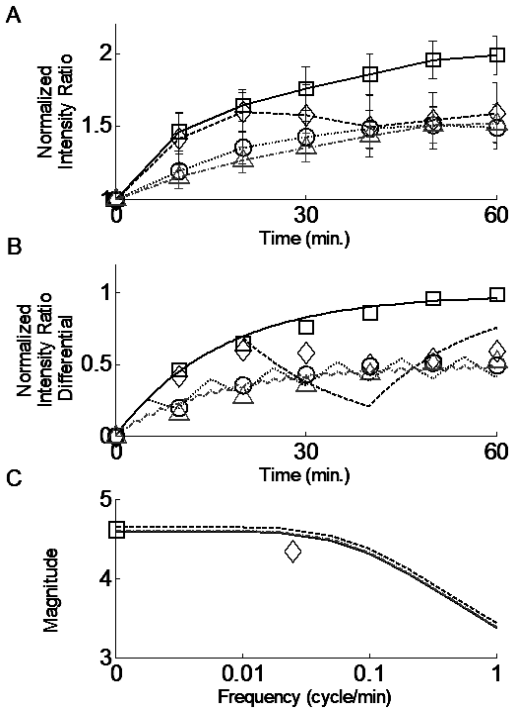

Figure 31. Experimental and first-order differential predicted responses of individual cells.

(A) Responses of 30 individual tracked cells from 3 different tissue explants to four different stimulation cases with different duty cycles: CS (squares), 40-minute 50% duty cycle PS (diamonds), 10-minute 50% duty cycle PS (circles), and 2-minute 50% duty cycle PS (triangles). Error bars indicate standard deviations. (B) Using the data from CS results, a mathematical model was constructed using a first-order differential equation. The parameters reproducing the response to CS were applied to the other PS cases to predict their response without any additional parameters (modeled CS, solid; modeled 40-minute PS, dashed; modeled 10-minute PS, dotted; and modeled 2-minute PS, dashdot). The modeled results closely approximate experimental results (CS, rectangles; 40-minute PS, diamonds; 10-minute PS, circles; 2-minute PS, triangles). (C) Frequency responses of three different PS profiles: 40-minute (0.025 cycle/min), 10-minute (0.1 cycle/min), and 2-minute (0.5 cycle/min). The lines come from the transfer function with a time constant of 16.6 minutes and the different constants K_{DC} for each stimulation case (see Materials and Methods; response in CS, square; response in 40-minute PS region, diamonds).

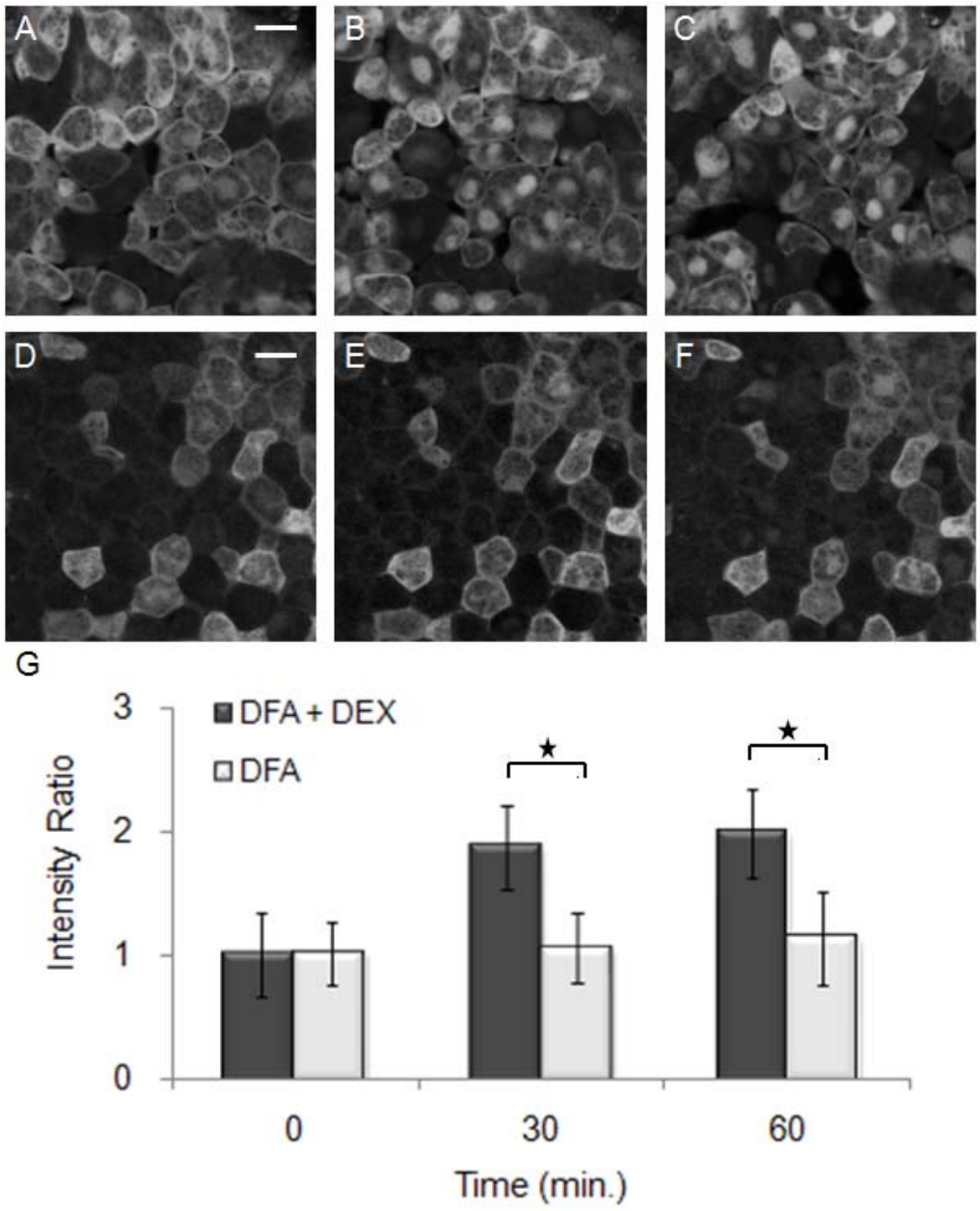

Figure 32. Microscopy images and responses of the tissue explant to continuous stimulation.

(A through C) Continuously stimulated AC explants with DEX at 0 minutes (A), 30 minutes (B), and 60 minutes (C). (D through F) Control regions without DEX at 0 minutes (D), 30 minutes (E), and 60 minutes (F). (G) Ratio of the intensity in the nucleus to the cytoplasm over time. Error bars represent standard deviations for 20 cells. The scale bar is 20 µm.

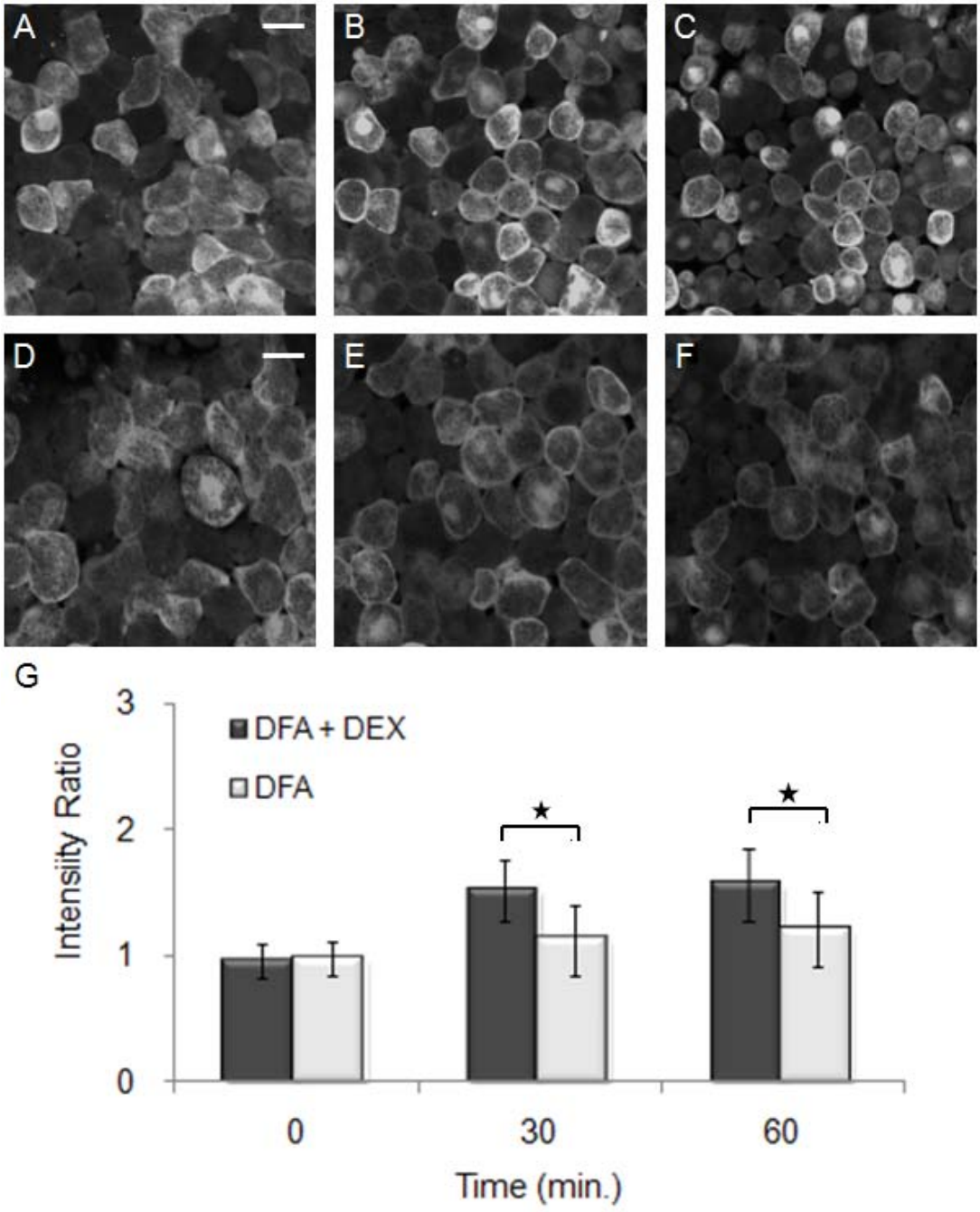

Figure 33. Response of the tissue explant to 40-minute 50% duty cycle periodic stimulation.

(A through C) 40-minute 50% duty cycle periodically stimulated AC explants with DEX at 0 minutes (A), 30 minutes (B), and 60 minutes (C). (D through F) Control regions without DEX at 0 minutes (D), 30 minutes (E), and 60 minutes (F). (G) Ratio of the intensity in the nucleus to the cytoplasm over time. Error bars represent standard deviations for 20 cells. The scale bar is 20 µm.

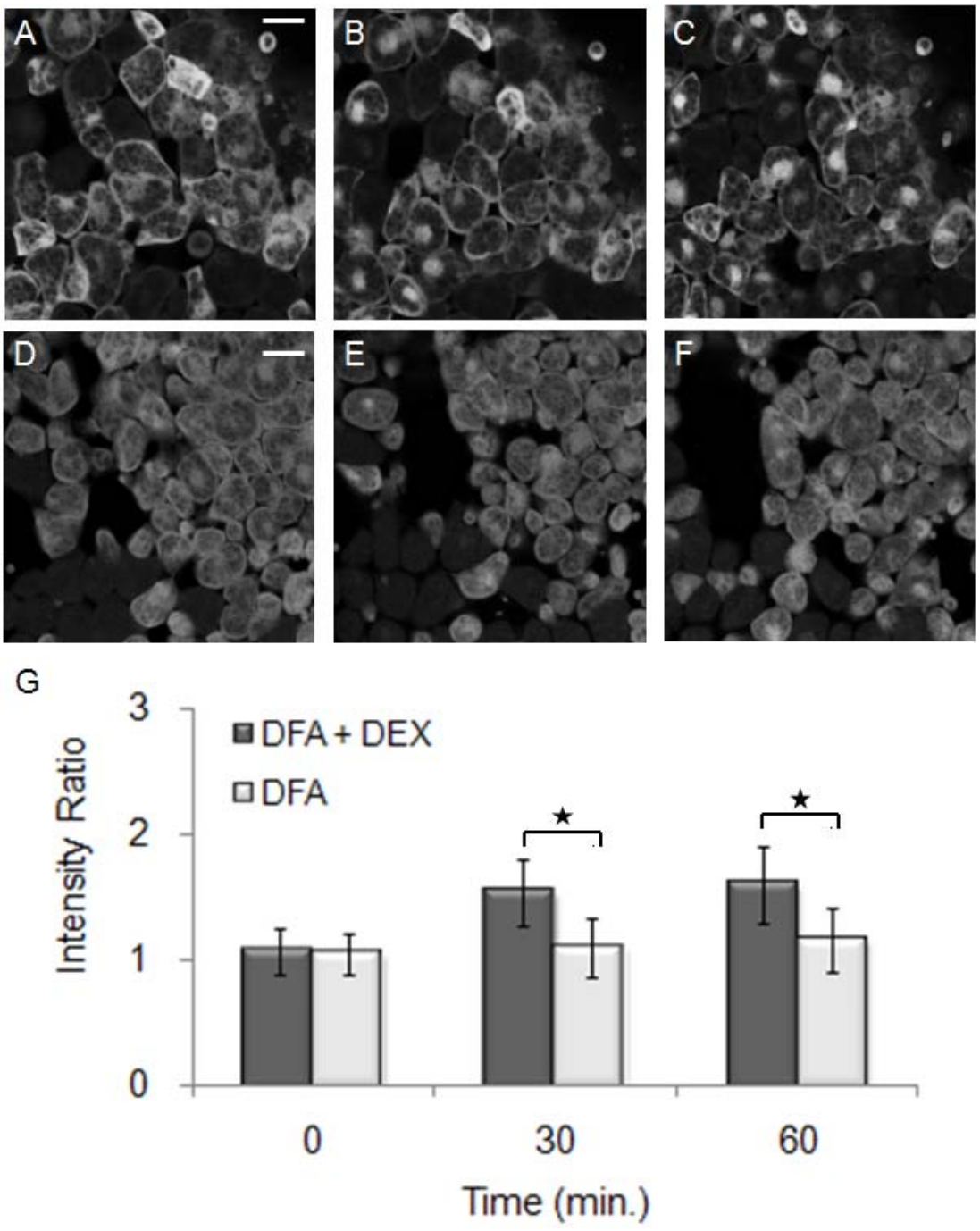

Figure 34. Response of the tissue explant to 10-minute 50% duty cycle periodic stimulation.

(A through C) 10-minute 50% duty cycle periodically stimulated AC explants with DEX at 0 minutes (A), 30 minutes (B), and 60 minutes (C). (D through F) Control regions without DEX at 0 minutes (D), 30 minutes (E), and 60 minutes (F). (G) Ratio of the intensity in the nucleus to the cytoplasm over time. Error bars represent standard deviations for 20 cells. The scale bar is 20 µm.

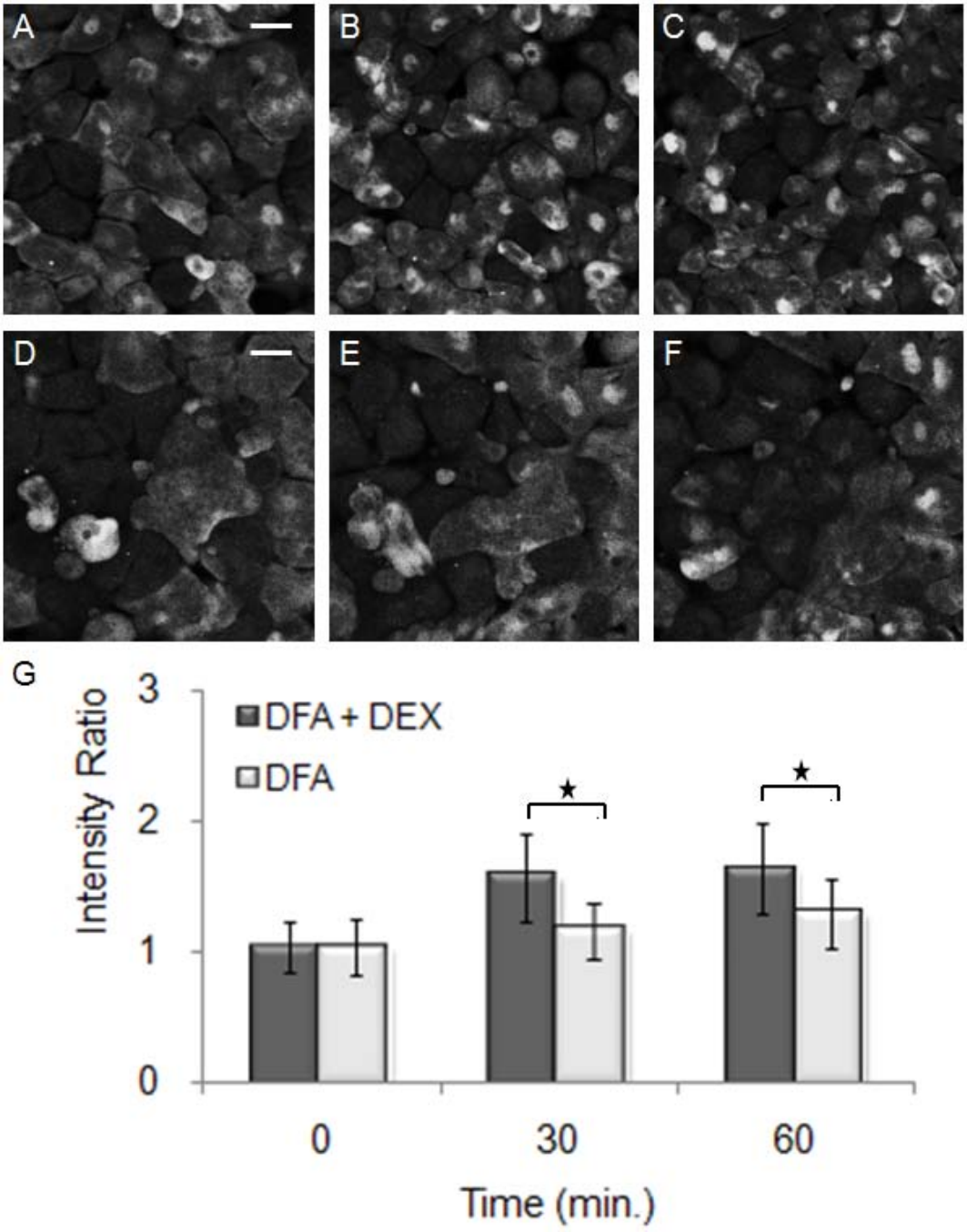

Figure 35. Response of the tissue explant to 2-minute 50% duty cycle periodic stimulation.

(A through C) 2-minute 50% duty cycle periodically stimulated AC explants with DEX at 0 minutes (A), 30 minutes (B), and 60 minutes (C). (D through F) Control regions without DEX at 0 minutes (D), 30 minutes (E), and 60 minutes (F). (G) Ratio of the intensity in the nucleus to the cytoplasm over time. Error bars represent standard deviations for 20 cells. The scale bar is 20 µm.

6.2.3.4 Modeling the response to temporally patterned stimulation

The response to the continuous stimulation suggested that input-output dynamics of the cellular responses could be modeled as a simple first-order function and that more complex stimulation programs could be understood within the same model framework. We chose to model response to continuous stimulation as a first-order differential equation (Figure 36). Using parameters that reproduced the response to continuous stimulation, we then used these equations to model the translocation response to more complex frequency-dependent stimulation by 40-, 10-, and 2-minute profiles with 50% duty cycle (Figure 31B). The simulated and observed responses are remarkably similar and reveal that the "input-output" response of a complex multicellular tissue to complex patterns of stimulation can be predicted by a systems-based model. Responses showed only slightly different magnitudes at zero frequency for CS and PS cases as steady-state responses to PS were approximately half the response to CS (Figure 31B). Transient responses between the “on” and “off” portions of the 10- and 2-minute periods lie below the temporal resolution of our experiments; however, the pattern of response is consistent with the signaling pathway acting as low-pass filter having a cut-off frequency of approximately 0.06 cycles per minute. Thus, quantification and close examination of the systematic response to different stimulation programs (i.e. complex time-dependent “input” functions) reveals the biophysical principles that may guide responses to spatially and temporally complex stimulation through the chemical microenvironment.

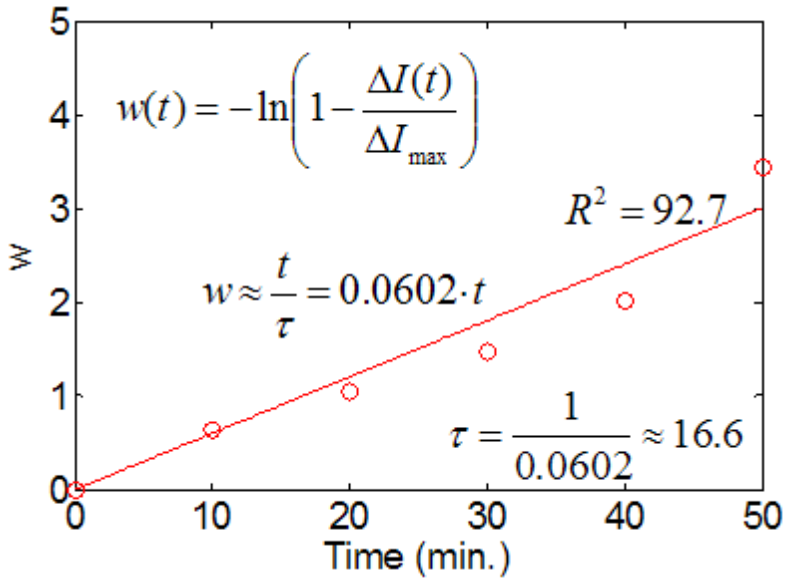

Figure 36. Plot and formulas showing a least square fitting to find the time constant.

The plot shows $w(t)$ over time, which was obtained from the exponential function of the intensity ratio. We applied a least square fitting to find the linear slope from the plot and the time constant.

6.3 DISCUSSION

Gradients of chemical factors drive emergent phenomena in embryos by stimulating cascades of cell signaling, gene regulatory networks, cell motility, and cell differentiation. Together, these cues provide positional information to establish distinct cell identities. As morphogenesis begins, gradients provide permissive polarity cues telling cells their orientation within a field and provide instructional guidance to direct cell rearrangement or movement. The extent and role of gradients in vivo continues to be debated (Wolpert 2009). By providing explicit spatial and temporal control over chemical gradients our study marks a key advance in studying the function of gradients as they interact with responsive embryonic tissues.

These spatiotemporal responses are hallmarks of a wide range of physical chemical and biological systems and understanding them provides tremendous insight to fundamental emergent patterns that may evolve within complex systems. For example, many systems can be approximated by first-order differential equations of constant coefficients. Examples include resistor-capacitor circuits, thermal systems (Close 2003), radioactive decay, decomposition of dinitrogen pentoxide (Ebbing 2002), and population growth (Campbell 1999). In each of these systems, the behaviors of individual components (e.g. electrons, atoms, molecules, or organisms) are quite complex, but collectively the components produce emergent behavior that can be simply modeled. The interaction of multitudes of components in an intricate arrangement, which results in emergent responses, has been a focus in the field of complexity (Waldrop 1992; Gell-Mann 1995). The concept of complexity has been successfully applied to study a range of problems from small scale systems such as cell and molecular interactions and large scale

systems such as population dynamics and the World Wide Web (Dorogovtsev and Mendes 2002; Newman 2003). We have found that the dynamics of an "input-output" system, DEX and GR-nuc-GFP, respectively, studied here resembles the dynamics of a resistor-capacitor network in that it has a well-defined input that can be externally manipulated, and the response of the system to standard test inputs (e.g. step inputs or pulses) are useful for deducing parameters of the collective behavior. Our system provides the methodology for manipulating these biochemical inputs to examine and model the collective behavior of many biochemical reactions.

In this study we observe a generalized response from a system comprised of hundreds of cells where each cell has millions of interacting molecules. Remarkably, the entire system of these molecular behaviors can be captured with a first-order reaction. Thus, by analogy with other complex biological systems our study reveals the emergence of potential governing or unifying relationships at the macro-scale.

7.0 SUMMARY AND CONCLUSIONS

7.1 SUMMARY OF FINDINGS

We carried out studies into the molecular and kinematic aspects of induced contraction in frog embryonic tissues and began an effort to utilize microfluidic-environment to have a spatiotemporal control over developmental processes in embryonic tissue explants. In Chapter 3, by comparing the contractions induced by three independent stimulation methods (Figure 37), we found 1) several similarities in the contraction kinematics (delay-to-contraction, contraction duration and time-to-peak) among the three methods 2) some dissimilarities where laser-activation method induced “overshoot” response as well as two contraction waves in comparison to just one contraction in the other two methods 3) rapid F-actin remodeling as a downstream effect of all the three induced contractions. Because there were many similarities in cellular responses, we utilized the unique and complementary advantages to answer questions about embryonic contractility from molecular, biochemical and mechanical perspectives. In Chapter 4 and 5, we wanted to by evaluate the developmental aspects of nano-perfusion induced contractility and utilize laser-activation to understand real-time changes in the dynamic cell cytoskeleton. We found: 1) extracellular nucleotides/ nucleosides were primary candidates within cell lysate capable of stimulating contraction, 2) embryos were sensitive to stimulations from the onset of gastrulation and remained sensitive throughout gastrulation, 3) cytoskeletal drugs reduced contraction strength and modulated contraction kinematics; strongest inhibition

was observed with blebbistatin, an inhibitor of myosin II heavy chain ATPase activity, 4) microtubules did not undergo dynamic polymerization as F-actin filaments and the rho-reporting protein. In Chapter 6, we extended our nano-perfusion approach to a microfluidics-controlled environment where we created spatiotemporal gradients of differentially responding cells in a single multicellular tissue. We found that the overall response of the embryonic tissue was first order.

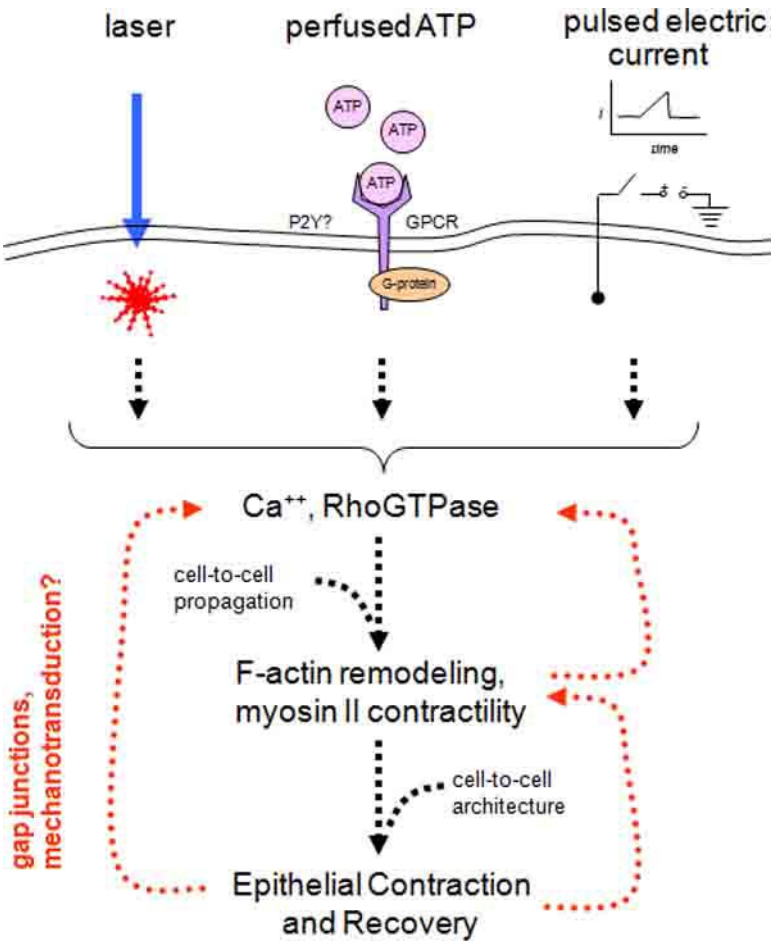

Figure 37. Three stimulation methods may a signaling pathway leading to contraction.

7.2 SIGNIFICANCE OF FINDINGS

Completion of the three aims allowed us to design and characterize four methods for manipulating embryonic cell behaviors. We were able to reveal the susceptibility of frog embryos to induced contractions as well as the ability of a multicellular tissue to follow a first order rate equation when subjected to spatiotemporal control. We identified trigger molecules and revealed the importance of contractility in embryonic development.

First, we found that three exogenous methods (electric stimulus, nano-perfusion and laser-activation) were able to induce consistent contractions in developing embryos. The contraction response to these three stimuli share several kinematic characteristics such as time duration of contractions and the delay between stimulus and the beginning of contractions. These studies of cell contraction allow us to develop tools to understand how cells change shape and to manipulate cell shapes. The three methods may share certain aspects of cell signaling leading to contraction (Figure 37).

Several birth defects are caused due to altered cell behaviors and our research can provide insight regarding these causes (Wallingford, Fraser et al. 2002; Kibar, Capra et al. 2007). Based on our studies, we suggest to combine these approaches to understand the contribution of the molecular, mechanical and morphological aspects to the changes in cell shapes.

Second, exogastrulation in frog embryos is a relatively common occurrence in a lab studying frog development. Traditionally, new graduate students in the lab are instructed to remove defective embryos from a dish of healthy embryos. It was thought that the defective embryos are harmful to surrounding healthy embryos. However, little was known about what factors or signaling mechanisms could harm healthy embryos. Our studies demonstrated that cell

lysate or wound extracts alone can induce contractions in healthy embryos. Continuous culture of the defective embryos with healthy ones could provide a constant source of contraction-stimulation which drives healthy embryos to exogastrulate. We also identified several nucleotides and nucleosides within cell lysate that can induce contraction and that ATP is a primary candidate, able to induce both transient contraction and induce exogastrulation. Our study suggests gastrulation defects can result from chronically induced cell contraction from signaling nucleotides.

Third, we extended our simple perfusion approaches by introducing microfluidic feedback control. We were able to culture frog tissues in the microfluidic environment. To the best of our knowledge this is the first time multicellular vertebrate tissues were cultured inside closed channels. Using microfluidic spatiotemporal control over fluid flow in a microchannel containing excised tissue, we demonstrated a first order response of the tissue to stimulation. This control system that can be further extended to answer long standing questions in development. Biological gradients have been studied using different experimental and computer simulation methods (Wilson and Melton 1994; Butler, Tsou et al. 2002; Green 2002; Kicheva, Pantazis et al. 2007; Francois, Vonica et al. 2009) and now we provide a sophisticated approach to study gradients and mimic different physiological tissue types within a single multicellular tissue. Forming and controlling gradients has been a dream among biologists and engineers and our studies provide a new methodology to realize that dream (Smith 2009).

7.3 FUTURE DIRECTIONS

We identified nucleotides as primary candidate stimuli capable of inducing contractions resulting in severe exogastrulation in developing frog embryos. We demonstrated that F-actin and Myosin II play significant roles in driving or coordinating cell contraction. We have also investigated the downstream effectors of cell contraction as well as the developmental consequences of these induced contractions. These results represent a significant step in the direction of identifying gastrulation defects from cell contraction. Many questions remain unanswered. First, what receptors transduce the ATP/ UTP signal? We have not yet identified the specific receptors that transduce these signals. Purinergic family of receptors, P2X and P2Y, may play a critical role to transduce the signal triggered by cell lysate or ATP. We suspect that one or more purinergic receptors of the P2Y class play a significant role in this process. There is evidence that P2Y receptors play significant roles during development (Yen, Herman et al. 1997; Devader, Drew et al. 2007; Burnstock 2008) and it is quite likely that one of the receptors plays the transduction role in case of the nucleotide-triggered cell contraction (Bogdanov, Dale et al. 1997; Bolego, Ceruti et al. 1997; Schwiebert and Zsembery 2003). Further studies will be needed to resolve physiological roles of nucleotides as well as provide a new methodology to permanently switch cells between contracted and relaxed morphologies.

Future molecular studies are necessary to reveal what factors mediate the contraction event, and what factors transduce the signals within cells and between neighbors. It is possible that there are different receptors for each nucleotide/ nucleoside and further in depth investigation is quite critical to identify this aspect of cell contraction.

We researched the multicellular contraction triggered by laser-activation of a single cell in a cell sheet and explored the downstream effects of the triggered contraction. Currently, we do

not understand the trigger mechanism underlying the laser-activation, but it is possible that reactive oxygen species are generated via laser-activation. We also do not understand the signal propagation in this phenomenon which is another avenue for investigation. Using cytoskeletal drugs we were not able to significantly reduce the contraction strength which could be a result of change in tissue properties. We hypothesize that softer tissue (tissues with smaller Young's modulus resulting from treatments with cytoskeletal drugs) can contract to the same extent as a normal tissue would, with a depleted cytoskeleton. Further studies involving simulation models will test this hypothesis.

We created a microfluidic environment to culture frog embryonic tissues. These studies demonstrated our capability to have control fluid flow spatiotemporally over several hours. In future, this method can be extended to 1) create biological gradients in a single multicellular tissue 2) induce cell contraction in a more precise and controlled manner.

BIBLIOGRAPHY

Adams, C. L., W. J. Nelson, et al. (1996). "Quantitative analysis of cadherin-catenin-actin reorganization during development of cell-cell adhesion." J Cell Biol **135**(6 Pt 2): 1899-911.

Alenghat, F. J., S. M. Nauli, et al. (2004). "Global cytoskeletal control of mechanotransduction in kidney epithelial cells." Exp Cell Res **301**(1): 23-30.

Anderson, R. H., M. J. Janse, et al. (1974). "A combined morphological and electrophysiological study of the atrioventricular node of the rabbit heart." Circ. Res. **35**: 909-922.

Andrew, D. J. and A. J. Ewald (2009). "Morphogenesis of epithelial tubes: Insights into tube formation, elongation, and elaboration." Dev Biol.

Ariizumi, T., M. Kinoshita, et al. (2003). "Amphibian in vitro heart induction: a simple and reliable model for the study of vertebrate cardiac development." International Journal of Developmental Biology **47**(6): 405-10.

Armstrong, M. T. and P. B. Armstrong (1992). "Mechanisms of epibolic tissue spreading analyzed in a model morphogenetic system. Roles for cell migration and tissue contractility." J Cell Sci **102 (Pt 2)**: 373-85.

Atkinson, M. M., S. L. Midland, et al. (1996). "Syringolide 1 Triggers Ca2+ Influx, K+ Efflux, and Extracellular Alkalization in Soybean Cells Carrying the Disease-Resistance Gene Rpg4." Plant Physiol **112**(1): 297-302.

Axelrod, J. D. (2006). "Cell shape in proliferating epithelia: a multifaceted problem." Cell **126**(4): 643-5.

Barry, V. A. and T. R. Cheek (1994). "Extracellular ATP triggers two functionally distinct calcium signalling pathways in PC12 cells." J Cell Sci **107 (Pt 2)**: 451-62.

Beloussov, L. V., A. V. Lakirev, et al. (1988). "The role of external tensions in differentiation of Xenopus laevis embryonic tissues." Cell Differ Dev **25**(3): 165-76.

Bement, W. M., C. A. Mandato, et al. (1999). "Wound-induced assembly and closure of an actomyosin purse string in Xenopus oocytes." Curr Biol **9**(11): 579-87.

Bendix, P. M., G. H. Koenderink, et al. (2008). "A quantitative analysis of contractility in active cytoskeletal protein networks." Biophys J **94**(8): 3126-36.

Benink, H. A. and W. M. Bement (2005). "Concentric zones of active RhoA and Cdc42 around single cell wounds." J Cell Biol **168**(3): 429-39.

Benko, R. and G. W. Brodland (2007). "Measurement of in vivo stress resultants in neurulation-stage amphibian embryos." Ann Biomed Eng **35**(4): 672-81.

Blacklow, S. C., R. T. Raines, et al. (1988). "Triosephosphate isomerase catalysis is diffusion controlled. Appendix: Analysis of triose phosphate equilibria in aqueous solution by 31P NMR." Biochemistry **27**(4): 1158-67.

Bogdanov, Y. D., L. Dale, et al. (1997). "Early expression of a novel nucleotide receptor in the neural plate of Xenopus embryos." J Biol Chem **272**(19): 12583-90.

Bolego, C., S. Ceruti, et al. (1997). "Characterization of the signalling pathways involved in ATP and basic fibroblast growth factor-induced astrogliosis." Br J Pharmacol **121**(8): 1692-9.

Botto, L. D., C. A. Moore, et al. (1999). "Neural-tube defects." N Engl J Med **341**(20): 1509-19.

Bourguignon, L. Y. (1980). "Simultaneous localization of intracellular myosin and surface concanavalin A receptor clusters using immuno-electron microscopy." Cell Biol Int Rep **4**(6): 541-7.

Brenner, M. P., L. S. Levitov, et al. (1998). "Physical mechanisms for chemotactic pattern formation by bacteria." Biophys J **74**(4): 1677-93.

Bub, G. and A. Shrier (2002). "Propagation through heterogeneous substrates in simple excitable media models." Chaos **12**: 747-753.

Bugyi, B., C. Le Clainche, et al. (2008). "How do in vitro reconstituted actin-based motility assays provide insight into in vivo behavior?" FEBS Lett **582**(14): 2086-92.

Burkel, B. M., G. von Dassow, et al. (2007). "Versatile fluorescent probes for actin filaments based on the actin-binding domain of utrophin." Cell Motil Cytoskeleton **64**(11): 822-32.

Burnstock, G. (2008). "Purinergic signalling and disorders of the central nervous system." Nat Rev Drug Discov **7**(7): 575-90.

Butler, P. J., T. C. Tsou, et al. (2002). "Rate sensitivity of shear-induced changes in the lateral diffusion of endothelial cell membrane lipids: a role for membrane perturbation in shear-induced MAPK activation." Faseb J **16**(2): 216-8.

Campbell, N. A., Reece, J. B., Mitchell, L. G. (1999). Biology, Addison Wesley Longman, Inc.

Charras, G. and E. Paluch (2008). "Blebs lead the way: how to migrate without lamellipodia." Nat Rev Mol Cell Biol **9**(9): 730-6.

Chen, C. S. (2008). "Mechanotransduction - a field pulling together?" J Cell Sci **121**(Pt 20): 3285-92.

Chen, C. S., M. Mrksich, et al. (1997). "Geometric control of cell life and death." Science **276**(5317): 1425-8.

Choi, E. Y., E. C. Kim, et al. (2004). "Iron chelator triggers inflammatory signals in human intestinal epithelial cells: involvement of p38 and extracellular signal-regulated kinase signaling pathways." J Immunol **172**(11): 7069-77.

Clark, A. G., A. L. Miller, et al. (2009). "Integration of single and multicellular wound responses." Curr Biol **19**(16): 1389-95.

Close, C. M., Frederick, D. K., Newell, J. C. (2003). Modeling and Analysis of Dynamic Systems, Wiley**:** 592.

Cohen, S., S. Au, et al. (2009). "Microinjection of *Xenopus laevis* oocytes." J Vis Exp(24).

Coudreuse, D. Y., G. Roel, et al. (2006). "Wnt gradient formation requires retromer function in Wnt-producing cells." Science **312**(5775): 921-4.

Cowin, S. C. (2000). "How is a tissue built?" J Biomech Eng **122**(6): 553-69.

Cross, M. K. and M. Powers (2008). "Obtaining eggs from *Xenopus laevis* females." J Vis Exp(18).

Cyr, J. L., R. A. Dumont, et al. (2002). "Myosin-1c interacts with hair-cell receptors through its calmodulin-binding IQ domains." J Neurosci **22**(7): 2487-95.

Daniels, B. R., B. C. Masi, et al. (2006). "Probing single-cell micromechanics in vivo: the microrheology of C. elegans developing embryos." Biophys J **90**(12): 4712-9.

Davidson, L. A., A. M. Ezin, et al. (2002). "Embryonic wound healing by apical contraction and ingression in *Xenopus laevis*." Cell Motil Cytoskeleton **53**(3): 163-76.

Davidson, L. A., R. Keller, et al. (2004). "Patterning and tissue movements in a novel explant preparation of the marginal zone of Xenopus laevis." Gene Expression Patterns **4**(4): 457-466.

Dawes-Hoang, R. E., K. M. Parmar, et al. (2005). "folded gastrulation, cell shape change and the control of myosin localization." Development **132**(18): 4165-78.

De Marco, P., E. Merello, et al. (2006). "Mutational screening of the CYP26A1 gene in patients with caudal regression syndrome." Birth Defects Res A Clin Mol Teratol **76**(2): 86-95.

Devader, C., C. M. Drew, et al. (2007). "A novel nucleotide receptor in Xenopus activates the cAMP second messenger pathway." FEBS Lett **581**(27): 5332-6.

Domingo, C. and R. Keller (1995). "Induction of notochord cell intercalation behavior and differentiation by progressive signals in the gastrula of Xenopus laevis." Development **121**(10): 3311-21.

Dorogovtsev, S. N. and J. F. F. Mendes (2002). "Evolution of networks." Advances in Physics **51**: 1079-1187.

Drews, U. and W. Mengis (1990). "Contraction wave in the chick blastoderm induced by muscarinic stimulation." Anat Embryol (Berl) **182**(5): 447-54.

Ebbing, D., Gammon, S. (2002). General Chemistry, Houghton Mifflin.

Fackler, O. T. and R. Grosse (2008). "Cell motility through plasma membrane blebbing." J Cell Biol **181**(6): 879-84.

Farge, E. (2003). "Mechanical induction of Twist in the Drosophila foregut/stomodeal primordium." Curr Biol **13**(16): 1365-77.

Ferguson, S. S. and M. G. Caron (1998). "G protein-coupled receptor adaptation mechanisms." Semin Cell Dev Biol **9**(2): 119-27.

Francois, P., A. Vonica, et al. (2009). "Scaling of BMP gradients in Xenopus embryos." Nature **461**(7260): E1; discussion E2.

Freeman, M. (2000). "Feedback control of intercellular signalling in development." Nature **408**(6810): 313-319.

Fristrom, D. (1988). "The cellular basis of epithelial morphogenesis. A review." Tissue Cell **20**(5): 645-90.

Frixione, E., R. Lagunes, et al. (2003). "Mechanical responses of single non-confluent epithelial cells to low extracellular calcium." J Muscle Res Cell Motil **24**(7): 477-85.

Gell-Mann, M. (1995). What is complexity?, John Wiley and Sons, Inc.

Ghosh, K. and D. E. Ingber (2007). "Micromechanical control of cell and tissue development: implications for tissue engineering." Adv Drug Deliv Rev **59**(13): 1306-18.

Gjorevski, N. and C. M. Nelson (2010). "Branch formation during organ development." Wiley Interdiscip Rev Syst Biol Med **2**(6): 734-41.

Glotzer, M. (1997). "The mechanism and control of cytokinesis." Curr Opin Cell Biol **9**(6): 815-23.

Gov, N. S. and S. A. Safran (2005). "Red blood cell membrane fluctuations and shape controlled by ATP-induced cytoskeletal defects." Biophys J **88**(3): 1859-74.

Green, J. (2002). "Morphogen gradients, positional information, and Xenopus: interplay of theory and experiment." Dev Dyn **225**(4): 392-408.

Haigo, S. L., J. D. Hildebrand, et al. (2003). "Shroom induces apical constriction and is required for hingepoint formation during neural tube closure." Curr Biol **13**(24): 2125-37.

Hardin, J. (1988). "The role of secondary mesenchyme cells during sea urchin gastrulation studied by laser ablation." Development **103**(2): 317-24.

Harland, R. M. (1991). "In situ hybridization: an improved whole-mount method for *Xenopus* embryos." Methods Cell Biol **36**: 685-95.

He, J. and L. G. Baum (2004). "Presentation of galectin-1 by extracellular matrix triggers T cell death." J Biol Chem **279**(6): 4705-12.

Heitzler, D., P. Crepieux, et al. (2009). "Towards a systems biology approach of-G protein-coupled receptor signalling: challenges and expectations." C R Biol **332**(11): 947-57.

Hlavacek, W. S. and J. R. Faeder (2009). "The complexity of cell signaling and the need for a new mechanics." Sci Signal **2**(81): pe46.

Hoque, M. T., G. Conseil, et al. (2009). "Involvement of NHERF1 in apical membrane localization of MRP4 in polarized kidney cells." Biochem Biophys Res Commun **379**(1): 60-4.

Htun, H., J. Barsony, et al. (1996). "Visualization of glucocorticoid receptor translocation and intranuclear organization in living cells with a green fluorescent protein chimera." Proc Natl Acad Sci U S A **93**(10): 4845-50.

Huang, S. and D. E. Ingber (2005). "Cell tension, matrix mechanics, and cancer development." Cancer Cell **8**(3): 175-6.

Hutson, M. S., Y. Tokutake, et al. (2003). "Forces for morphogenesis investigated with laser microsurgery and quantitative modeling." Science **300**(5616): 145-9.

Ingber, D. E. (2006). "Cellular mechanotransduction: putting all the pieces together again." FASEB J **20**(7): 811-27.

Jaalouk, D. E. and J. Lammerding (2009). "Mechanotransduction gone awry." Nat Rev Mol Cell Biol **10**(1): 63-73.

Jaeger, J., S. Surkova, et al. (2004). "Dynamic control of positional information in the early Drosophila embryo." Nature **430**(6997): 368-71.

Joshi, S. D. and L. A. Davidson "Live-cell imaging and quantitative analysis of embryonic epithelial cells in Xenopus laevis." J Vis Exp(39).

Joshi, S. D., M. von Dassow, et al. (2010). "Experimental control of excitable embryonic tissues: three stimuli induce rapid epithelial contraction." Exp Cell Res **316**(1): 103-14.

Joshi, S. D. and K. Webb (2008). "Variation of cyclic strain parameters regulates development of elastic modulus in fibroblast/substrate constructs." J Orthop Res **26**(8): 1105-13.

Kay, B. K. and H. B. Peng (1991). "*Xenopus laevis*: Practical Uses in Cell and Molecular Biology." Academic Press, New York.

Keller, R., L. A. Davidson, et al. (2003). "How we are shaped: the biomechanics of gastrulation." Differentiation **71**(3): 171-205.

Keller, R., J. Shih, et al. (1992). "The cellular basis of the convergence and extension of the Xenopus neural plate." Dev Dyn **193**(3): 199-217.

Keller, R. E. (1975). "Vital dye mapping of the gastrula and neurula of Xenopus laevis. I. Prospective areas and morphogenetic movements of the superficial layer." Dev Biol **42**(2): 222-41.

Keller, R. E. (1976). "Vital dye mapping of the gastrula and neurula of Xenopus laevis. II. Prospective areas and morphogenetic movements of the deep layer." Dev Biol **51**(1): 118-37.

Kelley, C. A. (1997). "Characterization of isoform diversity among smooth muscle and nonmuscle myosin heavy chains." Comp Biochem Physiol B Biochem Mol Biol **117**(1): 39-49.

Kessler, D. S. and D. A. Melton (1994). "Vertebrate embryonic induction: mesodermal and neural patterning." Science **266**(5185): 596-604.

Kibar, Z., C. M. Bosoi, et al. (2009). "Novel mutations in VANGL1 in neural tube defects." Hum Mutat **30**(7): E706-15.

Kibar, Z., V. Capra, et al. (2007). "Toward understanding the genetic basis of neural tube defects." Clin Genet **71**(4): 295-310.

Kicheva, A., P. Pantazis, et al. (2007). "Kinetics of morphogen gradient formation." Science **315**(5811): 521-5.

Kim, Y., B. Kuczenski, et al. (2009). "Modulation of fluidic resistance and capacitance for long-term, high-speed feedback control of a microfluidic interface." Lab Chip **9**(17): 2603-9.

Kintner, C. R. and J. P. Brockes (1984). "Monoclonal antibodies identify blastemal cells derived from dedifferentiating limb regeneration." Nature **308**(5954): 67-9.

Klemm, A. H., K. Suchodolski, et al. (2006). "Mechano-chemical signaling in F9 cells." Cell Biol Int **30**(9): 755-9.

Kolm, P. J. and H. L. Sive (1995). "Efficient hormone-inducible protein function in Xenopus laevis." Dev Biol **171**(1): 267-72.

Kowalczyk, B., M. Byrska, et al. (2009). "Nanoparticle-based solution deposition of gold films supporting bioresistant SAMs." Langmuir **25**(4): 1905-7.

Kroll, K. L. and E. Amaya (1996). "Transgenic Xenopus embryos from sperm nuclear transplantations reveal FGF signaling requirements during gastrulation." Development **122**(10): 3173-83.

Kucera, P. and M. B. Burnand (1987). "Mechanical tension and movement in the chick blastoderm as studied by real-time image analysis." J Exp Zool Suppl **1**: 329-39.

Kwan, K. M. and M. W. Kirschner (2005). "A microtubule-binding Rho-GEF controls cell morphology during convergent extension of Xenopus laevis." Development **132**(20): 4599-610.

Lagunes, R., L. Ruiz, et al. (1999). "Contraction of epithelial (MDCK) cells in response to low extracellular calcium is dependent on extracellular sodium." J Muscle Res Cell Motil **20**(8): 761-70.

Lecuit, T. and P. F. Lenne (2007). "Cell surface mechanics and the control of cell shape, tissue patterns and morphogenesis." Nat Rev Mol Cell Biol **8**(8): 633-44.

Lee, C., H. M. Scherr, et al. (2007). "Shroom family proteins regulate gamma-tubulin distribution and microtubule architecture during epithelial cell shape change." Development **134**(7): 1431-41.

Lee, J. Y. and R. M. Harland (2007). "Actomyosin contractility and microtubules drive apical constriction in Xenopus bottle cells." Dev Biol **311**(1): 40-52.

Leptin, M. and B. Grunewald (1990). "Cell shape changes during gastrulation in Drosophila." Development **110**(1): 73-84.

Lewis, J. (2008). "From signals to patterns: space, time, and mathematics in developmental biology." Science **322**(5900): 399-403.

Limouze, J., A. F. Straight, et al. (2004). "Specificity of blebbistatin, an inhibitor of myosin II." J Muscle Res Cell Motil **25**(4-5): 337-41.

Litman, P., M. R. Amieva, et al. (2000). "Imaging of dynamic changes of the actin cytoskeleton in microextensions of live NIH3T3 cells with a GFP fusion of the F-actin binding domain of moesin." BMC Cell Biol **1**: 1.

Lucchetta, E. M., J. H. Lee, et al. (2005). "Dynamics of Drosophila embryonic patterning network perturbed in space and time using microfluidics." Nature **434**(7037): 1134-8.

Maekawa, M., T. Ishizaki, et al. (1999). "Signaling from Rho to the actin cytoskeleton through protein kinases ROCK and LIM-kinase." Science **285**(5429): 895-8.

Mandato, C. A. and W. M. Bement (2001). "Contraction and polymerization cooperate to assemble and close actomyosin rings around Xenopus oocyte wounds." J Cell Biol **154**(4): 785-97.

Mandato, C. A. and W. M. Bement (2003). "Actomyosin transports microtubules and microtubules control actomyosin recruitment during Xenopus oocyte wound healing." Curr Biol **13**(13): 1096-105.

Mani, S. A., W. Guo, et al. (2008). "The epithelial-mesenchymal transition generates cells with properties of stem cells." Cell **133**(4): 704-15.

Marcelli, G., K. H. Parker, et al. (2005). "Thermal fluctuations of red blood cell membrane via a constant-area particle-dynamics model." Biophys J **89**(4): 2473-80.

Martin, A. C. (2009). "Pulsation and stabilization: Contractile forces that underlie morphogenesis." Dev Biol.

Martin, A. C., M. Gelbart, et al. (2010). "Integration of contractile forces during tissue invagination." J Cell Biol **188**(5): 735-49.

Martin, A. C., M. Kaschube, et al. (2008). "Pulsed contractions of an actin-myosin network drive apical constriction." Nature.

Mathews, T. J. and M. F. MacDorman (2008). "Infant Mortality Statistics from the 2005 Period Linked Birth/Infant Death Data Set. ." National Vital Statistics Reports **57**(2).

Matsumoto, T., J. Sasaki, et al. (2007). "Three-dimensional cell and tissue patterning in a strained fibrin gel system." PLoS ONE **2**(11): e1211.

Montell, D. J., H. Keshishian, et al. (1991). "Laser ablation studies of the role of the Drosophila oocyte nucleus in pattern formation." Science **254**(5029): 290-3.

Na, S., O. Collin, et al. (2008). "Rapid signal transduction in living cells is a unique feature of mechanotransduction." Proc Natl Acad Sci U S A **105**(18): 6626-31.

Nakajima, Y. and R. D. Burke (1996). "The initial phase of gastrulation in sea urchins is accompanied by the formation of bottle cells." Dev Biol **179**(2): 436-46.

Nakayama, T., H. M. Hiep, et al. "An optimal design method for preventing air bubbles in high-temperature microfluidic devices." Anal Bioanal Chem **396**(1): 457-64.

Narumiya, S., T. Ishizaki, et al. (2000). "Use and properties of ROCK-specific inhibitor Y-27632." Methods Enzymol **325**: 273-84.

Newman, M. E. J. (2003). "The structure and function of complex network." SIAM Rev. **45**: 167

Nieuwkoop, P. D. and J. Faber (1967). "Normal Tables of *Xenopus laevis* (Daudin)." Elsevier North-Holland Biomedical Press, Amsterdam.

Ninomiya, H. and R. Winklbauer (2008). "Epithelial coating controls mesenchymal shape change through tissue-positioning effects and reduction of surface-minimizing tension." Nat Cell Biol **10**(1): 61-9.

Nobes, C. D. and A. Hall (1995). "Rho, rac, and cdc42 GTPases regulate the assembly of multimolecular focal complexes associated with actin stress fibers, lamellipodia, and filopodia." Cell **81**(1): 53-62.

Orth, J. D., E. W. Krueger, et al. (2002). "The large GTPase dynamin regulates actin comet formation and movement in living cells." Proc Natl Acad Sci U S A **99**(1): 167-72.

Painter, K. J. (2009). "Continuous models for cell migration in tissues and applications to cell sorting via differential chemotaxis." Bull Math Biol **71**(5): 1117-47.

Peralta, X. G., Y. Toyama, et al. (2007). "Upregulation of Forces and Morphogenic Asymmetries in Dorsal Closure during Drosophila Development." Biophys J **92**(7): 2583-96.

Peskin, C. S., G. M. Odell, et al. (1993). "Cellular motions and thermal fluctuations: the Brownian ratchet." Biophys J **65**(1): 316-24.

Popoff, M. R. and B. Geny (2009). "Multifaceted role of Rho, Rac, Cdc42 and Ras in intercellular junctions, lessons from toxins." Biochim Biophys Acta **1788**(4): 797-812.

Pouille, P. A., P. Ahmadi, et al. (2009). "Mechanical signals trigger Myosin II redistribution and mesoderm invagination in Drosophila embryos." Sci Signal **2**(66): ra16.

Puri, M., A. Goyal, et al. (2008). "Building proteomic pathways using Drosophila ventral furrow formation as a model." Mol Biosyst **4**(11): 1126-35.

Rau, K. R., P. A. Quinto-Su, et al. (2006). "Pulsed laser microbeam-induced cell lysis: time-resolved imaging and analysis of hydrodynamic effects." Biophys J **91**(1): 317-29.

Rauzi, M., P. Verant, et al. (2008). "Nature and anisotropy of cortical forces orienting Drosophila tissue morphogenesis." Nat Cell Biol.

Reinhart-King, C. A., M. Dembo, et al. (2005). "The dynamics and mechanics of endothelial cell spreading." Biophys J **89**(1): 676-89.

Rodriguez-Diaz, A., Y. Toyama, et al. (2008). "Actomyosin purse strings: renewable resources that make morphogenesis robust and resilient." HFSP J **2**(4): 220-37.

Rolo, A., P. Skoglund, et al. (2009). "Morphogenetic movements driving neural tube closure in Xenopus require myosin IIB." Dev Biol **327**(2): 327-38.

Rubin, G. M. (1988). "Drosophila melanogaster as an experimental organism." Science **240**(4858): 1453-9.

Sakamoto, T., J. Limouze, et al. (2005). "Blebbistatin, a myosin II inhibitor, is photoinactivated by blue light." Biochemistry **44**(2): 584-8.

Salbreux, G., J. F. Joanny, et al. (2007). "Shape oscillations of non-adhering fibroblast cells." Phys Biol **4**(4): 268-84.

Sater, A. K., R. A. Steinhardt, et al. (1993). "Induction of neuronal differentiation by planar signals in Xenopus embryos." Dev Dyn **197**(4): 268-80.

Sawyer, J. M., J. R. Harrell, et al. (2009). "Apical constriction: A cell shape change that can drive morphogenesis." Dev Biol.

Schafer, D. A., M. D. Welch, et al. (1998). "Visualization and molecular analysis of actin assembly in living cells." J Cell Biol **143**(7): 1919-30.

Schock, F. and N. Perrimon (2002). "Molecular mechanisms of epithelial morphogenesis." Annu Rev Cell Dev Biol **18**: 463-93.

Schoenwolf, G. C. and M. V. Franks (1984). "Quantitative analyses of changes in cell shapes during bending of the avian neural plate." Dev Biol **105**(2): 257-72.

Schwiebert, E. M. and A. Zsembery (2003). "Extracellular ATP as a signaling molecule for epithelial cells." Biochim Biophys Acta **1615**(1-2): 7-32.

Sherrard, K., F. Robin, et al. (2010). "Sequential Activation of Apical and Basolateral Contractility Drives Ascidian Endoderm Invagination." Curr Biol.

Shook, D. and R. Keller (2003). "Mechanisms, mechanics and function of epithelial-mesenchymal transitions in early development." Mech Dev **120**(11): 1351-83.

Slack, J. M. (2008). "Origin of stem cells in organogenesis." Science **322**(5907): 1498-501.

Smith, J. C. (2009). "Forming and interpreting gradients in the early Xenopus embryo." Cold Spring Harb Perspect Biol **1**(1): a002477.

Smith, J. C., A. Hagemann, et al. (2008). "Understanding how morphogens work." Philos Trans R Soc Lond B Biol Sci **363**(1495): 1387-92.

Smith, J. L., G. C. Schoenwolf, et al. (1994). "Quantitative analyses of neuroepithelial cell shapes during bending of the mouse neural plate." J Comp Neurol **342**(1): 144-51.

Smutny, M., H. L. Cox, et al. (2010). "Myosin II isoforms identify distinct functional modules that support integrity of the epithelial zonula adherens." Nat Cell Biol **12**(7): 696-702.

Snow, M. H. (1981). "Autonomous development of parts isolated from primitive-streak-stage mouse embryos. Is development clonal?" J Embryol Exp Morphol **65 Suppl**: 269-87.

Sofer, W. and L. Tompkins (1994). "Drosophila genetics in the classroom." Genetics **136**(1): 417-22.

Solon, J., A. Kaya-Copur, et al. (2009). "Pulsed forces timed by a ratchet-like mechanism drive directed tissue movement during dorsal closure." Cell **137**(7): 1331-42.

Sparkes, I. A. (2010). "Motoring around the plant cell: insights from plant myosins." Biochem Soc Trans **38**(3): 833-8.

Stern, C. D. and B. C. Goodwin (1977). "Waves and periodic events during primitive streak formation in the chick." J Embryol Exp Morphol **41**: 15-22.

Straight, A. F., A. Cheung, et al. (2003). "Dissecting temporal and spatial control of cytokinesis with a myosin II Inhibitor." Science **299**(5613): 1743-7.

Theriot, J. A. (1994). "Regulation of the actin cytoskeleton in living cells." Semin Cell Biol **5**(3): 193-9.

Tinevez, J. Y., U. Schulze, et al. (2009). "Role of cortical tension in bleb growth." Proc Natl Acad Sci U S A **106**(44): 18581-6.

Toyama, Y., X. G. Peralta, et al. (2008). "Apoptotic force and tissue dynamics during Drosophila embryogenesis." Science **321**(5896): 1683-6.

Trinkaus (1969). "Cells into Organs; the forces that shape the embryo." Foundation of Developmental Biology Series.

Tuvia, S., A. Almagor, et al. (1997). "Cell membrane fluctuations are regulated by medium macroviscosity: evidence for a metabolic driving force." Proc Natl Acad Sci U S A **94**(10): 5045-9.

Vartiainen, M. K. (2008). "Nuclear actin dynamics--from form to function." FEBS Lett **582**(14): 2033-40.

Vasioukhin, V., C. Bauer, et al. (2000). "Directed actin polymerization is the driving force for epithelial cell-cell adhesion." Cell **100**(2): 209-19.

Vaughan, R. B. and J. P. Trinkaus (1966). "Movements of epithelial cell sheets in vitro." J Cell Sci **1**(4): 407-13.

Venugopalan, V., A. Guerra, 3rd, et al. (2002). "Role of laser-induced plasma formation in pulsed cellular microsurgery and micromanipulation." Phys Rev Lett **88**(7): 078103.

von Dassow, M. and L. A. Davidson (2007). "Variation and robustness of the mechanics of gastrulation: the role of tissue mechanical properties during morphogenesis." Birth Defects Res C Embryo Today **81**(4): 253-69.

von Dassow, M. and L. A. Davidson (2009). "Natural variation in embryo mechanics: gastrulation in Xenopus laevis is highly robust to variation in tissue stiffness." Dev Dyn **238**(1): 2-18.

Waldrop, M. (1992). Complexity: The Emerging Science at the Edge of Order and Chaos. New York, Simon and Schuster.

Wallingford, J. B., A. J. Ewald, et al. (2001). "Calcium signaling during convergent extension in Xenopus." Curr Biol **11**(9): 652-61.

Wallingford, J. B., S. E. Fraser, et al. (2002). "Convergent extension: the molecular control of polarized cell movement during embryonic development." Dev Cell **2**(6): 695-706.

Wallingford, J. B., B. A. Rowning, et al. (2000). "Dishevelled controls cell polarity during Xenopus gastrulation." Nature **405**(6782): 81-5.

Wardle, F. C. and H. L. Sive (2003). "What's your position? the Xenopus cement gland as a paradigm of regional specification." Bioessays **25**(7): 717-26.

Wayne Brodland, G. and C. J. Wiebe (2004). "Mechanical effects of cell anisotropy on epithelia." Comput Methods Biomech Biomed Engin **7**(2): 91-9.

Wells, K. L. and N. Patel (2010). "Lumen formation in salivary gland development." Front Oral Biol **14**: 78-89.

Wilson, P. A. and D. A. Melton (1994). "Mesodermal patterning by an inducer gradient depends on secondary cell-cell communication." Curr Biol **4**(8): 676-86.

Woehler, A. and E. G. Ponimaskin (2009). "G protein--mediated signaling: same receptor, multiple effectors." Curr Mol Pharmacol **2**(3): 237-48.

Wolpert, L. (2009). "Diffusible gradients are out - an interview with Lewis Wolpert. Interviewed by Richardson, Michael K." Int J Dev Biol **53**(5-6): 659-62.

Wolpert, L., R. Beddington, et al. (2002). "Principles of Development." Oxford University Press.

Wozniak, M. A. and C. S. Chen (2009). "Mechanotransduction in development: a growing role for contractility." Nat Rev Mol Cell Biol **10**(1): 34-43.

Yen, P. T., P. Herman, et al. (1997). "Extracellular ATP modulates ion transport via P2Y purinoceptors in a middle-ear epithelial cell line." ORL J Otorhinolaryngol Relat Spec **59**(3): 170-5.

Zhou, J., H. Y. Kim, et al. (2009). "Actomyosin stiffens the vertebrate embryo during crucial stages of elongation and neural tube closure." Development **136**(4): 677-88.

Zsembery, A., A. T. Boyce, et al. (2003). "Sustained calcium entry through P2X nucleotide receptor channels in human airway epithelial cells." J Biol Chem **278**(15): 13398-408.

Zsembery, A., J. A. Fortenberry, et al. (2004). "Extracellular zinc and ATP restore chloride secretion across cystic fibrosis airway epithelia by triggering calcium entry." J Biol Chem **279**(11): 10720-9.